Technische Universität München
Physik Department
Institut für Theoretische Physik T30d

The Cosmological Constant and Discrete Space-Times

Dipl.-Phys. Univ. Florian Bauer

Vollständiger Abdruck der von der Fakultät für Physik der Technischen Universität München zur Erlangung des akademischen Grades eines

Doktors der Naturwissenschaften (Dr. rer. nat.)

genehmigten Dissertation.

Vorsitzender:		Univ.-Prof. Dr. Lothar Oberauer
Prüfer der Dissertation:	1.	Prof. Dr. Manfred Lindner, Ruprecht-Karls-Universität Heidelberg
	2.	Hon.-Prof. Dr. Wolfgang Hillebrandt

Die Dissertation wurde am 31.07.2006 bei der Technischen Universität München eingereicht und durch die Fakultät für Physik am 23.08.2006 angenommen.

Abstract

In this thesis the cosmological constant is investigated from two points of view. First, we study the influence of a time-dependent cosmological constant on the late-time expansion of the universe. Thereby, we consider several combinations of scaling laws motivated by renormalisation group running and different choices for the interpretation of the renormalisation scale. Apart from well known solutions like de Sitter final states we also observe the appearance of future singularities. As the second topic we explore vacuum energy in the context of discrete extra dimensions, and we calculate the Casimir energy density as a contribution to the cosmological constant. The results are applied in a deconstruction scenario, where we propose a method to determine the zero-point energy of quantum fields in four dimensions. In a related way we find a lower bound on the size of a discrete gravitational extra dimension, and finally we discuss the graviton and fermion mass spectra in a scenario, where the extra dimensions form a discrete curved disk.

Zusammenfassung

In dieser Arbeit wird die kosmologische Konstante aus zwei verschiedenen Blickwinkeln untersucht. Als erstes behandeln wir den Einfluß einer zeitabhängigen kosmologischen Konstante auf die Entwicklung des Universums zu späten Zeiten. Dabei betrachten wir mehrere Skalengesetze, die vom Renormierungsgruppenlaufen herrühren, und außerdem verschiedene Möglichkeiten, die Renormierungsskala festzulegen. Neben bekannten Lösungen wie dem de Sitter Kosmos beobachten wir auch das Auftreten von Singularitäten in endlicher Zukunft. Der zweite Schwerpunkt dieser Arbeit stellt Vakuumenergie in diskreten extra Dimensionen dar, wo die Casimirenergiedichte als Beitrag zur kosmologischen Konstante berechnet wird. Im Rahmen von Deconstruction verwenden wir die Ergebnisse, um eine Möglichkeit zu finden, die Nullpunktsenergie von Quantenfeldern in vier Dimensionen zu bestimmen. Ebenso leiten wir eine untere Schranke für die Größe einer diskreten gravitativen extra Dimension her. Und schließlich diskutieren wir die Massenspektren von Gravitonen und Fermionen in einem Modell, bei dem die extra Dimensionen eine diskrete gekrümmte Scheibe bilden.

Contents

1 Introduction

Several years after the discovery of the accelerated cosmological expansion, the question what drives this behaviour is still open. Since general relativity with well known matter sources like dust and radiation always exhibits a decelerating universe, we have to expect something new that explains the observed behaviour, which has gained great support by recent observations [1, 2, 3, 4, 5, 6]. The name "dark energy" has become common to describe all energy forms that are able to yield the acceleration, although other origins are often put into the same category. The amount of possible frameworks and models that have been proposed to describe DE has grown quite huge as can be seen in recent reviews about this topic [7, 8, 9, 10, 11]. Interestingly, the first dark energy candidate was already introduced by Albert Einstein almost a century ago. He considered a positive cosmological constant (CC) in order to realise a static cosmos, where the CC compensates the dust matter. However, it turned out that this space-time was unstable and additionally not consistent with the afterwards observed cosmological expansion. These days, Einstein's CC has come back as the simplest candidate for dark energy since it is just a constant in the action for classical general relativity. Furthermore, in the context of quantum field theory the vacuum or zero-point energy of quantum fields contributes also to the CC. But this quantum origin also involves the so-called cosmological constant problem [12], which is generally considered to be one of the biggest mysteries in physics. The core of this problem is the fact that in quantum field theory the absolute value of the CC has not been determined yet, because the corresponding calculation leads to an infinite value. Furthermore, naive estimations using energy cutoffs are many orders of magnitude above its measured value. Due to this extreme discrepancy and the fact that dark energy has become dominant very lately in the cosmological evolution, other explanations have been proposed. Apart from new energy forms like, e.g., scalar field condensates (quintessence) [13], that contribute to the energy content of the universe, modifications of the theory of gravity or even of the space-time structure have become subject of intensive investigation. Instead of discussing all these possibilities, we will in this thesis concentrate on two subjects in the context of vacuum energy as a major source of dark energy. First, we will study a CC that becomes time-dependent due to quantum effects. In this framework we discuss the late time cosmological evolution and the occurrence of future singularities. The second topic of investigation are space-times with discrete compact extra dimensions, where the appearance of zero-point energy and the properties of fields will be discussed.

To introduce the first subject let us start on the classical level, where the CC is just a constant term in the action for general relativity, implying that it remains constant in Einstein's equations, too. Assume for the moment that the current cosmological acceleration

is just due to a positive CC in a universe with only cold dark matter (ΛCDM cosmology), then one finds that our space-time is approaching an empty and static de Sitter universe. However, other dark energy sources might change the cosmological fate significantly in comparison to the ΛCDM case. For instance, they could cause a final domination of matter or even future singularities [14], where space-time collapses to a big crunch or gets torn apart in a big rip event [15]. Especially the big rip singularity would require some very unusual energy forms like scalar fields with negative kinetic terms and other "exotic" things. But as we will show in this work, such extreme final states might also appear with the CC once it is allowed to be time-dependent or more generally scale-dependent. Constants that become scale-dependent occur quite generally in quantum theories like quantum electrodynamics, where the fine-structure constant becomes energy-dependent by renormalisation group effects. The corresponding renormalisation group equations (RGE) describe the "running" of the constant as a function of the renormalisation scale μ and masses of quantum fields that are involved in the theory. Similarly, one obtains the RGEs for the CC and also for Newton's constant from the effective action of quantum fields on curved space-times [16, 17, 18, 19]. For free fields the RGEs can be calculated exactly thereby leading to a scale dependence of the CC as we will see later. Also certain theories of quantum gravity [20, 21, 22] can be a source for a scale-dependent CC or Newton's constant. Unlike running coupling constants emerging from interacting quantum fields, where the renormalisation scale can be easily interpreted as external momentum or temperature, the identification of the scale for the CC is not always given by the theory since there is no external momentum. To study the RG running in a cosmological context we will therefore explore as candidates for the renormalisation scale several scales that are characteristic for the cosmological evolution. This will be the Hubble scale and the sizes of the particle and event horizons. In addition, the consequences of several RGEs following from different frameworks and motivations will be discussed as well. For each combination of RGEs and renormalisation scale identifications we will finally solve Einstein's equations and determine the possible final states of the universe. Apart from the pure curiosity of the researcher, the results of this analysis might be valuable also for deciding which of the above combinations are reasonable after one has accepted or rejected the idea of future singularities.

The second major part of this thesis deals with fact that vacuum energy is also sensitive to external conditions, which might come from a non-trivial space-time structure. The Casimir effect [23] is a famous example, where the quantum field zero-point energy depends on the boundary conditions that are imposed onto the quantum fields. In the original setup the boundary conditions follow from two parallel conducting plates in four dimensions, where the Casimir effect implies a force on the plates. While in this case the corresponding vacuum energy usually cannot be identified directly with contributions to the CC, a space-time with compact extra dimensions (ED) might lead to an effective four dimensional (4D) CC that depends on the properties of the EDs [24]. Generally, one can say that the resulting Casimir energy of massless fields scales inversely with the size of the EDs. Here, one encounters a severe problem because small EDs produce large contributions to the effective 4D CC in contrast to its observed tiny value. Too large EDs, on the other hand, could be easily observed by fifth force experiments and other

methods [25, 26, 27]. One has therefore to cope with stringent bounds on the size of the EDs. Instead of working with large EDs one can obtain small CC contributions also by considering massive quantum fields, which yield a suppression of the Casimir energy. This property allows to keep both the ED and the Casimir energy small. In this thesis we will investigate the Casimir effect and the behaviour of quantum fields more deeply in the context of discretised EDs. In contrast to continuous EDs the discrete structure implies some interesting features like a finite number of Kaluza-Klein modes or typical lattice theory attributes. More motivation comes from the fact that a discretised space-time structure exhibits a minimal physical length scale that could in principle regularise space-time singularities in general relativity and respectively ultra-violet (UV) divergences in quantum theories. It therefore represents a useful concept for quantum gravity [28]. By the way, as EDs have not been observed yet, the property of being discretised represents a reasonable possibility. One should just imagine some kind of higher dimensional solid state physics. Furthermore, it was recently found that discretised EDs can be described within a fully 4D context called "deconstruction" [29, 30]. This model-building approach avoids problems that emerge when extra-dimensional field momenta reach the fundamental Planck scale, which can be considerably below the 4D Planck scale. Coming back to the CC problem, the vacuum energy of 4D quantum fields in a deconstruction setup is, as expected, divergent, which just leads to the renormalisation group running effects mentioned above. Thus the overall CC scale is undetermined and has to fixed by observations. However, in this work we propose a well defined prescription to assign a finite value to the CC by employing the correspondence between deconstruction and discretised higher dimensions. We will demonstrate this idea within a specific deconstruction model, where also the suppression of the Casimir energy by massive fields will be applied.

Going one step further by discretising gravity in the EDs one approaches new effects in the form of strongly interacting massive 4D gravitons [31, 32]. This strong coupling behaviour leads to an upper limit for masses and energy scales appearing in the theory. Interestingly, the limit might depend also on the size of the ED. As a consequence, the ability to suppress the Casimir energies by large field masses is reduced since the masses have to lie below the strong coupling scale. In this context we will derive some limits on the ED size by requiring that the resulting CC does not exceed its observed value. Finally, we consider on a more formal level a six dimensional (6D) model, which involves a discretised curved disk. In this scenario we discuss the implementation of fermions and gravitons, and furthermore investigate the effect of the curvature and its influence on the mass spectra of the resulting 4D fields.

The structure of this thesis is given as follows: in Chap. 2 we introduce a number of scaling laws for the CC together with some renormalisation scale identifications. Afterwards we explain how to solve Einstein's equations with a time-dependent CC and Newton's constant and subsequently discuss cosmological late-time solutions and the corresponding fates of the universe. Chap. 3 is devoted the Casimir effect in continuous higher dimensions, where the vacuum energy for a five dimensional (5D) setup is derived. In Chap. 4 we introduce the discretisation of the fifth dimension and explicitly show how to calculate the Casimir energy in the corresponding scenario. Several effects like bulk masses and lattice artefacts are discussed, too. As an application we apply in Chap. 5 our results to

a deconstruction model and propose a way to determine the zero-point energy of the 4D fields. Discretised gravitational EDs are the main subject of Chap. 6, where we derive some bounds on the size of the ED. In Chap. 7 we investigate a 6D scenario with two curved and discretised EDs. We calculate the corresponding mass spectra of gravitons and fermions and close the chapter with a little application. Finally, we summarise the results of this work and present our conclusions.

Conventions

Throughout this work we use the Einstein sum convention, and we set the speed of light c, Planck's constant $\hbar$ and Boltzmann's constant k_{B} to unity. Other conventions are given in the text, where necessary.

2 Time-dependent Cosmological Constant

2.1 Quantum Effects and the Cosmological Constant

In this chapter we will investigate a positive CC as the most prominent candidate for dark energy. As a component in Einstein's equations of classical general relativity it can be treated as a perfect fluid with a constant energy density $\Lambda > 0$ and an equation of state $\omega = p/\Lambda = -1$ that corresponds to a negative pressure $p = -\Lambda$. On the quantum level the CC emerges as vacuum energy of quantum fields with the same equation of state as the classical CC. It is therefore an unavoidable constituent of the matter content of the universe. Unfortunately, one does not know how to calculate its value in a unique way, because it can be written in the form of a quartically divergent momentum (p) integral like $\int \mathrm{d}^3p \cdot p$. Respectively, for compact dimensions one obtains the infinite sum of zero-point energies $\sum \frac{1}{2}p$. In Minkowski space one usually eliminates the infinite vacuum energy by normal ordering in QFT since it has no influence on flat space-time physics. Gravity, on the other hand, is sensitive to all forms of energy and matter, and we thus have to deal with vacuum energy in cosmology. The naive assumption of an UV cutoff to regularise the infinite integral at some known energy scale M_x leads to an unobserved high value of the CC, which illustrates the old CC problem [12]. For example, let $M_\mathrm{x} \sim 10^3\,\mathrm{GeV}$ be the energy scale, where supersymmetry is assumed to be broken. This leads via

$$\int_0^{M_\mathrm{x}} \mathrm{d}^3p \cdot p \sim M_\mathrm{x}^4 \gg \rho_\mathrm{obs} \sim 10^{-47}\,\mathrm{GeV}^4 \tag{2.1}$$

to a mismatch of about 60 orders of magnitude. Without extreme fine-tuning in the theory the naive cutoff method for determining the CC obviously does not work and should be rejected. Fortunately, the procedure of renormalisation in QFT can handle infinities, thereby leading to a dependence of the renormalised constants on some energy scale μ. In many cases, this renormalisation scale can be identified with an external momentum, or at least with some characteristic scale (e.g., the temperature) of the environment. Studying QFT on curved space-time [16, 19] leads to infinities in the effective action or in the vacuum expectation values (VEV) of the energy-momentum tensors of the fields. This can be treated by renormalisation to yield a scale-dependent or running CC and a running Newton constant. However, the absolute values are still not calculable, but the change with respect to the renormalisation scale can be calculated via RGEs. In the following we will investigate the influence of RGEs originating in QFT [17, 33, 34] and quantum gravity [20]. Unlike the running coupling constants in the standard model of particles,

here, the physical meaning of the scale is not given by the theory since there is no external momentum. In the cosmological context that we consider, it is reasonable to identify the renormalisation scale with some characteristic scales in cosmology, which will be done in Sec. 2.3. For phenomenological reasons, we should request that the scale μ does not change too much over cosmological time scales. Once we have fixed the combination of RGE and scale identification we are able to discuss in Sec. 2.5 the late-time behaviour and the fate of the universe with a running CC. In addition to a running CC we will also consider a running of Newton's constant for one case in Sec. 2.6. Please note, that in contrast to dark energy scenarios with a time-dependent equation of state as in Refs. [13], here, the equation of state of the CC is still exactly $\omega = -1$. Nevertheless, it is possible to obtain an effective time-dependent equation of state [35] due to a non-standard scaling of the matter energy density with the cosmological time. This non-standard scaling is explained in Sec. 2.4, where we discuss how to solve Einstein's equations on a Robertson-Walker background when the CC and Newton's constant depend on the cosmological time.

2.2 Scaling Laws

According to QFT on curved space-times the CC and Newton's constant G are subject to renormalisation group running like the running of the fine-structure constant in quantum electrodynamics. The corresponding scaling laws of these constants depend crucially on the considered quantum fields and their masses. In the following we consider two different RGEs emerging in this framework and in addition one scaling law that emerges in the context of "quantum Einstein gravity" [20]. Throughout the text we will identify the CC with the corresponding vacuum energy density Λ.

Let us first start with non-interacting quantum fields on a curved space-time, namely a Friedmann-Robertson-Walker universe with a positive CC. For one fermionic and one bosonic degree of freedom with masses $m_{\rm F}$ and $m_{\rm B}$, respectively, the 1-loop effective action can be written in the form [16]

$$\begin{aligned} S_{\rm eff} &= \int {\rm d}^4x\sqrt{-g}\left[\frac{\rm Ric}{16\pi G} - \Lambda + \left(D + \ln\frac{m_{\rm F/B}}{\mu}\right)\right. \\ &\quad \left.\times\left(\frac{m_{\rm F}^4 - m_{\rm B}^4}{32\pi^2} - \frac{\rm Ric}{16\pi^2}\left[(\xi - \tfrac{1}{6})m_{\rm B}^2 - \tfrac{1}{12}m_{\rm F}^2\right]\right)\right] + C \end{aligned} \tag{2.2}$$

where $D = \frac{1}{2}\gamma_{\rm Euler} + \lim_{n\to 4}(n-4)^{-1}$ is a divergent term, which does not depend on the renormalisation scale μ. Furthermore, ξ is a coupling constant[1], and the variable C represents all further terms in the effective action, that are neither proportional to the Ricci scalar Ric nor to the vacuum energy density

$$\Lambda := \frac{\lambda}{8\pi G}.$$

[1] In the action $S = \int {\rm d}^4x\sqrt{-g}\left[\frac{\rm Ric - 2\lambda}{16\pi G} + \frac{1}{2}\phi_{;\alpha}\phi^{;\alpha} - \frac{1}{2}[m^2 + \xi{\rm Ric}]\phi^2\right]$ of a scalar field ϕ on a curved space-time, the constant ξ occurs in the coupling term $\xi \cdot {\rm Ric} \cdot \phi^2$ between the scalar field and the Ricci scalar Ric.

The relevant β-functions in the $\overline{\text{MS}}$-scheme for the vacuum energy density Λ and Newton's constant G are obtained by the requirement that the effective action S_{eff} must not depend on the renormalisation scale μ,

$$\mu \frac{\mathrm{d}S_{\text{eff}}}{\mathrm{d}\mu} = 0.$$

Because of this condition, Λ and G have to be treated as μ-dependent functions in Eq. (2.2), which consequently have to obey the RGEs given by

$$\mu \frac{\mathrm{d}\Lambda}{\mathrm{d}\mu} = -\frac{m_{\text{F}}^4 - m_{\text{B}}^4}{32\pi^2}, \quad \mu \frac{\mathrm{d}}{\mathrm{d}\mu}\left(\frac{1}{G}\right) = -\frac{1}{\pi}\left[(\xi - \tfrac{1}{6})m_{\text{B}}^2 - \tfrac{1}{12}m_{\text{F}}^2\right].$$

Note, that the divergent term D has dropped out, leaving over just the masses $m_{\text{F/B}}$ and ξ. Assuming constant masses, the RGEs can be integrated, hence, the equation for the vacuum energy density reads

$$\Lambda(\mu) = \Lambda_0(1 - q_1 \ln \tfrac{\mu}{\mu_0}), \quad \Lambda_0 := \Lambda(\mu_0), \tag{2.3}$$

where Λ_0 denotes the vacuum energy density today, when the renormalisation scale μ has the value μ_0. Moreover, the sign of the parameter

$$q_1 := \frac{1}{32\pi^2\Lambda_0}\left(m_{\text{F}}^4 - m_{\text{B}}^4\right) \tag{2.4}$$

depends on whether bosons or fermions dominate. In this context, a real scalar field counts as one bosonic degree of freedom, and a Dirac field as four fermionic ones. The generalisation to more than one quantum field in the RGE, can be achieved by summing over the fourth powers of their masses. For Newton's constant G we obtain the RGE in the integrated form

$$G(\mu) = \frac{G_0}{1 - q_2 \ln \frac{\mu}{\mu_0}}, \quad G_0 := G(\mu_0). \tag{2.5}$$

Again, we omit the generalisation to more fields, that follows from summing over the squared masses of the fields. For one bosonic and one fermionic degree of freedom the mass parameter q_2 is given by

$$q_2 := \frac{G_0}{\pi}\left[(\xi - \tfrac{1}{6})m_{\text{B}}^2 - \tfrac{1}{12}m_{\text{F}}^2\right]. \tag{2.6}$$

Finally, we remark, that Eq. (2.3) for the running vacuum energy density $\Lambda(\mu)$ was derived in a renormalisation scheme, which is usually associated with the high energy regime. It is therefore not known to what extend it can be applied at late times in cosmology. In addition, to avoid conflicts with observations, the field content has to be fine-tuned to obtain $|q_1| \leq O(1)$, which we assume for the rest of this work. Unfortunately, the corresponding covariantly derived equations for the low energy sector are not known yet [36]. Therefore, we prefer to work with the above RGEs, which were derived in a covariant way, and study the consequences and the constraints on the mass parameters q_1 and q_2.

The second scaling law follows from a RGE that shows a decoupling behaviour. Considering only the most dominant terms at low energy, the corresponding β-function for Λ is

given by $\mu\frac{\mathrm{d}\Lambda}{\mathrm{d}\mu} = A_1\mu^2$, where $A_1 \sim \pm M^2$ is set by the masses M and the spins of the fields. RGEs of this kind have been studied extensively in the literature, see Refs. [17]. Assuming constant masses and μ_0 to be of the order of today's Hubble scale H_0 one obtains

$$\frac{\Lambda(\mu)}{\Lambda_0} = L_0 + L_1\frac{\mu^2}{\mu_0^2}, \quad L_1 \sim \pm\frac{M^2}{M_\mathrm{P}^2}, \tag{2.7}$$

where $L_0 := 1 - L_1$ and M_P denotes the Planck mass today. Here, the running of Λ is suppressed since $|L_1| \ll 1$ for sub-Planckian masses M.

The last scaling laws come from the RGEs in quantum Einstein gravity [20, 21]. In this framework the effective gravitational action becomes dependent on a renormalisation scale μ, which leads to RGEs for Λ and G. An interesting feature is the occurrence of an UV fixed-point [37] in the renormalisation group flow of the dimensionless quantities[2] $\Lambda\mu^{-4}$ and $G\mu^2$ at very early times in cosmology corresponding to $\mu \to \infty$. Motivated by strong infrared (IR) effects in quantum gravity one has proposed that there might also exist an IR fixed-point in quantum Einstein gravity [38] leading to significant changes in cosmology at late times[3], where $\mu \to 0$. If this were true, one would obtain the RGEs

$$\frac{\Lambda}{\Lambda_0} = \frac{\mu^4}{\mu_0^4}, \quad \frac{G}{G_0} = \frac{\mu_0^2}{\mu^2}, \tag{2.8}$$

where μ_0 corresponds to $\Lambda = \Lambda_0$ and $G = G_0$. In the epoch between the UV and IR fixed-points, Λ and G vary very slowly with μ, and we will treat them as constants in this region. Therefore, we assume that the scaling laws (2.8) are valid from today until the end of the universe.

2.3 Renormalisation Scales

In order to study the effects on the cosmological expansion due to the scaling laws of Sec. 2.2, we have to define the physical meaning of the renormalisation scale μ. Unfortunately, the theories underlying the scaling laws often do not determine the scale explicitly[4], apart from the usual interpretations as an (IR) cutoff or a scale characterising the physical environment (temperature, external momenta). In our cosmological setting we will investigate three different choices for μ, given by the Hubble scale H, the inverse radius R^{-1} of the cosmological event horizon, and finally the inverse radius T^{-1} of the particle horizon.

Let us consider our universe on sufficiently large scales, where it is well described by the Robertson-Walker metric given by

$$\mathrm{d}s^2 = \mathrm{d}t^2 - a^2(t)\left(\frac{\mathrm{d}r^2}{1-kr^2} + r^2\mathrm{d}\Omega^2\right), \tag{2.9}$$

[2] In this work Λ denotes the vacuum energy density corresponding to a CC, whereas in many articles about quantum gravity Λ is the CC λ itself.

[3] However, it was argued in Ref. [39] that the region of strong IR effects can never be reached.

[4] In the framework of Refs. [40], Newton's constant was found to depend explicitly on the Hubble scale.

where k fixes the spatial curvature. In accordance with recent observation we will ignore the spatial curvature and consider in the following the spatially flat ($k = 0$) metric

$$\mathrm{d}s^2 = \mathrm{d}t^2 - a^2(t)\mathrm{d}\vec{x}^2, \tag{2.10}$$

where the scale factor $a(t)$ depends only on the cosmological time t and not on the spatial coordinates $\vec{x}$.

Our first candidate for the renormalisation scale μ is the Hubble scale

$$H(t) := \frac{\dot{a}(t)}{a(t)}, \tag{2.11}$$

which describes the actual expansion rate of the universe. On the other hand, the horizon scales R and T describe the cosmological evolution of the future and the past, respectively.

In universes with late-time acceleration like the ΛCDM model there usually exists a cosmological event horizon. Its proper radius R corresponds to the proper distance that a (light) signal can travel when it is emitted by a comoving observer at the time t:

$$R(t) := a(t) \int_t^\infty \frac{\mathrm{d}t'}{a(t')}. \tag{2.12}$$

In the case that the universe comes to an end within finite time the upper limit of the integral has to be replaced by this time. Similar to the event horizon of a black hole, the cosmological event horizon exhibits thermodynamical properties like the emission of radiation with the Gibbons-Hawking temperature [41].

The counterpart of R is the particle horizon radius T, which is given by the proper distance that a signal has travelled since the beginning of the world ($t = 0$):

$$T(t) := a(t) \int_0^t \frac{\mathrm{d}t'}{a(t')}. \tag{2.13}$$

In a simple cosmological model, where the universe begins at $t = 0$ and then evolves according to the decelerating scale factor $a(t) \propto t^n$ with $0 < n < 1$, the particle horizon radius reads $T(t) = t/(1-n)$. Now we assume that at some time t_0 a de Sitter phase sets in, which corresponds to a scale factor $a(t) \propto \exp(H_0(t - t_0))$ for $t > t_0$. This leads to a radius function T that grows exponentially with t at late times:

$$T(t > t_0) = \left(T(t_0) + \frac{1}{H_0}\right) \exp(H_0(t - t_0)) - \frac{1}{H_0}. \tag{2.14}$$

Since the asymptotic behaviour of the scales H, R and T plays a major role in this work, it is plotted in Fig. 2.1 for a universe with dust-like matter and Λ and G being positive and constant. Note that if one of the horizon radii diverges, one says that the horizon does not exist. The geometric meaning of the scales given here has been discussed, e.g., in Ref. [42], and some arguments for the event horizon in the context of the CC can be found in Refs. [43, 44].

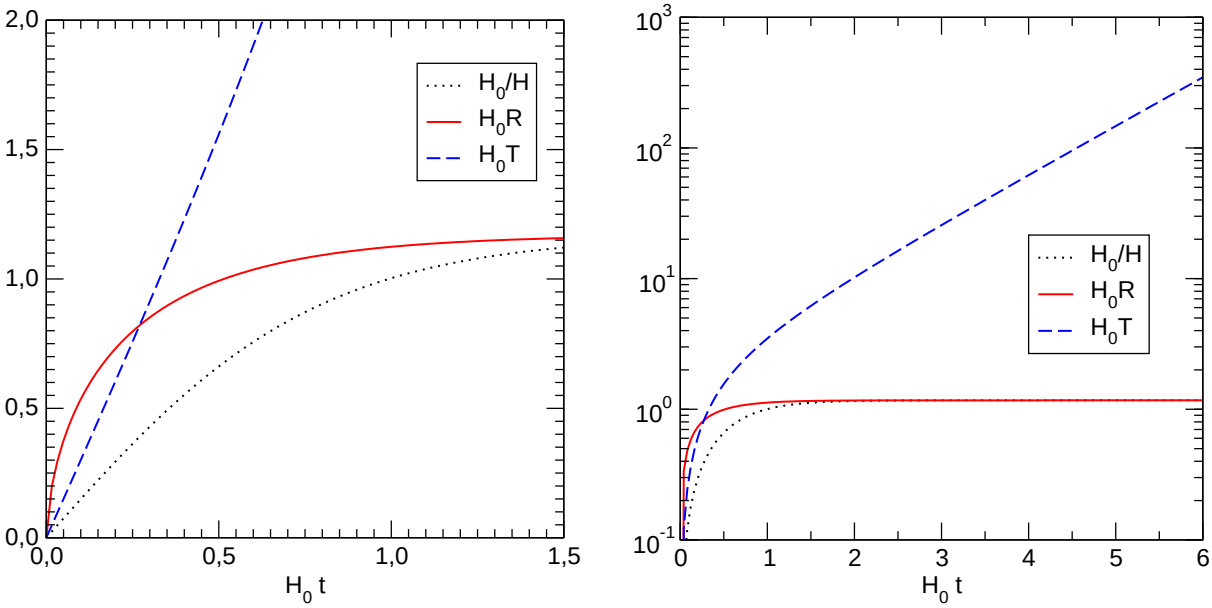

Figure 2.1: In a spatially flat ΛCDM universe with constant Λ and G the radii of the event horizon R and the Hubble horizon H^{-1} approach the same constant value for $t \to \infty$. At early times the particle horizon radius T grows linearly with time and exponentially with time for $t \to \infty$. At the time $t_0 = 0,99 H_0^{-1}$ (today) the relative vacuum energy is given by $\Omega_{\Lambda 0} = 0,73$.

2.4 General Relativity with Time-dependent Constants

In this section, we derive the evolution equation for the cosmic scale factor $a(t)$ in the framework of the spatially isotropic and homogeneous Friedmann-Robertson-Walker universe with a time-dependent CC and Newton's constant. On this background, radiation and pressureless matter (dust) can both be described by a perfect fluid with energy density ρ and pressure $p = \omega\rho$, where the constant ω characterises the equation of state. For instance, dust-like matter like CDM has the equation of state $\omega = 0$ and incoherent radiation $\omega = \frac{1}{3}$, respectively. The corresponding energy-momentum tensor for these energy forms reads

$$T^{\alpha\beta} = (\rho + p)u^\alpha u^\beta - p g^{\alpha\beta},$$

with u^α being the four-velocity vector field of the fluid. With our choices of the renormalisation scale, G and Λ depend only on the cosmic time t. From Einstein's equations

$$G^{\alpha\beta} = 8\pi G(\Lambda g^{\alpha\beta} + T^{\alpha\beta})$$

and from the contracted Bianchi identities $G^{\alpha\beta}{}_{;\beta} = 0$ for the Einstein tensor $G^{\alpha\beta}$, we obtain the generalised conservation equations

$$[G\Lambda g^{\alpha\beta} + G T^{\alpha\beta}]_{;\beta} = 0,$$

whose $\alpha = 0$ component reads

$$\dot{G}(\Lambda + \rho) + G(\dot{\Lambda} + \dot{\rho} + 3\tfrac{\dot{a}}{a}\rho(1 + \omega)) = 0.$$

Here the dot denotes the derivative with respect to the cosmological time t, and we do not assume $T^{\alpha\beta}_{\ \ ;\beta} = 0$. For constant Λ and G the last equation can be integrated to yield the usual scaling law for the matter energy density $\rho \propto a^{-2(Q+1)}$, where we have for our convenience introduced the equation of state parameter[5]

$$Q := \frac{1}{2}(1 + 3\omega). \tag{2.15}$$

Note that for non-constant Λ and G this simple scaling rule for the matter content is not valid anymore, because it is now possible to transfer energy between the matter and the vacuum, in addition to $\dot{G} \neq 0$. At this stage we have to admit that this energy transfer implies an effective interaction between the gravitational sector (Λ, G) and matter, which is not part of the original Lagrangian. In this sense it should be compared with gravitational particle production [45] resulting also from the interplay of gravity with quantum physics.

Since we have at this point no information about ρ as function of time or the scale factor, we have to combine the Friedmann equations for the Hubble scale $H := \frac{\dot{a}}{a}$ and the acceleration $\frac{\ddot{a}}{a}$,

$$\left(\frac{\dot{a}}{a}\right)^2 + \frac{k}{a^2} = \frac{8\pi}{3}G(t)(\Lambda(t) + \rho(t)), \tag{2.16}$$

$$\frac{\ddot{a}}{a} = \frac{8\pi}{3}G(t)(\Lambda(t) - Q\rho(t)), \tag{2.17}$$

in order to eliminate the matter energy density ρ. The left-hand side of the resulting is abbreviated by $F(t)$:

$$F(t) := \frac{\ddot{a}}{a} + Q\left[\left(\frac{\dot{a}}{a}\right)^2 + \frac{k}{a^2}\right] = \frac{8\pi}{3}G\Lambda \cdot (1 + Q). \tag{2.18}$$

By introducing the constant

$$K_0 := \frac{3}{8\pi G_0 \Lambda_0 (Q+1)} = \frac{H_0^{-2}}{\Omega_{\Lambda 0}(Q+1)}, \tag{2.19}$$

with the relative vacuum energy density $\Omega_{\Lambda 0} = 8\pi G_0 \Lambda_0/(3H_0^2)$ and the Hubble scale H_0 at the time $t = t_0$, we obtain the main equation in the compact form

$$K_0 F(t) = \frac{\Lambda G}{\Lambda_0 G_0} \tag{2.20}$$

Here, we can now insert the RGEs for Λ and G from Sec. 2.2 together with a choice of the renormalisation scale μ from Sec. 2.3. For the scale identifications $\mu = R^{-1}$ and $\mu = T^{-1}$ we have to solve integro-differential equations, whereas $\mu = H$ just leads to an ordinary differential equation.

[5] For a dominant matter energy density $\rho \gg \Lambda$ and flat spatial curvature, the acceleration quantity $q := \frac{\ddot{a}a}{\dot{a}^2}$ is given by the negative value of the Q.

2.5 Cosmological Evolution at Late Times

In this section we study the late-time evolution of the universe with variable Λ and G, thereby assuming from today on the validity of the scaling laws (2.3)–(2.8) and the correct identification of the renormalisation scale μ with the scales (2.11)–(2.13). Our aim is to determine in all nine cases the possible final states of the universe. This depends, of course, on the choice of parameters, but we restrict ourselves to parameter values which comply vaguely to current observations. Today, at the cosmological time $t_0 = 0,99H_0^{-1}$ we fix the initial values H_0 and $\Omega_{\Lambda 0} = 0,73$ by observations. Furthermore, the initial value T_0 of the particle horizon radius would be fixed if the past cosmological evolution was known from the Big Bang on. In contrast to this, the value R_0 of today's event horizon radius depends on the future cosmological evolution and is treated here as a free parameter. In the following we derive some properties of the solutions analytically, in particular, we study the stability of (asymptotic) de Sitter solutions and the occurrence of future singularities, where the scale factor or one of its derivatives diverge within finite time [14, 46]. For simplicity we denote a big rip or a big crunch by the lowest order divergent derivative that is positive or negative, respectively. Since some combinations of scaling laws and renormalisation scales lead to complicated equations we derive in some cases only approximate or numerical statements.

In order to solve Eq. (2.20) numerically, we have to remove the integrals in the definitions (2.12), (2.13) of R and T by a differentiation with respect to t. Using the relations

$$\dot{R} = RH - 1, \quad \dot{T} = TH + 1$$

an ordinary differential equation for the scale factor can be obtained. Let us, for instance, consider $\mu = R^{-1}$ in combination with the RGEs (2.3) and (2.5). First, we solve the main equation (2.20) for R,

$$\frac{\mu_0}{\mu(t)} = \frac{R(t)}{R_0} = \exp\left[\frac{K_0 F(t) - 1}{q_1 - q_2 K_0 F(t)}\right], \tag{2.21}$$

which has the time derivative

$$\left[\frac{\dot{a}}{a} + \frac{(q_2 - q_1)K_0\dot{F}}{(q_1 - q_2 K_0 F)^2}\right] \cdot \exp\left[\frac{K_0 F - 1}{q_1 - q_2 K_0 F}\right] - \frac{1}{R_0} = 0, \tag{2.22}$$

where we have substituted R by Eq. (2.21). This equation can be integrated numerically. Afterwards we have to check whether the functions R and T, calculated from the numerical solution of $a(t)$, agree with R and T that follow directly from Eq. (2.20). If they do not match, the numerical solution has to be discarded. Some of these cases are illustrated and discussed in Sec. 2.6. Furthermore, solutions involving a negative matter energy density are questionable on physical grounds. This happens when the vacuum energy density Λ becomes greater than the critical energy density $\rho_c = 3H^2/(8\pi G)$, which follows from the first Friedmann equation (2.16).

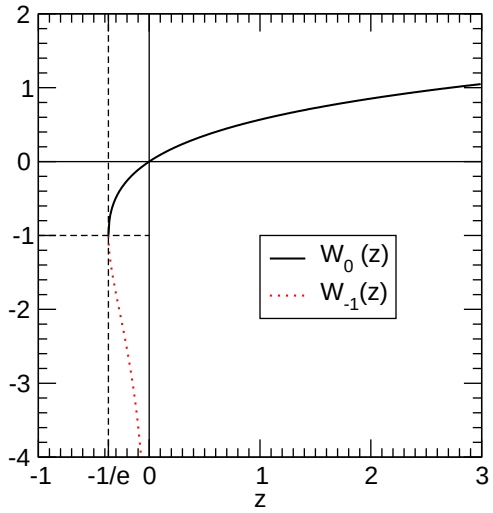

Figure 2.2: Lambert's W-function is the inverse function of $z = xe^x$. For $-1/e \leq z < 0$ it has two real-valued brunches $W_0(z)$ and $W_{-1}(z)$, and for $z \geq 0$ only $W_0(z)$ is real.

2.5.1 $\Lambda = \Lambda_0(1 - q_1 \ln \frac{\mu}{\mu_0})$, $\mu = H$

For the given scaling law and scale choice Eq. (2.20) reads

$$K_0(\dot{H} + (Q+1)H^2) = 1 - q_1 \ln \frac{H}{H_0}. \tag{2.23}$$

We first look for asymptotic de Sitter solutions by applying $\dot{H} = 0$ and $H \to H_\mathrm{e}$. Thus the final Hubble scale H_e is given by

$$\frac{H_\mathrm{e}^2}{H_0^2} = \frac{q_1}{2}\Omega_{\Lambda 0} W_u\left(\frac{2}{q_1\Omega_{\Lambda 0}} e^{2/q_1}\right). \tag{2.24}$$

Here, $W_u(z)$ with $u = 0, -1$ denotes one of the two real-valued branches of Lambert's W-function, which is the solution of $z = xe^x$, see Fig. 2.2. For $q_1 > 0$ there is always one solution for H_e, and for $q_1 < 0$ two solutions exist if the argument of W_u in Eq. (2.24) is greater than $-e^{-1}$. This means either $q_1 < n_1$ or $q_1 > n_2$ with

$$n_1 := \frac{2}{W_0(-\Omega_{\Lambda 0}e^{-1})} \quad \text{and} \quad n_2 := \frac{2}{W_{-1}(-\Omega_{\Lambda 0}e^{-1})} > n_1.$$

These solution are stable if

$$\left.\frac{\mathrm{d}(K_0\dot{H})}{\mathrm{d}H}\right|_{H\to H_\mathrm{e}} = -\frac{q_1}{H_\mathrm{e}} - 2H_\mathrm{e}K_0(Q+1) < 0,$$

where we used Eq. (2.23). For positive q_1 this condition is always fulfilled, whereas for negative q_1 it means $W_u(\frac{2}{q_1\Omega_{\Lambda 0}}e^{2/q_1}) < -1$, which follows from Eq. (2.24). Again, the argument of W_u is constrained yielding $q_1 > n_2$. Therefore only $q_1 > n_2$, which includes $q_1 > 0$, leads to stable de Sitter solutions. Using the phase space relation (2.23), which is plotted in Fig. 2.3, we conclude that for other values of q_1 the cosmological evolution will always end within finite time in a Big Crunch singularity, where $H \to 0$ and $\dot{H} \to -\infty$.

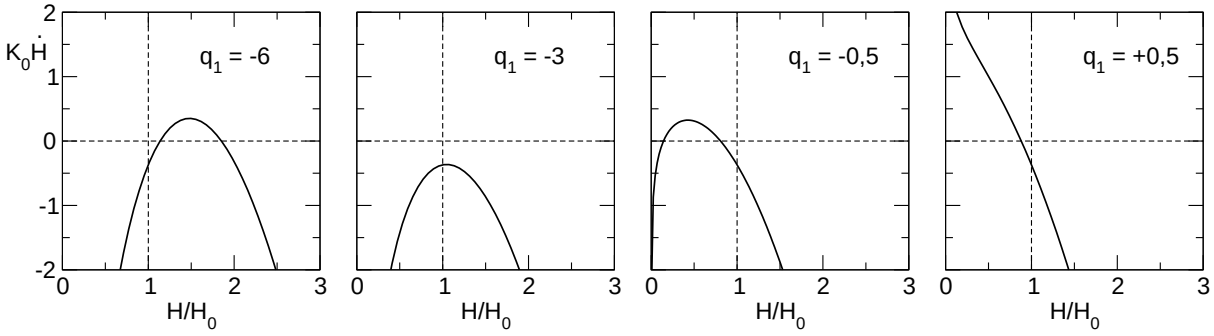

Figure 2.3: The phase space relation (2.23) is shown for $q_1 = -6; -3$, where the universe ends in a big crunch singularity, and respectively for $q_1 = -\frac{1}{2}; +\frac{1}{2}$, which leads to a de Sitter final state ($\dot{H} = 0$). In all cases the evolution begins at $H = H_0$, where $\Omega_{\Lambda 0} = 0,73$ and $\dot{H}_0 < 0$.

2.5.2 $\Lambda = \Lambda_0(L_0 + L_1\frac{\mu^2}{\mu_0^2})$, $\mu = H$

Using this choice for Λ and μ the main equation (2.20) becomes

$$\frac{\ddot{a}}{a} + H^2(Q - L_1(Q+1)\Omega_{\Lambda 0}) = H_0^2 L_0 \Omega_{\Lambda 0}(Q+1),$$

which has the exact solution

$$\frac{a(t)}{a_0} = \Big[\sinh([Q+1][\Omega_{\Lambda 0} L_0(1 - L_1\Omega_{\Lambda 0})]^{\frac{1}{2}} H_0 t)\Big]^n$$

with the parameter

$$n := [(Q+1)(1 - L_1\Omega_{\Lambda 0})]^{-1}.$$

At early times, $H_0 t \ll 1$, it describes a power-law expansion $a(t) \propto t^n$, whereas at late times it approaches the de Sitter expansion law $a(t) \propto \exp(H_e t)$ with the final Hubble scale H_e given by

$$H_e = H_0 \sqrt{\frac{\Omega_{\Lambda 0} L_0}{1 - L_1 \Omega_{\Lambda 0}}}.$$

Further aspects of this case have been studied, e.g., in Refs. [17].

2.5.3 $\Lambda G = \Lambda_0 G_0 \frac{\mu^2}{\mu_0^2}$, $\mu = H$

Following Sec. 2.2 we assume that this scaling law is valid from today on. Here, Eq. (2.20) is given by $\frac{\ddot{a}}{a} + BH^2 = 0$ with $B := Q - (Q+1)\Omega_{\Lambda 0}$. It has an exact power-law solution

$$\frac{a(t)}{a_0} = [(1+B)(t - t_1)]^{1/(B+1)}, \quad t_1 = \text{const.},$$

that exhibits a constant acceleration $\ddot{a}a/\dot{a}^2 = -B > 0$ as well as $\Omega_\Lambda = \text{const}$. Note that a similar solution was found in Refs. [38].

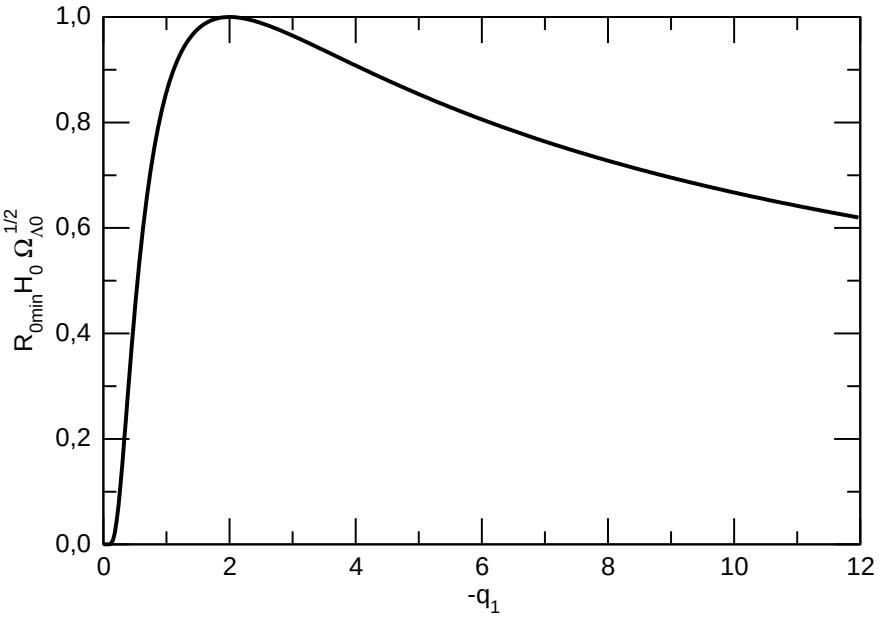

Figure 2.4: The lower bound $R_{0\min}$ of the initial event horizon radius R_0 from Eq. (2.26) for negative q_1. For $R_0 < R_{0\min}$ a final de Sitter state does not exist.

2.5.4 $\Lambda = \Lambda_0(1 - q_1 \ln \frac{\mu}{\mu_0})$, $\mu = R^{-1}$

At first we look for de Sitter solutions with $a(t) \propto \exp(H_e t)$, where the inverse Hubble scale and the event horizon radius approach $R \to R_e = H_e^{-1}$ in addition to $\dot{H} = 0$. Plugging this asymptotic form for $a(t)$ into Eq. (2.20), one arrives at

$$\frac{K_0(1+Q)}{R_e^2} = q_3 x^{-2} = 1 + q_1 \ln x,$$

where the variables $x := R_e/R_0$ and $q_3 := K_0(1+Q)/R_0^2 > 0$ have been introduced. The solutions for x are given by

$$x = \frac{R_e}{R_0} = \sqrt{\frac{2q_3}{q_1 \cdot W_u(\frac{2q_3}{q_1} e^{2/q_1})}}, \tag{2.25}$$

involving Lambert's W-function $W_u(z)$ with $u = 0, -1$ (Fig. 2.2). Since the W-function is real only for arguments $z \geq -e^{-1}$ and $z < 0$ for $W_{-1}(z)$ we obtain for negative q_1 the constraint $q_3 \leq -\frac{q_1}{2} \exp(-\frac{2}{q_1} - 1)$, which implies an lower bound for the initial value R_0 of the horizon radius as shown in Fig. 2.4:

$$R_0 \geq R_{0\min} := \sqrt{-\frac{2}{q_1 \Omega_{\Lambda 0} H_0^2} \exp\left(\frac{2}{q_1} + 1\right)}. \tag{2.26}$$

If R_0 is smaller than this minimal value, then Eq. (2.25) has no positive solutions and a final de Sitter state does not exist. For $R_0 = R_{0\min}$ there is exactly one solution $x =$

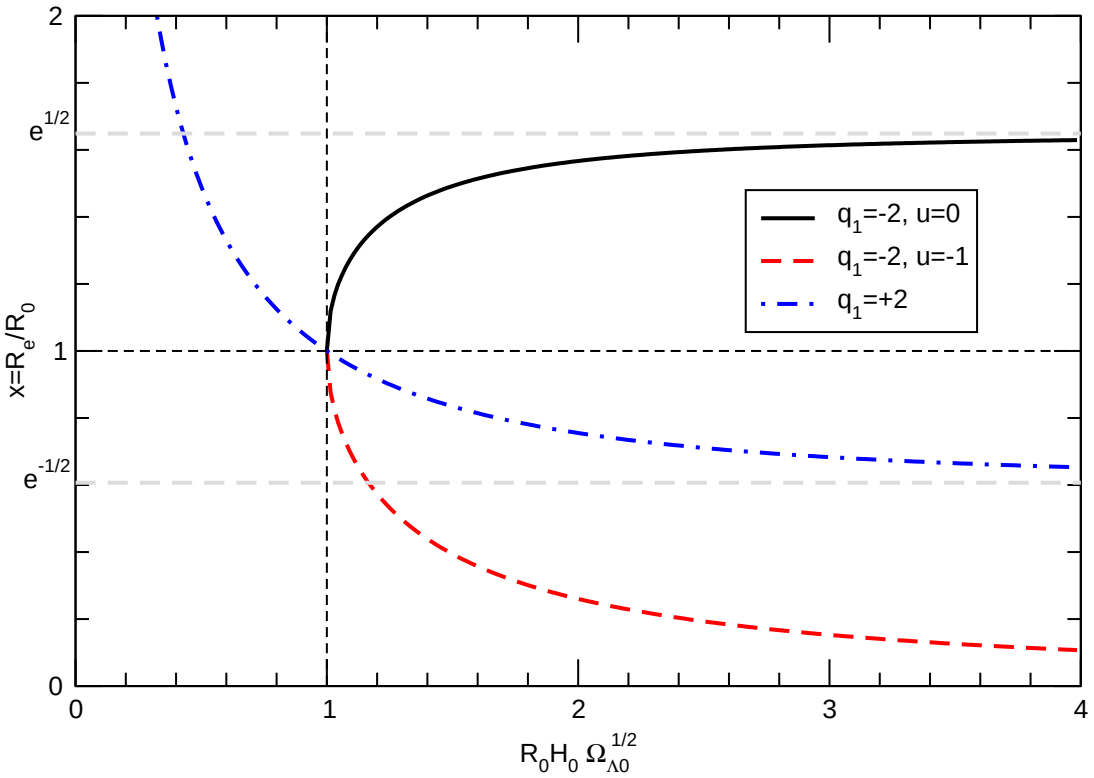

Figure 2.5: The ratio x between the final event horizon radius R_e and the initial radius R_0 as a function of R_0, Eq. (2.25). Here q_1 is set to ± 2. All stable de Sitter final states lie on the curve $u = 0$.

$\exp(-\frac{1}{q_1} - \frac{1}{2})$, for higher values R_0 there are two solutions. In the case of a positive value of the parameter q_1, the initial value R_0 must be smaller than $1/\sqrt{H_0^2 \Omega_{\Lambda 0}}$. Otherwise the final horizon radius R_e is smaller than the initial one, $x < 1$. Both cases are plotted in Fig. 2.5.

Since we have found several de Sitter solutions, we now have to study the stability of these final states. Therefore, we write $K_0 \dot{F}$ as a function of $K_0 F = K_0(\dot{H} + (Q+1)H^2)$,

$$K_0 \dot{F} = q_1 \left[H - \frac{1}{R_0} \exp\left(\frac{1 - K_0 F}{q_1} \right) \right],$$

where we used $\dot{R} = RH - 1$. In the final de Sitter state we have $K_0 \dot{F} = 0$ and $R = R_\mathrm{e} = 1/H_\mathrm{e} = \mathrm{const}$. Near this point we can neglect $\dot{H}$ in the function F and replace H by

$$\sqrt{\frac{K_0 F}{K_0 (Q+1)}}.$$

For a stable solution it is required that

$$\left. \frac{\mathrm{d}(K_0 \dot{F})}{\mathrm{d}(K_0 F)} \right|_{\mathrm{dS}} = \frac{q_1}{2} [K_0^2 F (Q+1)]^{-\frac{1}{2}} + \frac{1}{R_0} \exp\left[\frac{1 - K_0 F}{q_1} \right] < 0, \qquad (2.27)$$

in the final point, where $K_0F = K_0(Q+1)H_\mathrm{e}^2 = q_3 x^{-2}$. With q_3 and x from above, this yields the stability condition

$$\left[W_u\left(\frac{2q_3}{q_1}e^{2/q_1}\right)\right]^{-1} < -1,$$

implying that there are no stable de Sitter solutions for positive values of q_1, because the W-function is positive. Thus a big crunch singularity ($F, \dot{H} \to -\infty$, $R \to 0$) might happen for certain values of initial conditions and parameters, or there exists no solution. A big rip singularity ($F, \dot{H} \to \infty$, $R \to 0$) does not exist because it is not compatible with $R \to \infty$.

For negative q_1 we get the condition

$$W_u\left(\frac{2q_3}{q_1}e^{2/q_1}\right) > -1,$$

which means that only the solution with $u = 0$ is stable. This renders the final event horizon radius $R_\mathrm{e} = R_0 x$ unique.

Finally, we take a closer look at the ratio R_e/R_0 as a function of the mass parameter q_1. For initial values $R_0 < 1/(H_0\sqrt{\Omega_{\Lambda 0}})$, which means $q_3 > 1$, there is a certain range of values of q_1 where no solutions for R_e exist. This range is again given by the requirement that the argument of the W-function must be greater than or equal to $-e^{-1}$, leading to the conditions

$$q_1 \leq \frac{2}{W_0(-\frac{1}{eq_3})} \quad \text{or} \quad q_1 \geq \frac{2}{W_{-1}(-\frac{1}{eq_3})}. \tag{2.28}$$

In Fig. 2.6 the exclusion range for q_1 is obvious for $q_3 > 1$. In the case that q_1 lies above this range, the unstable solution for R_e is reached first during the future cosmic evolution. For q_1 below this range, the stable solution is nearer to the initial value R_0 than the unstable one, however, both solutions for R_e lie below R_0. Initial values $R_0 > 1/(H_0\sqrt{\Omega_{\Lambda 0}})$ (i.e. $q_3 < 1$) lead to stable final states with $R_\mathrm{e} > R_0$ for all negative values of q_1. Moreover, all stable de Sitter solutions are realised except the last one corresponding to the parameter region

$$R_0^2 H_0^2 \Omega_{\Lambda 0} < 1, \quad q_1 > \frac{2}{W_0[-1/(e^1 q_3)]}.$$

Numerical solutions show that in this last case the universe will end in a big rip singularity, where $F, \dot{H} \to \infty$ and $R \to 0$. A big crunch ($F \to -\infty$) is not possible for negative q_1 because it contradicts $R \to 0$. This can also be seen from the time-derivative of the function K_0F given by

$$K_0\dot{F} = q_1\frac{\dot{R}}{R} = q_1\left(H - \frac{1}{R}\right), \quad q_1 < 0.$$

This becomes positive for $H < 0$ (big crunch), thus preventing a further decrease of K_0F and the final collapse of the scale factor.

More on the numerical solutions of this case can be found in Sec. 2.6 and Ref. [33], where additionally the running of Newton's constant is taken into account.

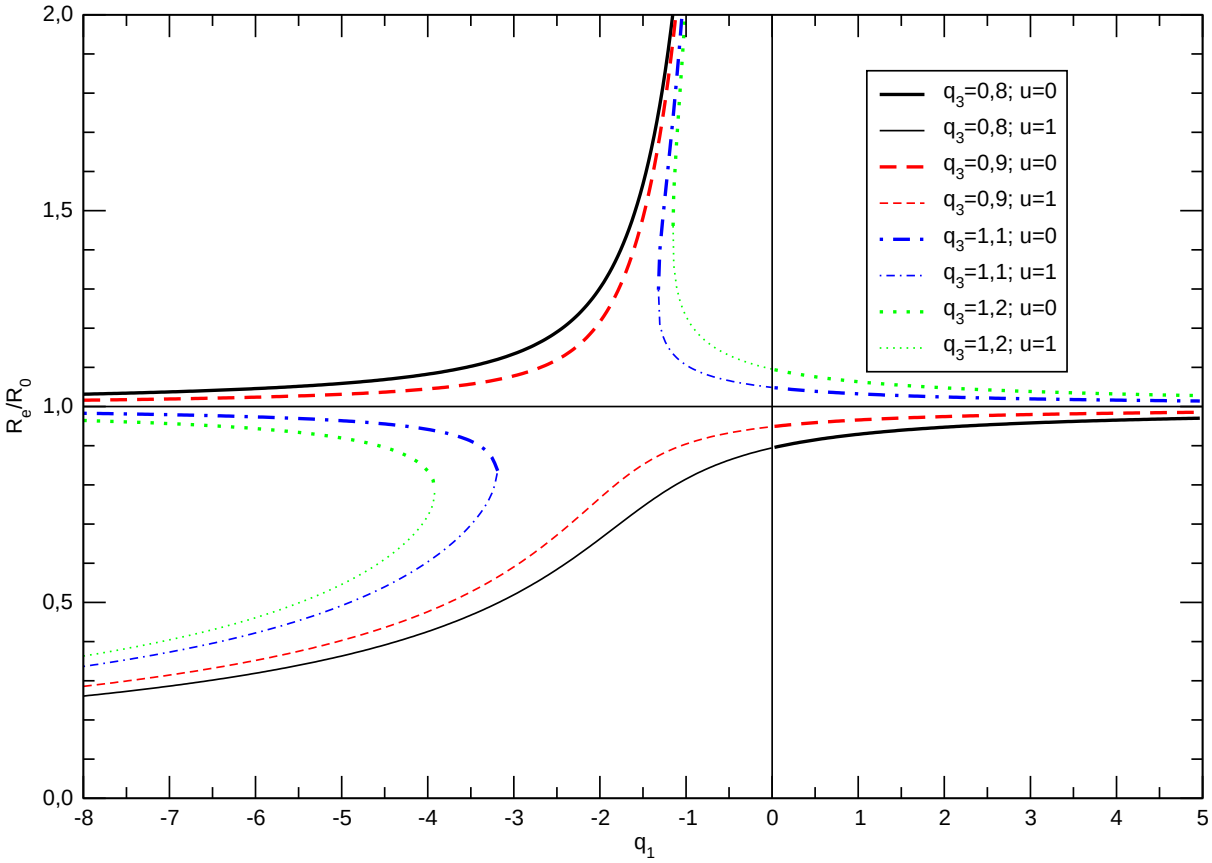

Figure 2.6: This figure shows the ratio R_e/R_0 from Eq. (2.25) between the final and the initial event horizon radius as a function of q_1. We plotted four cases for different values of $q_3 = 1/(H_0^2 R_0^2 \Omega_{\Lambda 0})$, where the choice $q_3 = 0,8;\, 0,9$ corresponds to an initial radius $R_0 > 1/(H_0\sqrt{\Omega_{\Lambda 0}})$, and $q_3 = 1,1;\, 1,2$ to $R_0 < 1/(H_0\sqrt{\Omega_{\Lambda 0}})$. In the latter case there are no solutions for a certain range of values of q_1 as described by Eq. (2.28). The thick lines show the $(u = 0)$-branch of R_e/R_0, and the thin lines the $(u = -1)$-branch, respectively.

2.5.5 $\Lambda = \Lambda_0(L_0 + L_1 \frac{\mu^2}{\mu_0^2})$, $\mu = R^{-1}$

In the de Sitter limit, $\dot{H} = 0$ and $R \to R_\mathrm{e} = H_\mathrm{e}^{-1}$, we find here the solution

$$R_\mathrm{e}^2 = (H_0^{-2}\Omega_{\Lambda 0}^{-1} - L_1 R_0^2)/L_0,$$

but it is unstable for all possible values of L_1, which follows from

$$\left.\frac{\mathrm{d}(K_0\dot{F})}{\mathrm{d}(K_0 F)}\right|_{\mathrm{dS}} = R_\mathrm{e} H_0^2 L_0 \Omega_{\Lambda 0} > 0.$$

For $L_1 < 0$ our numerical calculations did not yield any solution that is compatible with Eqs. (2.12) and (2.20). This is also true in a certain parameter range for $L_1 > 0$, where otherwise a Big Rip singularity occurs, where $F, \dot{H} \to \infty$ and $R \to 0$, see Fig. 2.7. A big crunch is not possible since $K_0 F$ is bounded from below.

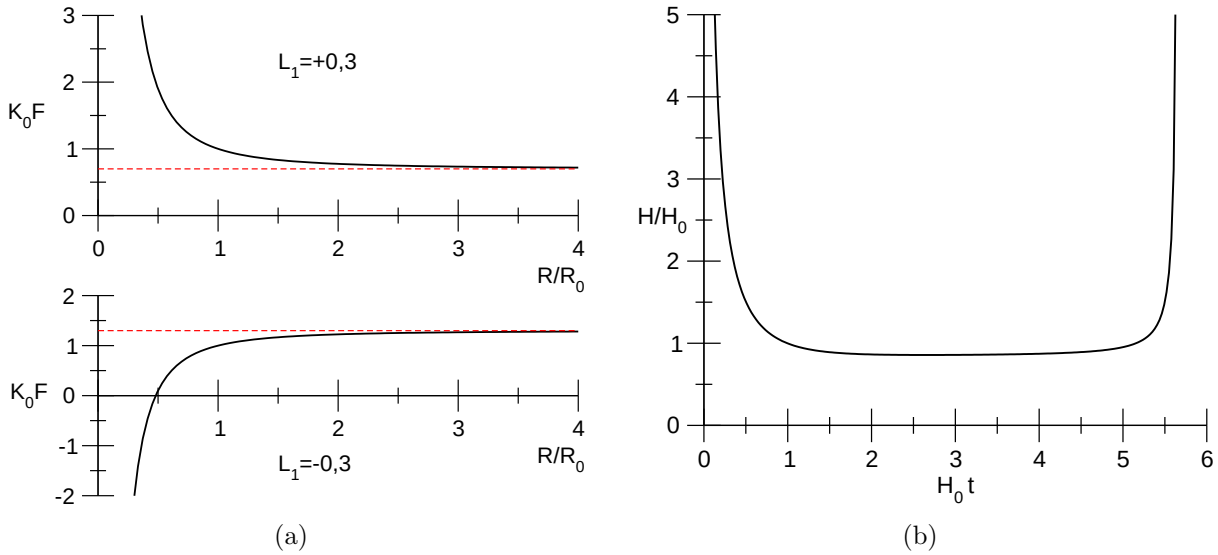

Figure 2.7: Corresponding to Sec. 2.5.5 we plot (a) the function $K_0F = L_0 + L_1\frac{R_0^2}{R^2}$ for $L_1 = \pm 0,3$ and (b) the Hubble scale $H(t)$ for $L_1 = +0,1$; $R_0 = 1,1$; $\Omega_{\Lambda 0} = 0,73$ and $Q = \frac{1}{2}$ (dust), where a big rip singularity occurs.

2.5.6 $\Lambda G = \Lambda_0 G_0 \frac{\mu^2}{\mu_0^2}$, $\mu = R^{-1}$

Here, one cannot find a prediction for R_e in the de Sitter limit ($\dot{H} = 0$, $R \to R_\mathrm{e} = H_\mathrm{e}^{-1}$) since Eq. (2.20) only leads to the constraint $R_0^2 = 1/(H_0^2\Omega_{\Lambda 0})$. To find solutions corresponding to other values of R_0 we impose the ansatz $a(t) = a_0(t-t_1)^n$ with $a_0, n, t_1 =$ const. The Hubble scale is given by $H = n(t-t_1)^{-1}$ which implies due to $H_0 > 0$ that $t_1 < t$ for $n > 0$ and $t_1 > t$ for $n < 0$, respectively. For $0 < n < 1$ the event horizon does not exist, in the other cases R can be calculated exactly via Eq. (2.12):

$$R(t) = a(t)\int_t^{t_\mathrm{E}} \frac{\mathrm{d}t'}{a(t')} = (t-t_1)^n \cdot \frac{(t_\mathrm{E}-t_1)^{(1-n)} - (t-t_1)^{(1-n)}}{1-n}.$$

Note that for negative n there is a big rip singularity at $t \to t_1$, where $a(t)$ diverges and the universe ends: $t_\mathrm{E} = t_1$. For $n > 1$ the scale factor $a(t)$ describes power-law acceleration and there is no future singularity which means $t_\mathrm{E} \to \infty$. As a result, both cases yield

$$R(t) = \frac{(t-t_1)}{n-1}.$$

Thus Eq. (2.20) can be solved exactly, which determines the constant n, see Fig. 2.8:

$$n_{1,2}(x) = \frac{(x-\frac{1}{2}) \pm \sqrt{(x-\frac{1}{2})^2 - x(x-(Q+1))}}{x-(Q+1)} \tag{2.29}$$

$$\text{with } x := \frac{R_0^2}{K_0} = R_0^2 H_0^2 \Omega_{\Lambda 0}(Q+1). \tag{2.30}$$

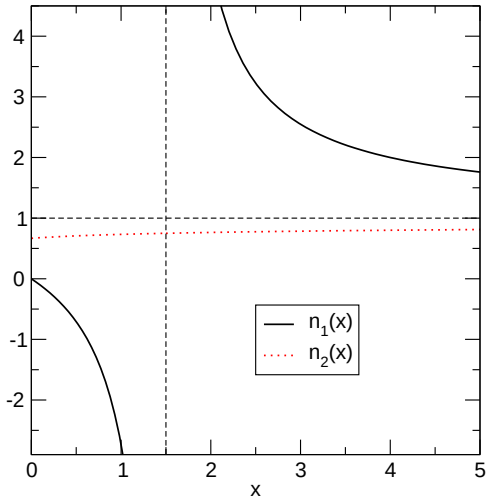

Figure 2.8: The exponents $n_{1,2}(x)$ from Eq. (2.29), which occur in the power-law expansion scale factor $a(t) = a_0(t - t_1)^n$, are shown. In Sec. 2.5.6 we find $n = n_1(R_0^2/K_0)$, whereas $n = n_2(T_0^2/K_0)$ in Sec. 2.5.9.

For $Q > 0$ we find $(Q + 1)^{-1} < n_2 < 1$ for all positive values of x, therefore n_2 can be dropped as the event horizon does not exist. In the case $R_0^2 < 1/(H_0^2\Omega_{\Lambda 0})$ the constant $n = n_1$ is negative leading to a big rip singularity at the time $t = t_1$, and $R_0^2 > 1/(H_0^2\Omega_{\Lambda 0})$ implies a positive n corresponding to power-law acceleration.

2.5.7 $\Lambda = \Lambda_0(1 - q_1 \ln \frac{\mu}{\mu_0})$, $\mu = T^{-1}$

Solving Eq. (2.20) for this choice of Λ and μ can be done approximately. First we propose the ansatz

$$a(t) = a_0 \exp[u^2(t - t_1)^2] \tag{2.31}$$

for the scale factor with the constants a_0, u and t_1. Therefore

$$H = 2u^2(t - t_1), \quad \frac{\ddot{a}}{a} = 4u^4(t - t_1)^2 + 2u^2, \quad F = 2u^2 + 4u^4(Q + 1)(t - t_1)^2,$$

and the particle horizon radius at late times reads

$$\begin{aligned} T &= \exp(u^2(t - t_1)^2) \int_{t_x}^{t} \exp(-u^2(t' - t_1)^2)\mathrm{d}t', \quad t > t_x = \text{const.} \\ &= \exp(u^2(t - t_1)^2) \cdot \left[\frac{\sqrt{\pi}}{2u} \mathrm{erf}(u(t - t_1)) \right]_{t_x}^{t}. \end{aligned}$$

For $t \to \infty$ the series expansion of the square brackets reads $C + \mathcal{O}(t^{-1})$ with $C > 0$ and thus $T \approx C \exp(u^2(t - t_1)^2)$. In this limit the given ansatz for $a(t)$ solves $K_0 F = 1 - q_1 \ln \frac{T_0}{T}$ exactly and determines the constant $u^2 = \frac{1}{4} q_1 H_0^2 \Omega_{\Lambda 0}$. Therefore we have found that Eq. (2.31) represents an approximate late-time solution in the case $q_1 > 0$, which we call super-exponential accelerated expansion.

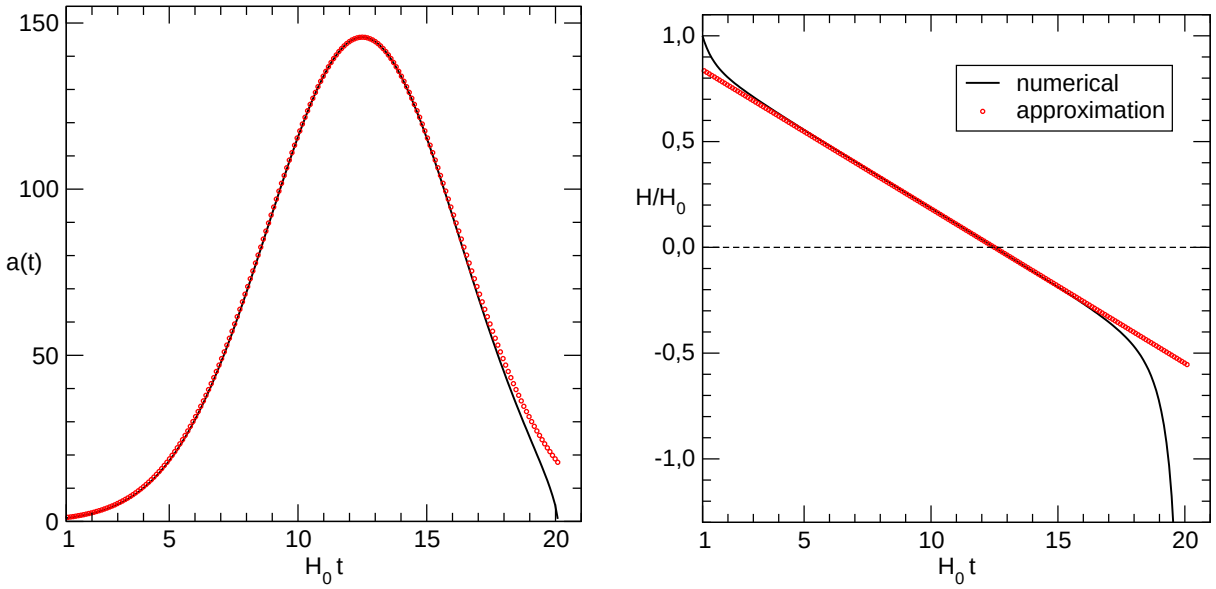

Figure 2.9: Here, the numerical and the approximate solutions for the scale factor $a(t)$ and the Hubble scale $H(t)$ from Sec. 2.5.7 are shown for negative $q_1 = -0,2$. Furthermore, we have used $\Omega_{\Lambda 0} = 0,73$; $T_0 H_0 = 3$ and $Q = \frac{1}{2}$ (dust). In this case a big crunch singularity will occur in the future. Note that the analytical approximation from Eq. (2.32) works very well except near the future singularity.

The numerical solutions in the case $q_1 < 0$ exhibits a future big crunch singularity. However, at times sufficiently before this event the scale factor can be well approximated by the ansatz

$$a(t) = a_0 \exp[-u^2(t - t_1)^2], \tag{2.32}$$

which implies $F = -2u^2 + 4u^4(Q + 1)(t - t_1)^2$ and

$$T = \exp(-u^2(t - t_1)^2) \cdot \left[\frac{\sqrt{\pi}}{2iu}\mathrm{erf}(iu(t - t_1))\right]_{t_x}^{t}, \quad t > t_x = \text{const.}$$

We expand the square bracket term around $t \to t_1$, where the scale factor is maximal, and find $T \approx C \exp(-u^2(t - t_1)^2)$ with $C > 0$. Solving $K_0 F = 1 - q_1 \ln \frac{T_0}{T}$ leads to $u^2 = -\frac{1}{4} q_1 H_0^2 \Omega_{\Lambda 0}$ in accordance with $q_1 < 0$. The numerical and approximate solutions are shown in Fig. 2.9.

2.5.8 $\Lambda = \Lambda_0(L_0 + L_1 \frac{\mu^2}{\mu_0^2})$, $\mu = T^{-1}$

In the late-time de Sitter limit, $a(t) \propto \exp(H_e t)$, the particle horizon radius has the asymptotic form

$$T \propto \exp(H_e t) \to \infty \quad \text{for} \quad t \to \infty,$$

which follows from Eq. (2.14). This means that $K_0F \to L_0$ and thus determines $H_\mathrm{e}^2 = H_0^2\Omega_{\Lambda 0}L_0$. To verify the stability of this solution we calculate

$$K_0\dot{F} = -2L_1\frac{\dot{T}}{T}\cdot\frac{T_0^2}{T^2} = -2L_1\frac{T_0^2}{T^2}\left(H+\frac{1}{T}\right).$$

At the initial time (today) $K_0\dot{F}$ is negative for $L_1 > 0$ and K_0F keeps on approaching the de Sitter limit unless a sign change in $K_0\dot{F}$ would occur. But this requires a negative H, which is only possible if $K_0F = \dot{H} + (Q+1)H^2 < 0$ at some time. Since $K_0F \geq L_0 > 0$ we conclude that the de Sitter limit will be reached always. For $L_1 < 0$ the initial values of K_0F and $K_0\dot{F}$ are positive and K_0F approaches the de Sitter limit. Again, a sign change in $K_0\dot{F}$ is only possible for $H < 0$, which requires $K_0F < 0$ at some time. These conditions cannot be realised because $K_0F > 0$ as long as $K_0\dot{F} > 0$. In summary all reasonable values of L_1 lead to a stable de Sitter final state.

2.5.9 $\Lambda G = \Lambda_0 G_0 \frac{\mu^2}{\mu_0^2}$, $\mu = T^{-1}$

By using at late times the power-law ansatz $a(t) = a_0(t-t_1)^n$ with $a_0, t, n = \text{const.}$, we find

$$F = (n^2(Q+1) - n)(t-t_1)^{-2},$$

and the particle horizon radius is given by

$$T = a_0(t-t_1)^n\left[\int_0^{t_0}\frac{\mathrm{d}t'}{a(t')} + \int_{t_0}^{t}\frac{\mathrm{d}t'}{a(t')}\right] = \frac{t-t_1}{1-n} + (t-t_1)^n\left[T_0 - \frac{(t_0-t_1)^{1-n}}{1-n}\right], \quad (2.33)$$

where $T_0 = T(t_0) > 0$ depends on the past evolution of the scale factor. In the case $n < 0$ a positive Hubble scale $H = n(t-t_1)^{-1}$ requires $t, t_0 < t_1$, which implies $T < 0$ and thus the non-existence of the particle horizon. For $0 < n < 1$ the second term in Eq. (2.33) can be neglected at late times, and Eq. (2.20) can be solved exactly, leading to

$$\begin{aligned} n_{1,2}(x) &= \frac{(x-\frac{1}{2}) \pm \sqrt{(x-\frac{1}{2})^2 - x(x-(Q+1))}}{x-(Q+1)} \\ \text{with } x &:= \frac{T_0^2}{K_0} = T_0^2H_0^2\Omega_{\Lambda 0}(Q+1). \end{aligned}$$

This is the same equation as in Sec. 2.5.6 with R_0 replaced by T_0, see also Fig. 2.8. Here, solution n_2 is the physical one because of $(Q+1)^{-1} < n_2 < 1$, that corresponds to a decelerating universe for $t \to \infty$. In comparison with Sec. 2.5.6 the identification of the particle horizon radius as renormalisation scale yields a complementary cosmological behaviour.

2.6 Time-dependent Cosmological and Newton's Constant

In the previous sections we have discussed only the running of the CC except for the scaling laws (2.8), where the change of Newton's constant is comparable with that of the CC. For the scaling law (2.3) we have required that the mass parameter q_1 is small in order to obtain a viable phenomenology. Since the largest known field masses are of the order of $10^2\,\mathrm{GeV}$ we had to assume fine-tuning or some unknown suppression mechanism to achieve the smallness of q_1. What happens to Newton's constant when it is controlled by the RGE (2.5)? As we can see from Eq. (2.6), the corresponding mass parameter q_2 is of the order $m^2 G_0 = m^2/M_{\mathrm{Pl}}^2$ and therefore strongly suppressed by the Planck mass M_{Pl} even for larger masses m. Obviously, the running of G is suppressed from the beginning, which agrees with the strong bounds on the time-variation of G, see, e.g., Ref. [47]. Additionally, this property has the advantage, that today we are far away from the Landau pole of $G(\mu)$, where the function F diverges in Eq. (2.20). Since the RGE for G follows directly from the effective action (2.2), we are interested in its influence on the cosmological evolution.

As an example we will discuss the combination of the RGEs (2.3) for the CC and (2.5) for G that were both derived from the effective action (2.2). As renormalisation scale μ we use, according to Eq. (2.12), the inverse of the cosmological event horizon, $\mu = R^{-1}$. With these preliminaries Eq. (2.20) reads

$$K_0 F = \frac{1 + q_1 \ln \frac{R}{R_0}}{1 + q_2 \ln \frac{R}{R_0}}, \tag{2.34}$$

leading to the ordinary differential equation (2.22) for the scale factor $a(t)$. Unfortunately, finding explicit solutions of this equation seems to be rather difficult because of the strongly non-linear form of the equation. Therefore, we solve it numerically to show the characteristic future cosmic evolution corresponding to four different cases, which result from the parameter choices $q_1 = \pm 2$ and $q_2 = \pm 0, 1$. These values for q_1 mean that the relevant mass scale m should be near $\Lambda_0^{1/4} \sim 10^{-3}\,\mathrm{eV}$. Actually, the only known particles with such a low mass are neutrinos. This indicates that the influence of higher mass fields is suppressed, or these fields have decoupled, respectively. Note that due to the suppression by the Planck scale, the realistic value of q_2 should be much lower than $\pm 0, 1$. Here, we used a large value for q_2 just to explore the differences due to the sign of q_2. Concerning the differential equation, we fix the initial conditions by using observational results, i.e., the relative vacuum energy density is given by $\Omega_{\Lambda 0} = 0,73$, no spatial curvature ($\Omega_k = 0$) and only dust (with an equation of state parameter $Q = 0,5$) and the CC as relevant energy forms in the present-day universe. The acceleration parameter $q_0 = \frac{\ddot{a}a}{\dot{a}^2}(t_0)$ is determined by Eq. (2.18): $q = \Omega_\Lambda(1+Q)+Q(\Omega_k-1)$. Today's value of the horizon radius R_0 is unknown, so we have to estimate it. Since it should be the largest physical length scale and the universe seems to be almost de Sitter-like, we assume the horizon radius to be a bit larger than the inverse Hubble scale, $R_0 \gtrsim H_0^{-1}$. Finally, all dimensionful quantities are expressed in terms of today's Hubble scale H_0 (Hubble units). Figures 2.10–2.13 show the numerical results for different values of the initial radius R_0 of the event horizon. The

graphs in each of the four figures illustrate the scale factor $a(t)$, the Hubble scale $H(t)$, the acceleration $q(t)$, the event horizon radius $R(t)$, and $F(t)$ as functions of the cosmic time t, respectively. The last graph displays Eq. (2.34), i.e., K_0F as a function of the radius R/R_0.

The first observation from the numerical solutions is, that for a positive value of q_1 the cosmic age decreases with respect to the age t_0 of the standard ΛCDM universe, whereas for a negative q_1 the age increases. In the latter case, we observe only big rip solutions and de Sitter final states. However, for positive q_1 a big crunch may also occur, but no stable de Sitter states exist. For positive values of q_1 and q_2 (see Fig. 2.13), we have not observed any big rip solutions. Hence, the final state may be either a big crunch or a forever expanding universe, where the Hubble scale approaches a finite positive value, but the event horizon radius R goes to infinity. This is a contradiction, because an asymptotically constant Hubble scale $H > 0$ implies a finite event horizon radius $R \approx H^{-1}$ in the far future, which is not the case here. Obviously, this numerical solution is not a solution of the original equation (2.20). For $q_1 > 0$ and $q_2 < 0$ (see Fig. 2.12) the big rip events in the numerical solutions occur at a finite and large value of the horizon radius R. Again, this behaviour is not compatible with the vanishing of the horizon radius at such an event. Therefore, we can reject these numerical solutions, too. For positive q_1 we thus observe that if a solution exists it has to be a big crunch.

In summary, we conclude that the cosmological final states occurring in the numerical solutions in this section do not differ from the case with constant G, discussed in Sec. 2.5.4.

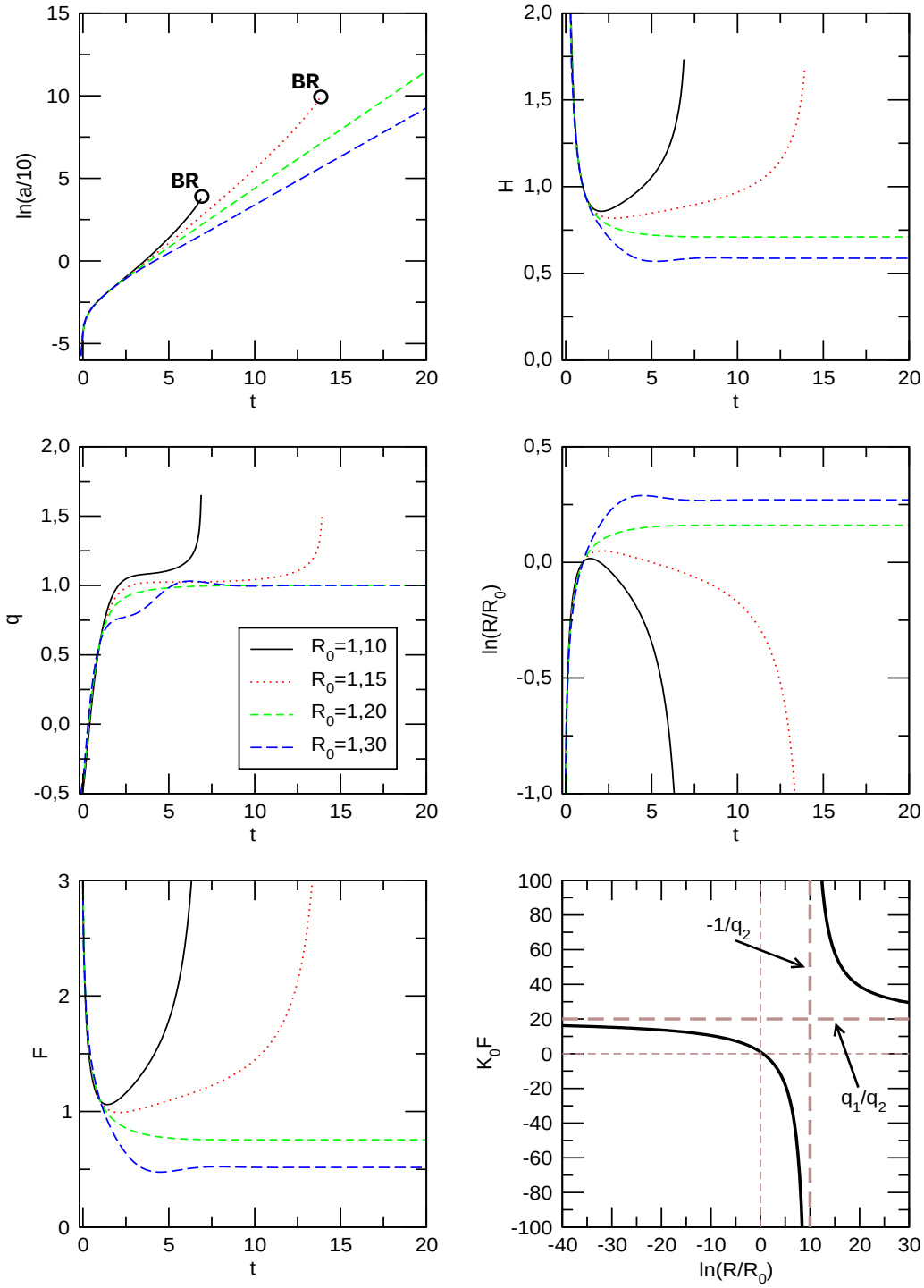

Figure 2.10: The cosmological evolution for the parameter choice $q_1 = -2$ and $q_2 = -0,1$ and different values of the initial event horizon radius R_0. The fate of this universe is either a stable de Sitter state when choosing $R_0 = 1,20;\ 1,30$, or a big rip (BR) in the case $R_0 = 1,10;\ 1,15$. K_0F is bounded from above. Nomenclature: Scale factor a, Hubble scale $H = \frac{\dot{a}}{a}$, acceleration $q = \frac{\ddot{a}a}{\dot{a}^2}$, event horizon radius R and its initial value R_0. For the function K_0F see Eqs. (2.34), and (2.19), for the mass parameters q_1, q_2 see Eqs. (2.4) and (2.6).

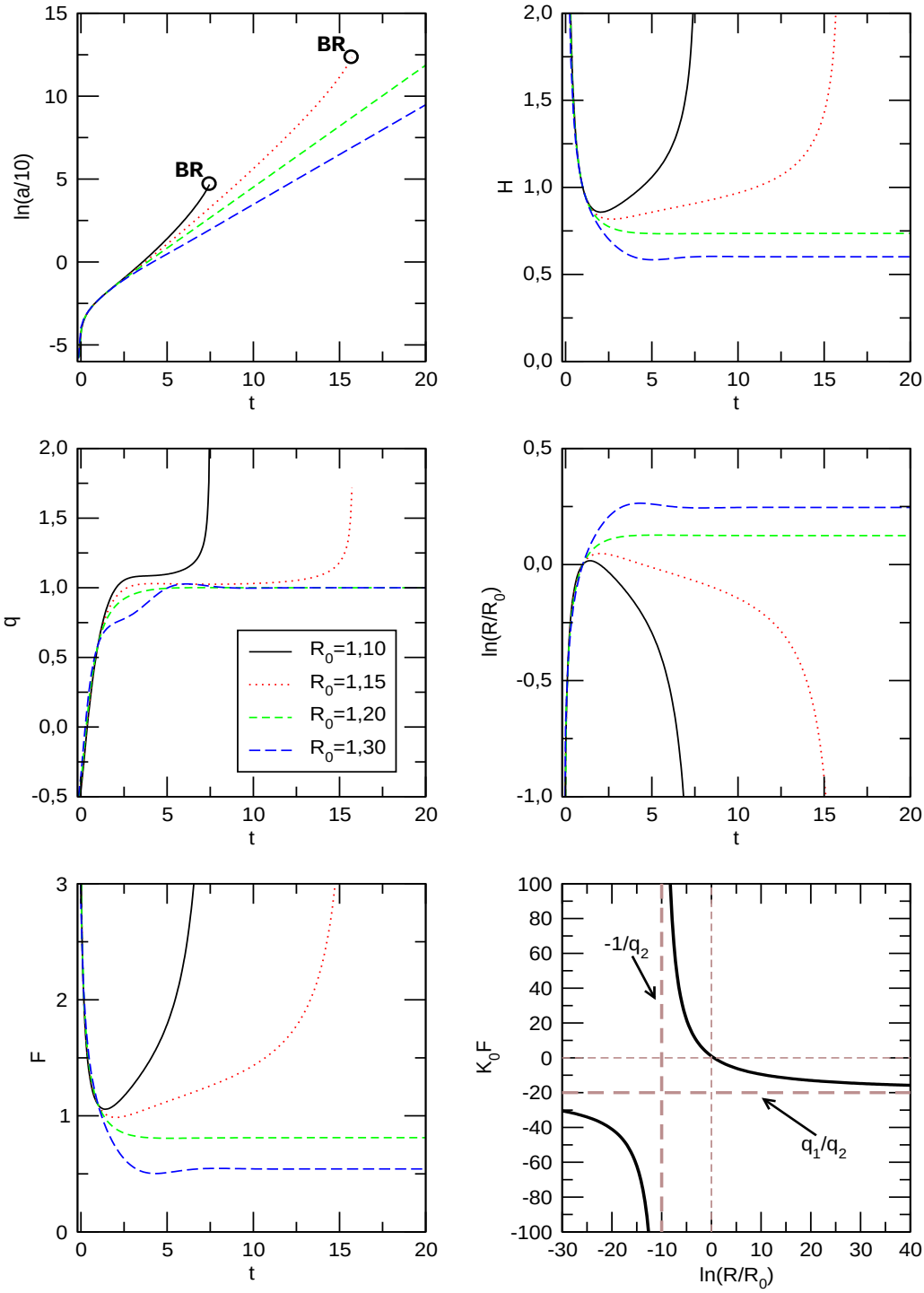

Figure 2.11: For the parameter choice $q_1 = -2$ and $q_2 = +0,1$ the cosmic evolution is not very different from the case $q_2 = -0,1$ (Fig. 2.10). In the future, there is either a stable de Sitter state for $R_0 = 1,20;\ 1,30$, or a big rip (BR) when $R_0 = 1,10;\ 1,15$. K_0F is bounded from below. Nomenclature: Scale factor a, Hubble scale $H = \frac{\dot{a}}{a}$, acceleration $q = \frac{\ddot{a}a}{\dot{a}^2}$, event horizon radius R and its initial value R_0. For the function K_0F see Eqs. (2.34) and (2.19), for the mass parameters q_1, q_2 see Eqs. (2.4) and (2.6).

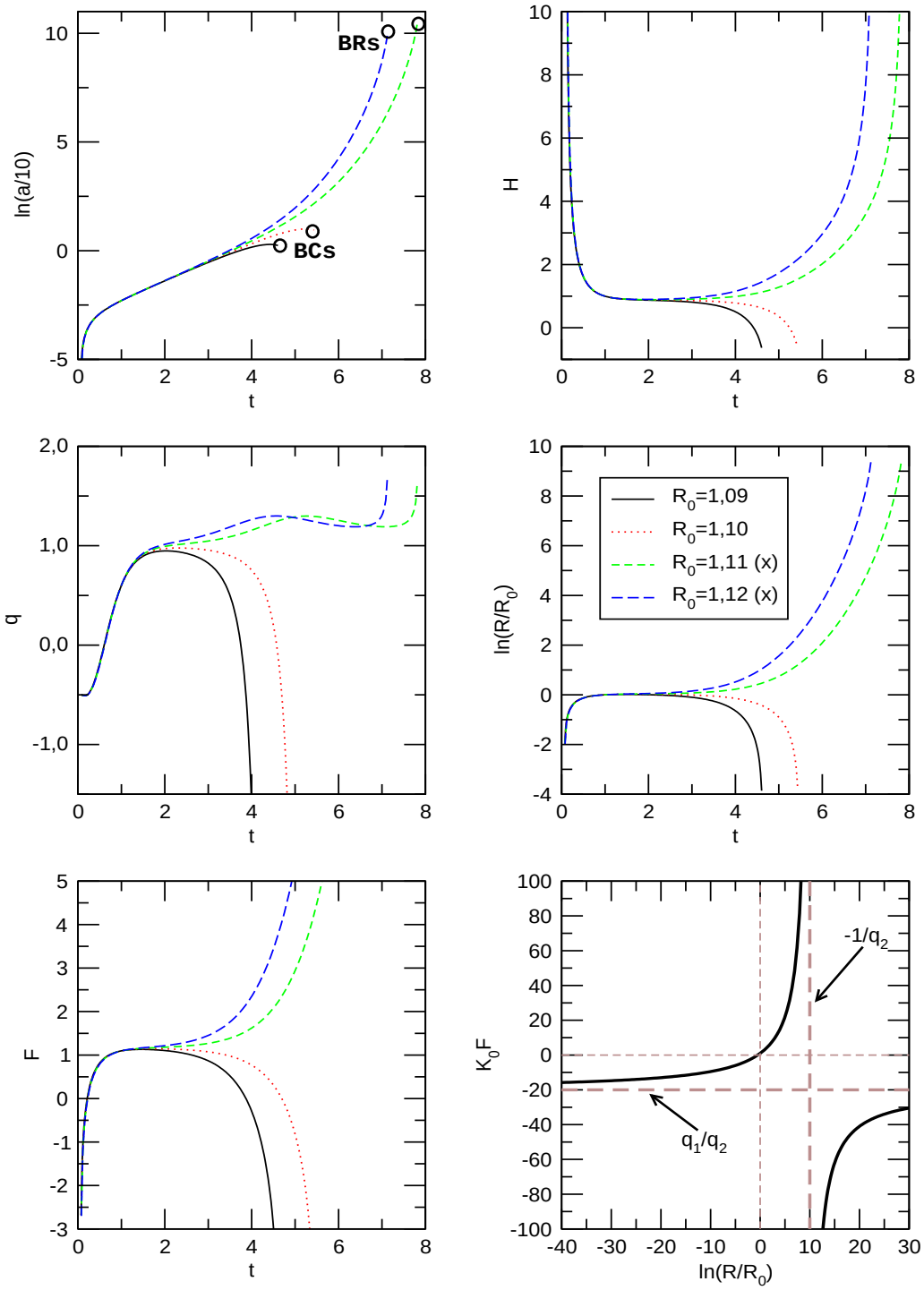

Figure 2.12: The cosmological evolution for different values of today's horizon radius R_0 for the case $q_1 = +2$ and $q_2 = -0,1$. The solutions for $R_0 = 1,09;\ 1,10$ exhibit a big crunch (BC), whereas the initial conditions $R_0 = 1,11;\ 1,10$ lead to a big rip (BR). K_0F is bounded from below. The numerical solutions marked by (x) are not compatible with the main equation (2.34), see Secs. 2.5 and 2.6 for further details. Nomenclature: Scale factor a, Hubble scale $H = \frac{\dot{a}}{a}$, acceleration $q = \frac{\ddot{a}a}{\dot{a}^2}$, event horizon radius R and its initial value R_0. For the function K_0F see Eqs. (2.34) and (2.19), for the mass parameters q_1, q_2 see Eqs. (2.4) and (2.6).

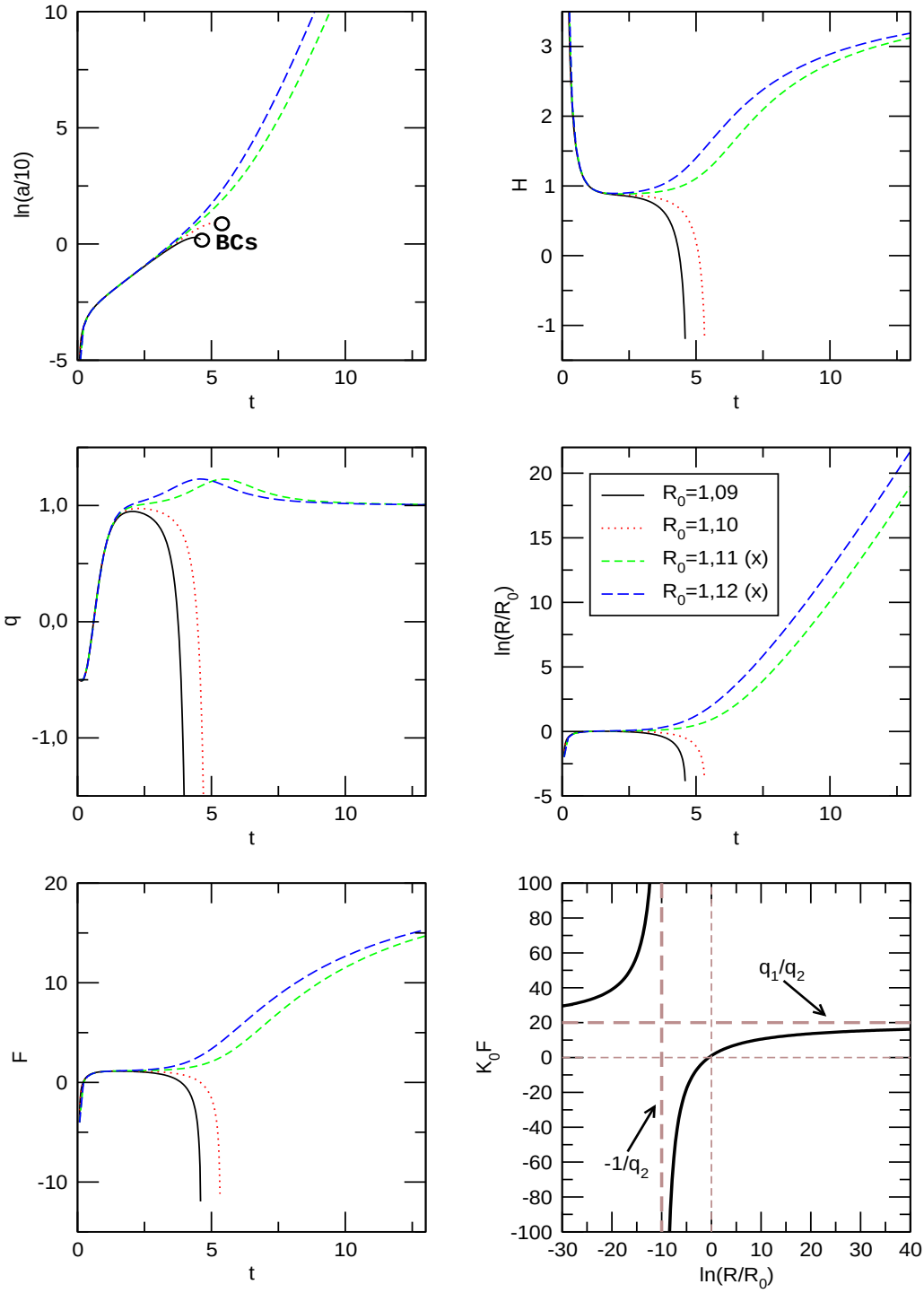

Figure 2.13: The cosmological evolution for different values of today's horizon radius R_0. Here, we choose $q_1 = +2$ and $q_2 = +0,1$. The solutions for $R_0 = 1,09;\ 1,10$ exhibit a big crunch (BC), where K_0F is unbounded from below. For the initial conditions $R_0 = 1,11;\ 1,10$ the function F and the Hubble scale H approach a finite value, where the horizon radius R diverges. The numerical solutions marked by (x) are not compatible with the main equation (2.34), see Secs. 2.5 and 2.6 for further details. Nomenclature: Scale factor a, Hubble scale $H = \frac{\dot{a}}{a}$, acceleration $q = \frac{\ddot{a}a}{\dot{a}^2}$, event horizon radius R and its initial value R_0. For the function K_0F see Eqs. (2.34) and (2.19), for the mass parameters q_1, q_2 see Eqs. (2.4) and (2.6).

	$\Lambda = \Lambda_0(1 - q_1 \ln \frac{\mu}{\mu_0})$	$\Lambda = \Lambda_0(L_0 + L_1 \frac{\mu^2}{\mu_0^2})$	$\Lambda G = \Lambda_0 G_0 \frac{\mu^2}{\mu_0^2}$
$\mu = H$	dS, BC	dS	P
$\mu = R^{-1}$	dS, BR, BC	BR	P, BR
$\mu = T^{-1}$	$\exp(\pm t^2)$, BC	dS	P

Table 2.1: This table shows all types of cosmological final states that we have found in Sec. 2.5 for the all combinations of scaling laws for the CC Λ (and G for the third law) from Sec. 2.2 and the choices for the renormalisation scale μ of Sec. 2.3. Here, dS denotes de Sitter solutions, P power-law solutions, BR big rip and BC big crunch future singularities, respectively. With $\exp(\pm t^2)$ we mean the late-time behaviour of the scale factor, where $a \propto \exp(-t^2)$ finally leads to a big crunch.

2.7 Summary

Before we summarise the cosmological final states that we have found in the previous sections, we have to mention that not all of the solutions are likely to be realised even if the underlying assumptions were correct. This is especially important for the extreme solutions that exhibit future singularities. For these cases the strength of the gravitational field becomes so large that other effects, e.g., higher orders in the curvature scalar or unknown quantum gravity effects, cannot be neglected anymore. Also matter sources like radiation would become again dominant over dust matter in big crunch scenarios. Therefore, it is possible that these cosmological final states are replaced by other solutions. For instance, the avoidance of a big rip in phantom cosmologies by such effects has been discussed in Refs. [48]. On the other hand, in Ref. [49] one has an example, where quantum effects were not able to prevent a big rip.

Nevertheless, we stay in this analysis on the basic level and use the results we found as an indicator for the (in)stability of the cosmological fate. Indeed, we have found regular solutions in many cases, which can be considered as realisable in nature. In this sense, we have found de Sitter solutions in the cases of Secs. 2.5.1, 2.5.2, 2.5.4 and 2.5.8. Also accelerating and decelerating power-law solutions for the scale factor can be called regular, we have found them for all cases with the scaling law (2.8) in Secs. 2.5.3, 2.5.6 and 2.5.9. Moreover, we have found in Sec. 2.5.7 a super-exponential expansion law of the type $a(t) \sim \exp(ct^2)$, which however implies negative values of the matter energy density. Future singularities of the big rip type are found for all cases with the event horizon as renormalisation scale, see Secs. 2.5.4, 2.5.5 and 2.5.6. Big crunch solutions, on the other hand, occur only for the scaling law (2.3) as described in Secs. 2.5.1, 2.5.4 and 2.5.7. In Sec. 2.6 we have finally analysed numerically the effect of a running Newton's constant G, but we did not observe any changes in the cosmological fates in comparison to the cases with constant G. To finish this chapter we give a comprehensive overview of our results in Tab. 2.1.

3 Vacuum Energy in Extra Dimensions

3.1 Introduction

With this chapter we start to investigate the occurrence of dark energy in models, where space-time has some non-trivial properties. One of the most famous approaches for space-time modifications represents the introduction of extra spatial dimensions. With the concept of Kaluza-Klein (KK) compactification [50] one has found a framework to unite gravity with electrodynamics. Decades later EDs are still a popular way to obtain 4D theories from a simpler higher-dimensional setup [51]. In this approach, the 4D theory which emerges after dimensional reduction is generally characterised by a tower of KK modes [52]. Also in string theories EDs are a crucial ingredient [53] and are needed for consistency reasons. Therefore EDs have become a common component for modern model-building.

Another interesting aspect of compactified EDs is, that quantum fields in such a non-trivial space-time give rise to the Casimir effect [23]. In this scenario the bulk fields have to obey certain boundary conditions thereby inducing a finite Casimir energy density, which depends on the size and the topology of the EDs. The associated Casimir force can be attractive and contract the compactified EDs to a size which is sufficiently small so as to have escaped experimental detection so far [24, 54, 55]. Upon integrating out the EDs, the Casimir energies have additionally the interesting property that they appear as an effective CC Λ or vacuum energy in the 4D subspace. In the following chapters we will focus mainly on this last point since the Casimir contributions to the vacuum energy budget must be smaller than the observed value of the CC in order to avoid fine-tuning. One can imagine that this requirement leads to stringent bounds on the size of the ED. Later on in Chaps. 4 and 5 we will investigate the Casimir effect for discretised EDs and its applications in the context of deconstruction. To prepare for this task we will first discuss the calculation the Casimir energy density in the continuum. After that the results can be transferred easily to the discretised case.

3.2 The Casimir Effect

The Casimir effect is a notable exception from the normal ordering procedure in quantum field theories. It occurs when quantum fields have to obey certain boundary conditions, for instance the electric component of the photon field, restricted between two parallel conducting plates, has to vanish on the plates. This causes a geometry dependent vacuum

energy density inducing a force on the plates. Therefore, the Casimir effect is a macroscopic quantum phenomenon, which is experimentally well established [56]. For some recent reviews of the effect and its applications see Refs. [57, 58]. Global properties of a non-trivial space-time may also be probed by the Casimir effect which is sensitive to the IR structure of a theory.

Let us now consider the Casimir effect for a scalar field ϕ in a 5D theory, where the ED is compactified on the circle $\mathcal{S}^1$ with circumference R. Hence, the whole manifold has the topology $\mathcal{M} \times \mathcal{S}^1$, where $\mathcal{M}$ denotes Minkowski space. In order to find the possible field theory configurations we have to specify the boundary conditions for the scalar field on the circle. Motivated by periodicity one obvious choice is given by

$$\phi(y + R) = \phi(y), \tag{3.1}$$

where y is the coordinate in the fifth dimension. This choice implies a cylinder-like structure. But this not the only one. According to Ref. [59] one can also form a structure with the properties of a Möbius band, where ϕ obeys anti-periodic boundary conditions

$$\phi(y + mR) = (-1)^m \phi(y), \quad m \in \mathbb{Z}, \tag{3.2}$$

In this case one must cycle twice through the circle $\mathcal{S}^1$ to completely traverse the Möbius band. In the latter case, the field ϕ is called a twisted field, whereas the fields with periodic boundary conditions are called untwisted fields. Locally, both cases have the same product structure, but globally they differ significantly. Since they yield inequivalent degrees of freedom of the field ϕ, both must be considered in the Casimir effect.

Turning to the calculation of the Casimir energy, we call q the momentum corresponding to the position y in the extra-dimensional space. Since the 5D manifold is flat, it is sensible to use for the scalar field a plane wave ansatz given by

$$\phi(t, \vec{x}, y) = J \cdot \exp(i\omega t - i\vec{p}\vec{x} - iqy), \tag{3.3}$$

where J is a normalisation factor, ω the energy and $\vec{p}$ the 3-momentum corresponding to the time t and respectively the 3-coordinates $\vec{x}$. As discussed above, the untwisted field configuration is fixed by periodic boundary conditions,

$$\phi(y + R) = \phi(y) \quad \Longrightarrow \quad e^{-iqR} = 1,$$

implying a discrete momentum spectrum,

$$q = 2\pi \frac{n}{R}, \quad n \in \mathbb{Z}. \tag{3.4}$$

For twisted fields we have to use anti-periodic boundary conditions

$$\phi(y + mR) = (-1)^m \phi(y), \quad m \in \mathbb{Z} \quad \Longrightarrow \quad e^{-iqR} = -1,$$

which yield the discrete momentum spectrum

$$q = 2\pi \frac{(n - \frac{1}{2})}{R}, \quad n \in \mathbb{Z}. \tag{3.5}$$

Since this is the only difference which is relevant for the following calculations, we will work with untwisted fields and replace n by $n - 1/2$ when needed.

To normalise the field modes in Eq. (3.3), we define the following scalar product for two modes $\phi_{1,2}(\vec{p}, n)$ by

$$(\phi_1, \phi_2) := i \int \mathrm{d}^3x \int \mathrm{d}y \left(\phi_1^\dagger (\partial_t \phi_2) - (\partial_t \phi_1)^\dagger \phi_2 \right),$$

so that the normalisation factor J can be fixed by demanding the orthonormality relation

$$(\phi(\vec{p}, n), \phi(\vec{p}', n')) = -V_3^{-1} \delta^{(3)}(\vec{p} - \vec{p}') \delta_{nn'}, \tag{3.6}$$

where V_3 is an arbitrary 3-volume factor, which leaves the scalar product dimensionless. With the ansatz in Eq. (3.3), we find

$$J^\dagger J = \frac{1}{2\omega (2\pi)^3 V_3 R}, \tag{3.7}$$

where we have applied the relations

$$\int \mathrm{d}^3x \cdot \exp(i\vec{x}(\vec{p} - \vec{p}')) = (2\pi)^3 \delta^{(3)}(\vec{p} - \vec{p}') \quad \text{and} \quad \int_0^R \mathrm{d}y \, \exp(2\pi i y \frac{n - n'}{R}) = R \delta_{nn'}.$$

The equation of motion for the real 5D scalar field ϕ with a bulk mass M_s is given by the Klein-Gordon equation

$$\left[\frac{\partial^2}{\partial t^2} - \nabla^2 - \partial_5^\dagger \partial_5 + M_\mathrm{s}^2 \right] \phi = 0, \tag{3.8}$$

which determines the energy ω of a field mode with the momenta $\vec{p}$ and q:

$$\omega^2 = \vec{p}^2 + m^2.$$

Here we have introduced the squared effective 4D mass

$$m^2 := q^2 + M_\mathrm{s}^2.$$

Furthermore, we need the 5D energy-momentum tensor T_{AB} of the real scalar field ϕ to calculate the energy density and pressure of the field. It has the form [16]

$$T_{AB} = (\phi_{,A})^\dagger (\phi_{,B}) - \frac{1}{2} g_{AB} g^{CD} (\phi_{,C})^\dagger (\phi_{,D}) + \frac{1}{2} g_{AB} M_\mathrm{s}^2 \phi^\dagger \phi, \tag{3.9}$$

where $A, B, C, \ldots$ are 5D coordinate indices. Here, $A = 0$ is the time-like index, $A = 1, 2, 3$ are spatial indices, corresponding to the uncompactified 3-space, and $A = 5$ characterises the extra spatial dimension. The 5D energy density ρ_5 is then given by the 00-component of T_{AB}:

$$\rho_5 = T_{00} = \frac{1}{2} (\partial_0 \phi)^\dagger (\partial_0 \phi) + \frac{1}{2} (\nabla \phi)^\dagger (\nabla \phi) + \frac{1}{2} (\partial_5 \phi)^\dagger (\partial_5 \phi) + \frac{1}{2} M_\mathrm{s}^2 \phi^\dagger \phi. \tag{3.10}$$

By averaging over all directions of the isotropic 3-space, we obtain the pressure p_5 of the scalar field ϕ:

$$p_5 = \frac{1}{3}\sum_{i=1}^{3} T_{ii} = \frac{1}{3}\left[(\nabla\phi)^\dagger(\nabla\phi) + \frac{1}{2}(\partial_0\phi)^\dagger(\partial_0\phi) - \frac{1}{2}(\nabla\phi)^\dagger(\nabla\phi) - \frac{1}{2}(\partial_5\phi)^\dagger(\partial_5\phi) - \frac{1}{2}M_{\rm s}^2\phi^\dagger\phi\right]. \tag{3.11}$$

Let us now perform the canonical quantisation of the field ϕ by introducing the field operator

$$\hat{\phi}(t,\vec{x},y) = \sqrt{V_3}\int \mathrm{d}^3p \sum_{n=1}^{N}\left(\phi(\vec{p},n)a_{\vec{p},n} + \phi^\dagger(\vec{p},n)a^\dagger_{\vec{p},n}\right), \tag{3.12}$$

where $a_{p,n}$ and $a^\dagger_{p,n}$ obey bosonic commutator relations:

$$[a_{\vec{p},n}, a^\dagger_{\vec{p}',n'}] = V_3^{-1}\delta(\vec{p}-\vec{p}')\delta_{nn'}\,, \quad [a,a] = [a^\dagger,a^\dagger] = 0.$$

Now, the 00-component $\hat{T}_{00}$ and the averaged ii-components $\frac{1}{3}\sum_{i=1}^{3}\hat{T}_{ii}$ of the energy-momentum operator $\hat{T}_{AB}$ follow from substituting the field operator $\hat{\phi}$ in Eq. (3.12) into Eqs. (3.10) and (3.11). Here, it is useful to consider the relations

$$\begin{aligned}
(\partial_0\hat{\phi})^\dagger(\partial_0\hat{\phi}) &= V_3^2\int \mathrm{d}^3p\int d^3p' \sum_{n,n'=-\infty}^{\infty}\left[\partial_0\phi(\vec{p},n)a_{\vec{p},n}\cdot\partial_0\phi(\vec{p}',n')^\dagger a^\dagger_{\vec{p}',n'} + \cdots\right] \\
&= V_3\int \mathrm{d}^3p \sum_{n=-\infty}^{\infty} A^\dagger A\cdot\omega^2 + \cdots \\
(\partial_b\hat{\phi})^\dagger(\partial_b\hat{\phi}) &= V_3\int \mathrm{d}^3p \sum_{n=-\infty}^{\infty} A^\dagger A\cdot p_b^2 + \cdots \quad \forall\, b = 1,2,3 \\
(\partial_5\hat{\phi})^\dagger(\partial_5\hat{\phi}) &= V_3\int \mathrm{d}^3p \sum_{n=-\infty}^{\infty} A^\dagger A\cdot q^2 + \cdots,
\end{aligned} \tag{3.13}$$

where the ellipses $(\cdots)$ denote the terms which vanish in the VEVs $\langle 0|\,\hat{T}_{AB}\,|0\rangle$ due to $\langle 0|\,a^\dagger = a\,|0\rangle = 0$. When we insert the terms from Eqs. (3.13) into Eqs. (3.10) and (3.11), one obtains, after taking the VEVs of $\hat{T}_{00}$ and $\hat{T}_{ii}$, the energy density ρ_5 and the pressure p_5 of the quantised field ϕ,

$$\begin{aligned}
\rho_5 = \langle 0|\,\hat{T}_{00}\,|0\rangle &= V_3\int \mathrm{d}^3p \sum_{n=-\infty}^{\infty} J^\dagger J\cdot\left[\frac{1}{2}\omega^2 + \frac{1}{2}\vec{p}^{\,2} + \frac{1}{2}q^2 + \frac{1}{2}M_{\rm s}^2\right] \\
&= V_3\int \mathrm{d}^3p \sum_{n=-\infty}^{\infty} J^\dagger J\cdot\omega^2,
\end{aligned}$$

$$\begin{aligned}
p_5 = \frac{1}{3}\sum_{i=1}^{3}\langle 0|\,\hat{T}_{ii}\,|0\rangle &= V_3\int \mathrm{d}^3p \sum_{n=-\infty}^{\infty} J^\dagger J\cdot\left[\frac{1}{3}\vec{p}^{\,2} + \frac{1}{2}\omega^2 - \frac{1}{2}\vec{p}^{\,2} - \frac{1}{2}q^2 - \frac{1}{2}M_{\rm s}^2\right] \\
&= V_3\int \mathrm{d}^3p \sum_{n=-\infty}^{\infty} J^\dagger J\cdot\frac{\vec{p}^{\,2}}{3\omega},
\end{aligned}$$

where we have used the energy-momentum relation $\omega^2 = \vec{p}^2 + q^2 + M_s^2$. With the normalisation factor J from Eq. (3.7) we finally obtain the energy density ρ_5 and the pressure p_5 of the quantised 5D field ϕ,

$$\rho_5 = \langle 0| \hat{T}_{00} |0\rangle = \frac{1}{2(2\pi)^3 R} \int \mathrm{d}^3 p \sum_{n=-\infty}^{\infty} \omega, \tag{3.14}$$

$$p_5 = \frac{1}{3} \sum_{i=1}^{3} \langle 0| \hat{T}_{ii} |0\rangle = \frac{1}{2(2\pi)^3 R} \int \mathrm{d}^3 p \sum_{n=-\infty}^{\infty} \frac{\vec{p}^2}{3\omega}. \tag{3.15}$$

The momentum integral $\int \mathrm{d}^3 p = 4\pi \int_0^\infty \mathrm{d}p \cdot p^2$ in these equations and thus ρ_5 and p_5 are divergent. We therefore have to apply a regularisation procedure to obtain meaningful, finite expressions. Consider first Eq. (3.14). By introducing an exponential suppression factor $e^{-(dp)^2}$ as regulator function for $d > 0$, we find

$$\begin{aligned} \int \mathrm{d}p \cdot p^2 \omega &\longrightarrow \int_0^\infty \mathrm{d}p \cdot p^2 \omega e^{-(dp)^2} \\ &= \frac{1}{4} m^2 d^{-2} e^{\frac{1}{2}(dm)^2} K_1\left(\tfrac{1}{2} d^2 m^2\right) \\ &= \frac{1}{2} d^{-4} + \frac{1}{4} m^2 d^{-2} + \frac{1}{8} m^4 \left(\frac{1}{4} + \frac{1}{2}\gamma - \ln 2 + \ln(dm)\right) + \mathcal{O}(d^6 m^6), \end{aligned} \tag{3.16}$$

where $\omega = \sqrt{\vec{p}^2 + m^2}$ and $K_n(x)$ denotes the modified Bessel function of the second kind of the order n and $\gamma = 0,577\ldots$ is the Euler-Mascheroni constant. The limit $d \to 0$ removes the regulator and recovers the divergence. Before taking this limit, a renormalisation has to be carried out to remove the potentially divergent terms. Alternatively to the exponential regulator function in Eq. (3.16), one can also apply dimensional regularisation by moving to n space-time dimensions. To be specific,

$$\begin{aligned} \int \mathrm{d}^3 p \cdot \omega &\longrightarrow \mu^{(4-n)} S(n-1) \cdot \int_0^\infty \mathrm{d}p \cdot p^{(n-2)} \cdot \omega \\ &= -\frac{1}{2} m^4 \left(\frac{\mu}{m}\right)^{(4-n)} \pi^{(n/2-1)} \Gamma\left(-\frac{n}{2}\right) \\ &\overset{n\to 4}{=} (4\pi) \frac{1}{8} m^4 \left[(n-4)^{-1} + \frac{1}{2}\gamma + \ln\left(\frac{m}{\mu}\right) + \mathcal{O}(n-4)\right]_{n\to 4}, \end{aligned}$$

where the renormalisation scale μ has been introduced to keep the mass dimension of the whole term constant, and $S(n)$ is the surface area of an n-ball. The regularisation of the divergent integral in Eq. (3.15) with the exponential suppression factor with $d > 0$ goes along the same lines as above:

$$\begin{aligned} \int \mathrm{d}p \cdot p^2 \frac{p^2}{\omega} &\longrightarrow \int_0^\infty \mathrm{d}p \cdot p^2 \frac{p^2}{\omega} e^{-(dp)^2} \\ &= \frac{1}{4} m^2 d^{-2} e^{\frac{1}{2}(dm)^2} \left(d^2 m^2 K_0\left(\tfrac{1}{2} d^2 m^2\right) + (1 - d^2 m^2) K_1\left(\tfrac{1}{2} d^2 m^2\right)\right) \\ &= \frac{1}{2} d^{-4} - \frac{1}{4} m^2 d^{-2} - \frac{3}{8} m^4 \left(\frac{7}{12} + \frac{\gamma}{2} - \ln 2 + \ln(dm)\right) + \mathcal{O}(d^6 m^6). \end{aligned} \tag{3.17}$$

In the next step we have to remove the potential divergences in the regularised expressions. For a curved background space-time [16], one would therefore decompose ρ into a divergent and a finite term, so that the former one has the form of a cosmological term in Einsteins´s equations. Then the divergences would be absorbed to yield renormalised coupling constants (which is the origin of some RGEs for Λ and G in Chap. 2), and the finite remainder is called the renormalised energy density or, in our case, the Casimir energy density. Here, such a general treatment is not necessary because the divergence also arises in flat space-time, like our $\mathcal{M} \times \mathcal{S}^1$-manifold, but there are neither cosmological terms nor Einstein´s equations. In order to get rid of the divergence, one simply subtracts the corresponding part of the energy density of the same field in a Minkowski-like space-time with the same dimensions, i.e., $\mathcal{M} \times \mathbb{R}^1$ in our case. In this case there is no IR cutoff and one has to integrate over the 5-momentum instead of summing over it. This kind of renormalisation works because the 5D Minkowski space suffers from the same divergence as the $\mathcal{M} \times \mathcal{S}^1$ space-time but exhibits no Casimir effect. For the energy density ρ_5 from Eq. (3.14), where the p-integral has been regularised by using Eq. (3.16), the renormalisation subtraction can be written as

$$\rho_{5,\text{renorm}} \quad \propto \quad \sum_{n=-\infty}^{\infty} f(n) - \int_{-\infty}^{\infty} \mathrm{d}n\, f(n) \tag{3.18}$$

with

$$f(n) := \frac{1}{2} d^{-4} + \frac{1}{4} m^2 d^{-2} + \frac{1}{8} m^4 \left(\frac{1}{4} + \frac{1}{2}\gamma - \ln 2 + \ln(dm) \right) + \mathcal{O}(d^6 m^6).$$

Above we have applied the substitution $q = 2\pi n/R$ to rewrite the integral over q:

$$\int \frac{\mathrm{d}q}{2\pi}\, f(q) = \frac{1}{R} \int \mathrm{d}n\, f(2\pi \frac{n}{R}).$$

Notice that when keeping in Eqs. (3.16) and (3.17) only terms proportional to $m^4 \ln m$, we obtain the equation of state $p = -\rho$ of the CC. As we will see next, all other terms including the divergences will vanish due to the subtraction in Eq. (3.18) and the subsequent regularisation removal with $d \to 0$. The finite result of the subtraction can be calculated by using the Abel-Plana formulas [60] given by

$$\sum_{n=0}^{\infty} f(n) - \int_0^{\infty} \mathrm{d}n \cdot f(n) \;=\; \frac{1}{2} f(0) + i \int_0^{\infty} \mathrm{d}n \cdot \frac{f(+in) - f(-in)}{\exp(2\pi n) - 1}, \tag{3.19}$$

$$\sum_{n=0}^{\infty} f(n + \tfrac{1}{2}) - \int_0^{\infty} \mathrm{d}n \cdot f(n) \;=\; -i \int_0^{\infty} \mathrm{d}n \cdot \frac{f(+in) - f(-in)}{\exp(2\pi n) + 1}. \tag{3.20}$$

With $m = \sqrt{k^2 n^2 + M_s^2}$ and $k := 2\pi/R$ we immediately see that terms like m^0, m^2, m^4 in the function $f(n)$ are cancelled on the right-hand side. And the term $\frac{1}{2} f(0)$ can be dropped as well since we consider the range $n = -\infty \ldots \infty$. Only terms of the form $m^4 \ln m$ survive, which we write for untwisted fields in the form

$$A := \sum_{n=-\infty}^{\infty} m^4(n) \ln[m(n)] - \int_{-\infty}^{\infty} \mathrm{d}n \cdot m^4(n) \ln[m(n)].$$

By applying the first Abel-Plana formula (3.19) we therefore obtain

$$A = 2i \int_0^\infty \mathrm{d}n \; \frac{m^4(+in)\ln[m(+in)] - m^4(-in)\ln[m(-in)]}{\exp(2\pi n) - 1}.$$

Assuming $k, n, M \geq 0$, we have to consider two cases for the root $m(\pm in)$ in the last equation:

$$\left[k^2(\pm in)^2 + M^2\right]^{\frac{1}{2}} = \begin{cases} (M^2 - k^2n^2)^{\frac{1}{2}} & \text{for } M > kn, \\ \pm i(k^2n^2 - M^2)^{\frac{1}{2}} & \text{for } M < kn. \end{cases}$$

For $a > 0$ we can write the logarithm as $\ln(\pm i \cdot a) = \pm i\pi/2 + \ln a$, and with $x := M/k$ we obtain the result

$$A(M) = -2\pi k^4 \int_x^\infty \mathrm{d}n \frac{(n^2 - x^2)^2}{\exp(2\pi n) - 1}, \tag{3.21}$$

which has, in the massless case ($x = 0$), the value

$$A = -2\pi k^4 \frac{3}{4\pi^5} \cdot \zeta(5) = -8R^{-4}3\zeta(5).$$

For twisted fields we have to use the second Abel-Plana formula (3.20). Analogously, we write

$$B(M) = -2i \int_0^\infty \mathrm{d}n \frac{m^4(+in)\ln[m(+in)] - m^4(-in)\ln[m(-in)]}{\exp(2\pi n) + 1},$$

using $m(n) = \sqrt{k^2n^2 + M^2}$, and not $m(n) = \sqrt{k^2(n + \frac{1}{2})^2 + M^2}$. Thus, the result becomes

$$B(M) = +2\pi k^4 \int_x^\infty \mathrm{d}n \frac{(n^2 - x^2)^2}{\exp(2\pi n) + 1}, \tag{3.22}$$

which has for massless fields ($x = 0$) the value

$$B = +2\pi k^4 \frac{45}{64\pi^5} \cdot \zeta(5) = \frac{15}{2} R^{-4} 3\zeta(5).$$

For large masses ($x \gg 1$), approximate expressions for $A(M)$ and $B(M)$ can be given by neglecting the 1 in the denominator of the Eqs. (3.21) and (3.22):

$$\int_x^\infty \mathrm{d}n \frac{(n^2 - x^2)^2}{\exp(2\pi n) \pm 1} \overset{x \gg 1}{\approx} \int_x^\infty \mathrm{d}n \frac{(n^2 - x^2)^2}{\exp(2\pi n)} = \frac{4\pi^2x^2 + 6\pi x + 3}{4\pi^5} e^{-2\pi x}. \tag{3.23}$$

Combining the prefactors in Eq. (3.14) and the finite results $A(M)$, $B(M)$ from the renormalisation in Eq. (3.18) we have found the finite 5D energy density. To obtain the effective 4D Casimir energy ρ_4 density we just have to integrate over the fifth dimension $\int_0^R \mathrm{d}y$, which simply yields a factor R. Finally, we find for untwisted scalar fields

$$\rho_4 \;=\; \frac{1}{8(2\pi)^2} \cdot A(M) \;\overset{M=0}{=}\; -1 \cdot (2\pi)^{-2} R^{-4} 3\zeta(5), \tag{3.24}$$

whereas twisted scalar fields yield

$$\rho_4 \;=\; \frac{1}{8(2\pi)^2}\cdot B(M) \;\stackrel{M=0}{=}\; +\frac{15}{16}\cdot(2\pi)^{-2}R^{-4}3\zeta(5). \tag{3.25}$$

Obviously, untwisted and twisted fields provide energy densities ρ_4 of different sign. Note that the values for ρ_4 in Eqs. (3.24) and (3.25) agree with the results in Refs. [55, 61] for $M = 0$.

As explained above, the corresponding effective 4D pressure p_4 is just the negative of ρ_4. Therefore the Casimir energy density from the ED represents a finite contribution to the 4D CC. From these results we see that ρ_4 scales like the inverse fourth power of the size R of the fifth dimension. For small EDs this could cause problems with the observed tiny value of the CC. Apart from fine-tuning the field content, there is another possibility to solve this problem. From expression (3.23) we obtain an approximately exponential suppression of the Casimir energy by bulk field masses $M = xk$. We will make use of this behaviour in Secs. 4.5 and 5.2, where the Casimir energy becomes small for large bulk masses even when the ED is small.

Finally, we mention that from statistical arguments and counting degrees of freedom one can immediately conclude that the Casimir energy densities for Dirac fermions are just (-4) times the values of real scalars. We will use this later in Sec. 4.3.

4 Discretised Extra Dimensions

4.1 Introduction

In the Chap. 3 we have discussed dark energy in the form of Casimir energy in the context of a continuous ED. We have found there that the Casimir effect yields a contribution the effective 4D CC. In this chapter we go one step further and consider discretised EDs. As already mentioned in Chap. 1 a discrete space-time structure might not only serve as an UV regulator in theories of quantum gravity but it is also a crucial ingredient of deconstruction. In this framework the phenomenology of discretised higher dimensions is exactly reproduced by a deconstruction model working in a 4D continuous space-time. This concept helps to circumvent some disadvantages occurring in extra-dimensional theories.

In the following sections we will derive the Casimir energy density for scalar and fermion fields in a discretised ED. Since we we are working effectively on a transverse lattice we expect to encounter typical lattice effects like fermion doubling. Furthermore, the scaling of the Casmir energy density with the number of lattice sites and the suppression by bulk masses will be discussed in detail. In Chap. 5 we will apply these results to a deconstruction model and propose a prescription to calculate the absolute value of the vacuum energy of 4D quantum fields in the deconstruction framework.

4.2 Casimir Effect for a Scalar Field

In this section, we consider a scalar quantum field ϕ in a space-time with the topology $\mathcal{M} \times \mathcal{S}^1_{\text{lat}}$, where $\mathcal{M}$ is the continuous Minkowski space and $\mathcal{S}^1_{\text{lat}}$ denotes the discrete fifth dimension compactified on the circle. Taking the discrete nature of the fifth dimension into account, the discretisation of the circle $\mathcal{S}^1$ also forces the coordinate y in the fifth dimension to be discrete. Assuming N lattice sites with a universal lattice spacing a, the circumference of the fifth dimension is given by $R = Na$, and the position y of each site can be described by a coordinate index j,

$$y = a \cdot j, \quad j = 1, \ldots, N. \tag{4.1}$$

From the standard definition for a derivative in the continuum,

$$\frac{\partial \phi}{\partial y}(y) = \lim_{a \to 0} \frac{\phi(y+a) - \phi(y)}{a},$$

follows the discrete forward and backward difference operators $\partial_5\phi$ and $(\partial_5\phi)^\dagger$:

$$\begin{aligned}\frac{\partial\phi}{\partial y} \longrightarrow (\partial_5\phi) &:= \frac{\phi(j+1)-\phi(j)}{a},\\ \left(\frac{\partial\phi}{\partial y}\right)^\dagger \longrightarrow (\partial_5\phi)^\dagger &:= \frac{\phi(j)-\phi(j-1)}{a}.\end{aligned}$$

By inserting the ansatz (3.3) for ϕ we find

$$\partial_5\phi = a^{-1}(e^{-iqa}-1)\phi, \quad (\partial_5\phi)^\dagger = a^{-1}(1-e^{iqa})\phi,$$

and therefore

$$\partial_5^\dagger\partial_5\phi = -2a^{-2}(1-\cos qa)\phi.$$

Taking into account the discrete derivatives ∂_5 and $\partial_5^\dagger$, the continuum Klein-Gordon equation (3.8) for a real 5D scalar field ϕ with bulk mass M_s becomes

$$\left[\frac{\partial^2}{\partial t^2} - \nabla^2 - \partial_5^\dagger\partial_5 + M_\mathrm{s}^2\right]\phi = 0.$$

Thus the the energy ω of a field mode with the momenta $\vec{p}$ and q reads

$$\omega^2 = \vec{p}^{\,2} + m^2, \quad m^2 := 2a^{-2}(1-\cos qa) + M_\mathrm{s}^2, \tag{4.2}$$

where the values q depend on the boundary conditions as in Eqs. (3.4) and (3.5). However, here n has to be in the range $1\ldots N$ since the lattice introduces an UV cutoff. Values of n outside the range $1\ldots N$ are mapped back into this range due to the 2π-periodicity in the discrete derivatives. Therefore, the momentum spectrum is finite and given by

$$q = 2\pi\frac{n}{R} = \frac{2\pi}{a}\cdot\frac{n}{N}, \quad n = 1\ldots N \tag{4.3}$$

for untwisted fields. For twisted fields we respectively find

$$q = 2\pi\frac{(n-\frac{1}{2})}{R} = \frac{2\pi}{a}\frac{(n-\frac{1}{2})}{N}, \quad n = 1\ldots N. \tag{4.4}$$

We can now easily transfer many of the continuum results from Sec. 3.2 to the discretised case by replacing the infinite sum $\sum_{n=-\infty}^{\infty}$ by the finite sum $\sum_{n=1}^{N}$. For instance, the scalar product for the field modes now reads

$$(\phi_1,\phi_2) := i\int \mathrm{d}^3x\, a\sum_{j=1}^{N}\left(\phi_1^\dagger(\partial_t\phi_2) - (\partial_t\phi_1)^\dagger\phi_2\right),$$

which yields via Eq. (3.6) the normalisation factor J from Eq. (3.7) by using the relation

$$\sum_{j=1}^{N}\exp\left(2\pi i\frac{n-n'}{N}j\right) = N\delta_{nn'}.$$

The quantisation of the scalar field and the determination of the corresponding energy density ρ_5 and pressure p_5 goes along the same lines as in the continuum case:

$$\rho_5 = \langle 0|\, \hat{T}_{00}\, |0\rangle \;=\; \frac{1}{2(2\pi)^3 R} \int \mathrm{d}^3p \sum_{n=1}^{N} \omega, \tag{4.5}$$

$$p_5 = \frac{1}{3}\sum_{i=1}^{3} \langle 0|\, \hat{T}_{ii}\, |0\rangle \;=\; \frac{1}{2(2\pi)^3 R} \int \mathrm{d}^3p \sum_{n=1}^{N} \frac{\vec{p}^2}{3\omega}. \tag{4.6}$$

Also, the regularisation of the momentum integral $\int \mathrm{d}^3p$ can be performed exactly like in the continuum case. Here, we also consider the method with the exponential regulator function $e^{-(dp)^2}$ with $d > 0$. However, in the renormalisation procedure we cannot make use of the Abel-Plana formulas since they only treat infinite sums. In order to obtain the finite Casimir energy density, it is necessary to compare the discrete mode sums belonging to the momenta in $\mathcal{S}^1_{\text{lat}}$ with the energy density and pressure of a field in a space-time with a non-compactified but still discretised ED. Regarding Eqs. (4.5) and (4.6), the mode sum with respect to the fifth momentum coordinate $q = 2\pi n/(aN)$ is of the type

$$\sum_{n=1}^{N} f(n/N),$$

where $f(n/N)$ summarises the terms

$$\frac{1}{2}d^{-4} + \frac{1}{4}m^2 d^{-2} + \frac{1}{8}m^4\left(\frac{1}{4} + \frac{1}{2}\gamma - \ln 2 + \ln(d)\right) + \mathcal{O}(d^6 m^6),$$

following from the last line in Eq. (3.16). From this sum, the mode integral corresponding to a non-compactified $\mathbb{R}^1$-dimension can be obtained by cutting out a section of length R of an $\mathbb{R}^1$-dimension. This means, that we take the limit of an infinite number M of lattice sites, $M \to \infty$, while keeping the spacing a constant:

$$\frac{R}{Ma}\sum_{n=1}^{M} f\left(\frac{n}{M}\right)\bigg|_{M\to\infty} = \frac{R}{a}\left[\sum_{n=1}^{M}\frac{\Delta n}{M} f\left(\frac{n}{M}\right)\right]_{M\to\infty} \overset{s:=n/M}{=} N \cdot \int_0^1 \mathrm{d}s \cdot f(s),$$

where Ma becomes the infinite "length" of $\mathbb{R}^1$ and $f(s)$ is the same function as in the $\mathcal{S}^1_{\text{lat}}$ mode sum. In the last equation, we have substituted $s := n/M$ and inserted $\Delta n = 1$ so that $\mathrm{d}s = \Delta n/M$ for $M \to \infty$. Both the sum and the integral are finite since the lattice introduces an UV cutoff. Then the renormalisation is performed by subtracting the integral from the sum,

$$\sum_{n=1}^{N} f\left(\frac{n}{N}\right) - N \cdot \int_0^1 \mathrm{d}s \cdot f(s) = \sum_{n=1}^{N} m^4 \ln m - N \cdot \int_0^1 \mathrm{d}s \cdot m^4 \ln m, \tag{4.7}$$

where only $m^4 \ln m$ survives since all other terms like m^0, m^2, m^4 either vanish when the regularisation is removed for $d \to 0$ or are completely subtracted due to the following

identities:

$$\sum_{n=1}^{N}(1-\cos 2\pi\tfrac{n}{N}+\tfrac{1}{2}a^2M_{\rm s}^2) = N\cdot\int_0^1 \mathrm{d}s\cdot(1-\cos 2\pi s+\tfrac{1}{2}a^2M_{\rm s}^2) \quad (4.8)$$

$$= N(1+\tfrac{1}{2}a^2M_{\rm s}^2), \quad (4.9)$$

$$\sum_{n=1}^{N}(1-\cos 2\pi\tfrac{n}{N}+\tfrac{1}{2}a^2M_{\rm s}^2)^2 = N\cdot\int_0^1 \mathrm{d}s\cdot(1-\cos 2\pi s+\tfrac{1}{2}a^2M_{\rm s}^2)^2 \quad (4.10)$$

$$= N(\tfrac{3}{2}+a^2M_{\rm s}^2+(\tfrac{1}{2}a^2M_{\rm s}^2)^2). \quad (4.11)$$

This is also the case for twisted fields, where n is replaced by $n-\frac{1}{2}$. Note that in the discretised case we obtain the CC equation of state $p=-\rho$, too. Finally, we find the renormalised Casimir energy density to be

$$\rho_5 = \frac{1}{2(2\pi)^3R}\cdot\frac{4\pi}{8}\left[\sum_{n=1}^{N}m^4\ln m - N\cdot\int_0^1\mathrm{d}s\cdot m^4\ln m\right]$$
$$= +R^{-5}S_1(N) = -p_5, \quad \text{(untwisted)} \quad (4.12)$$

where $m^2=2a^{-2}(1-\cos qa)+M_{\rm s}^2$ and where we have introduced the function

$$S_1(N) := \frac{1}{4(2\pi)^2}N^4\cdot\left[\sum_{n=1}^{N}\left(1-\cos 2\pi\frac{n}{N}+\frac{1}{2}a^2M_{\rm s}^2\right)^2\ln\left(1-\cos 2\pi\frac{n}{N}+\frac{1}{2}a^2M_{\rm s}^2\right)\right.$$
$$\left. - N\cdot\int_0^1\mathrm{d}s\cdot\left(1-\cos 2\pi s+\frac{1}{2}a^2M_{\rm s}^2\right)^2\ln\left(1-\cos 2\pi s+\frac{1}{2}a^2M_{\rm s}^2\right)\right]. \quad (4.13)$$

In the limit $N\to\infty$ and $M_{\rm s}=0$, the function $S_1(N)$ converges to the value of a continuous fifth dimension:

$$\lim_{N\to\infty}S_1(N) = -\frac{1}{4(2\pi)^2}3\zeta(5)\cdot 4.$$

By integrating out the fifth dimension, we obtain the 4D energy density

$$\rho_4 = \int_0^R \mathrm{d}r\cdot\rho_5 = R\cdot\rho_5 = -\frac{3\zeta(5)}{(2\pi)^2R^4} = \frac{1}{R^4}\cdot(-0,0787970\ldots). \quad \text{(untwisted)} \quad (4.14)$$

In the case of a twisted scalar field everything is like above, but the energy density reads

$$\rho_5 = +R^{-5}S_2(N)$$
$$= -p_5, \quad \text{(twisted)}$$

where $S_2(N)$ is the function $S_1(N)$ with n replaced by $n-\frac{1}{2}$. For massless fields ($M_{\rm s}=0$) we obtain in the continuum limit

$$\lim_{N\to\infty}S_2(N) = +\frac{1}{4(2\pi)^2}3\zeta(5)\cdot(4-\tfrac{1}{4}),$$

and after integrating out the fifth dimension the 4D energy density reads

$$\rho_4 = R \cdot \rho_5 = +\frac{15}{16} \cdot \frac{3\zeta(5)}{(2\pi)^2 R^4} = \frac{1}{R^4} \cdot (+0,0738722\ldots). \quad \text{(twisted)} \tag{4.15}$$

In the continuum limit the lattice results for ρ_4 found here are consistent with the continuum Casimir energy densities from Eqs. (3.24) and (3.25).

4.3 Casimir Effect for a Dirac Fermion

In analogy with the treatment of scalar fields in previous section, we will now calculate the Casimir energy density of Dirac fermions. Therefore, a plane wave Ansatz for Dirac spinor fields Ψ in the $\mathcal{M} \times \mathcal{S}^1$ manifold is a convenient choice, too:

$$\Psi = \psi \exp(-i\omega t + i\vec{p}\vec{x} + iqy). \tag{4.16}$$

The boundary conditions, associated with the compactified $\mathcal{S}^1$-dimension, provide the discrete momentum spectra. For twisted and untwisted fields we have as before $q = 2\pi(n - \frac{1}{2})/(aN)$ and $q = 2\pi n/(aN)$, respectively. Like in Eq. (4.1) the coordinate y corresponding to the fifth dimension is discrete, $y = a \cdot j$, where $j = 1, \ldots, N$, and implies an upper bound for the momentum q.

Unlike the Klein-Gordon equation for scalars fields, the Dirac equation is linear in the derivatives, and therefore we need a symmetric derivative operator for the discrete y-coordinate:

$$\partial_5 \Psi(j) := \frac{1}{2a} \left(\Psi(j+1) - \Psi(j-1)\right).$$

With the Ansatz (4.16) we obtain

$$\begin{aligned} \partial_5 \Psi(j) &= \frac{1}{2a} \psi \cdot \exp(-i\omega t + i\vec{p}\vec{x}) \left[\exp(iqa(j+1)) - \exp(iqa(j-1))\right] \\ &= \Psi(j) \cdot \left(+\frac{i}{a} \sin(qa)\right), \end{aligned}$$

and together with the 5D Dirac equation[1] for a Dirac field with mass M_f,

$$(i\gamma^A \partial_A - M_\mathrm{f})\Psi = 0, \quad A = 0, \ldots, 3, 5,$$

the energy-momentum relation is determined to be

$$\omega^2 = \vec{p}^{\,2} + m^2, \quad m^2 := a^{-2} \sin^2 qa + M_\mathrm{f}^2. \tag{4.17}$$

The energy-momentum tensor T_{AB} for the Dirac field Ψ has the form [16]

$$T_{AB} = \frac{1}{4} i[\overline{\Psi}\gamma_A \partial_B \Psi + \overline{\Psi}\gamma_B \partial_A \Psi - \overline{(\partial_A \Psi)}\gamma_B \Psi - \overline{(\partial_B \Psi)}\gamma_A \Psi],$$

[1] A fifth Dirac matrix $\gamma^5 := i\gamma^5_{4\mathrm{D}}$ has to be introduced, where $\gamma^5_{4\mathrm{D}}$ is the usual γ^5 matrix of the 4D Dirac theory [62].

and the usual canonical quantisation procedure parallels that for scalar fields up to replacing the bosonic commutator relations by the fermionic anti-commutator relations, which give an overall minus sign in the result. The Dirac fermion also has four times the degrees of freedoms of a real scalar, describing particles and anti-particles with two spin states each. In total, the energy density ρ_5 and pressure p_5 of a quantised Dirac field differ from the scalar results of Eqs. (4.5) and (4.6) only by a factor of (-4) and in the modified energy-momentum relation of Eq. (4.17), i.e.,

$$\rho_5 = -\frac{2}{(2\pi)^3 R} \sum_{n=1}^{N} \int \mathrm{d}^3 p \cdot \omega, \tag{4.18}$$

$$p_5 = -\frac{2}{(2\pi)^3 R} \sum_{n=1}^{N} \int \mathrm{d}^3 p \cdot \frac{\vec{p}^2}{\omega}, \tag{4.19}$$

where $\omega^2 = \vec{p}^2 + a^{-2} \sin^2 qa + M_\mathrm{f}^2$. By replacing back the sum $\sum_{n=1}^{N}$ to the continuum version $\sum_{n=-\infty}^{\infty}$ and additionally using the continuum energy momentum relation $\omega^2 = \vec{p}^2 + q^2 + M_\mathrm{f}^2$, we now explicitly see by comparison with Eqs. (3.14) and (3.15) that the corresponding fermionic Casimir energy density would indeed be (-4) times the scalar values. In the following, however, we will observe that on the lattice this is not true anymore due to fermion doublers.

From here on, the regularisation and renormalisation procedures are identical to the scalar case in Sec. 4.2. This also implies that the equation of state of the fermionic vacuum energy is that of a cosmological constant, $p = -\rho$. Thus, it is sufficient to give the renormalised energy density in five dimensions

$$\begin{aligned} \rho_5 &= -\frac{2}{(2\pi)^3 R} 4\pi \frac{1}{8} \left[\sum_{n=1}^{N} m^4 \ln m - N \cdot \int_0^1 \mathrm{d}s \cdot m^4 \ln m \right] \\ &= +R^{-5} F_1(N), \end{aligned} \tag{4.20}$$

where the function $F_1(N)$ in the last equation is defined as

$$\begin{aligned} F_1(N) &:= -\frac{1}{4(2\pi)^2} N^4 \cdot \left[\sum_{n=1}^{N} \left(\sin^2 2\pi \frac{n}{N} + a^2 M_\mathrm{f}^2 \right)^2 \ln \left(\sin^2 2\pi \frac{n}{N} + a^2 M_\mathrm{f}^2 \right) \right. \\ &- \left. N \cdot \int_0^1 \mathrm{d}s \cdot \left(\sin^2 2\pi \frac{n}{N} + a^2 M_\mathrm{f}^2 \right)^2 \ln \left(\sin^2 2\pi \frac{n}{N} + a^2 M_\mathrm{f}^2 \right) \right], \end{aligned} \tag{4.21}$$

with $R = Na$. For the twisted Dirac field we have

$$\rho_5 = R^{-5} F_2(N),$$

where $F_2(N)$ is the function $F_1(N)$ with n replaced by $n - \frac{1}{2}$. Unlike the functions $S_{1,2}(N)$ for the scalar fields, the functions $F_{1,2}(N)$ for the fermionic fields have two limit points each, which depend on whether the number of lattice sites N is even or odd. For massless

fermions ($M_\mathrm{f} = 0$) and even N we obtain

$$\begin{aligned}\lim_{N\to\infty} F_1(N) &= -\frac{1}{4(2\pi)^2}\cdot 3\zeta(5)\cdot(-32), \quad \text{(untwisted)}\\ \lim_{N\to\infty} F_2(N) &= -\frac{1}{4(2\pi)^2}\cdot 3\zeta(5)\cdot(+30). \quad \text{(twisted)}\end{aligned}$$

After integrating out the fifth dimension, the 4D Casimir energy densities read

$$\rho_4 = \frac{32\cdot 3\zeta(5)}{4(2\pi)^2R^4} = \frac{1}{R^4}\cdot(+0,630376\ldots), \quad \text{(untwisted)} \tag{4.22}$$

$$\rho_4 = \frac{-30\cdot 3\zeta(5)}{4(2\pi)^2R^4} = \frac{1}{R^4}\cdot(-0,590978\ldots). \quad \text{(twisted)} \tag{4.23}$$

In the case of odd N, both functions have the same limit

$$\lim_{N\to\infty} F_1(N) = \lim_{N\to\infty} F_2(N) = \frac{1}{4(2\pi)^2}\cdot 3\zeta(5),$$

$$\rho_4 = \frac{3\zeta(5)}{4(2\pi)^2R^4} = \frac{1}{R^4}\cdot(+0,019699\ldots).$$

Obviously, this behaviour is an effect of the lattice, in Ref. [63] it is called an odd-even artefact. We also notice, that the $N\to\infty$ limit of the sum of twisted and untwisted results does not depend on whether N is even or odd. Therefore, it is reasonable to consider only this sum as a physical quantity. For finite N, this odd-even artefact is illustrated in Fig. 4.1. Note again, that the continuum results for ρ_4 in Eqs. (4.22) and (4.23) are identical with the values in Ref. [55].

4.4 Massless Fields

The calculations of Sec. 4.2 show that the Casimir effect for a real scalar field in the transverse lattice space-time $\mathcal{M}\times\mathcal{S}^1_\mathrm{lat}$ induces a negative vacuum energy density ρ and therefore a negative contribution to the effective 4D CC. On the other hand, the fermionic Dirac field of Sec. 4.3 yields a positive contribution to the CC.

We have already concluded that only the sum of twisted and untwisted fields can be regarded as a physical quantity, and we note that its sign is independent of N. Moreover, for a constant circumference R and small N, the Casimir energy density $\rho_4(N)$ in the transverse lattice setup has already the same order of magnitude as the energy density $\rho_4(N\to\infty)$ in the continuum limit. Specifically, for $N\gtrsim 10$ the continuum result is approximated at the few percent level. Even for a number of lattice sites which is as small as $N = 3$, the results differ at most by a factor of 2, which is clearly shown in Fig. 4.2.

In the limit $N\to\infty$ (Tab. 4.1), the results for real scalars are the same as in the non-lattice calculation [55, 61], but for the fermions there is an extra factor of 2 in the energy

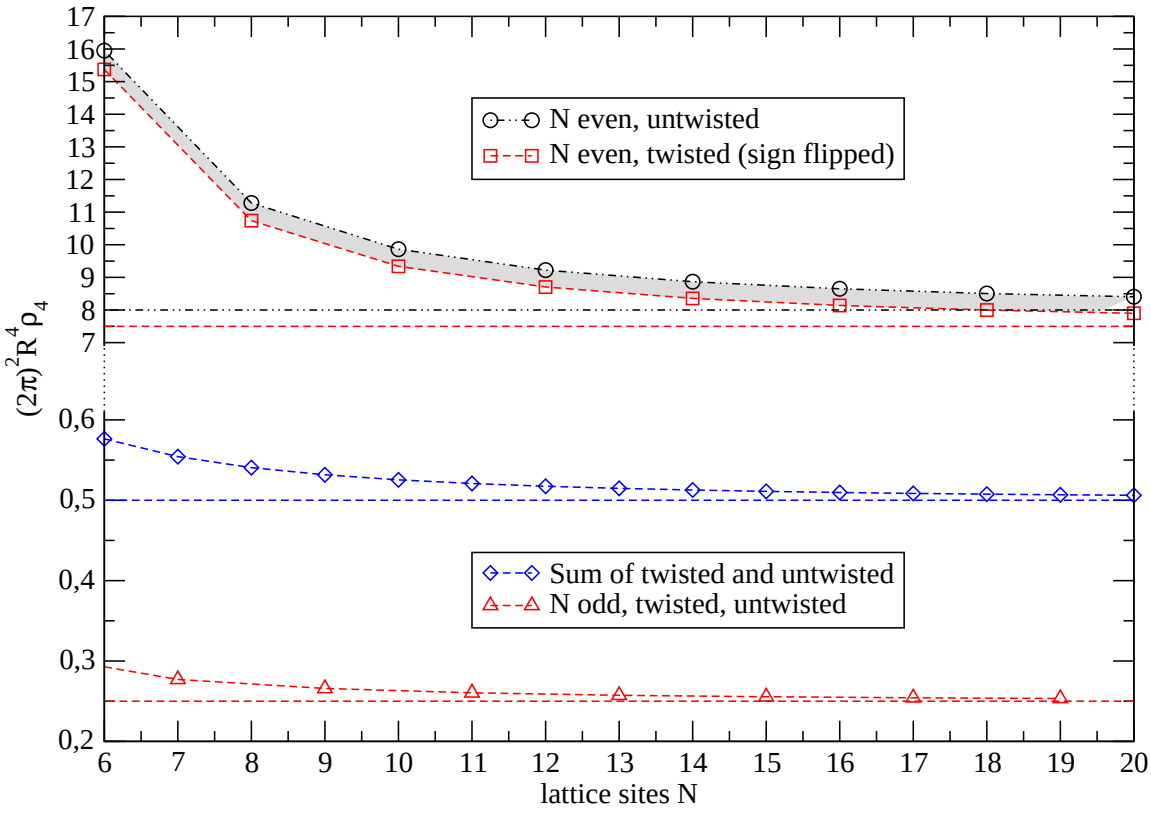

Figure 4.1: Illustration of the odd-even artefact for fermion fields. The cases of odd and even N are plotted separately, and the circumference R of the fifth dimension is kept constant. For a better representation, we flipped the sign in the results for twisted fields and even N. The horizontal lines correspond to the continuum values given in Table 4.1.

density of our lattice calculation because of the fermion doubling phenomenon in lattice theory. In a calculation for continuous dimensions, one usually expects, from counting degrees of freedom, that the energy density for Dirac fermions is (-4) times the value of real scalars.

Up to now, we have investigated the Casimir effect for Dirac fermions and real scalars having twisted and untwisted field configurations. When passing to a complex scalar field which transforms under a $U(1)$ gauge group there exist only trivial (untwisted) structures and therefore the charged scalar obeys only periodic boundary conditions. For fermions, on the other hand, the appearance of twisted field modes is related to the double covering map $SL(2,\mathbb{C}) \to SO(3,1)$ which gives rise to inequivalent spin connections [59]. Consequently, even in presence of a simply connected gauge group like $U(1)$ we still have also the anti-periodic boundary condition for the fermions.

$\rho_4 R^4$	untwisted	twisted	sum
real scalar	$-1 \cdot (2\pi)^{-2} 3\zeta(5)$	$+\frac{15}{16} \cdot (2\pi)^{-2} 3\zeta(5)$	$-\frac{1}{16} \cdot (2\pi)^{-2} 3\zeta(5)$
fermion, N even	$+8 \cdot (2\pi)^{-2} 3\zeta(5)$	$-\frac{15}{2} \cdot (2\pi)^{-2} 3\zeta(5)$	$+\frac{1}{2} \cdot (2\pi)^{-2} 3\zeta(5)$
fermion, N odd	$+\frac{1}{4} \cdot (2\pi)^{-2} 3\zeta(5)$	$+\frac{1}{4} \cdot (2\pi)^{-2} 3\zeta(5)$	$+\frac{1}{2} \cdot (2\pi)^{-2} 3\zeta(5)$

Table 4.1: The Casimir energy density ρ_4 multiplied by R^4 for real massless scalars and Dirac fermions ($M_{\mathrm{s,f}} = 0$) in the limit of an infinite number of lattice sites ($N \to \infty$).

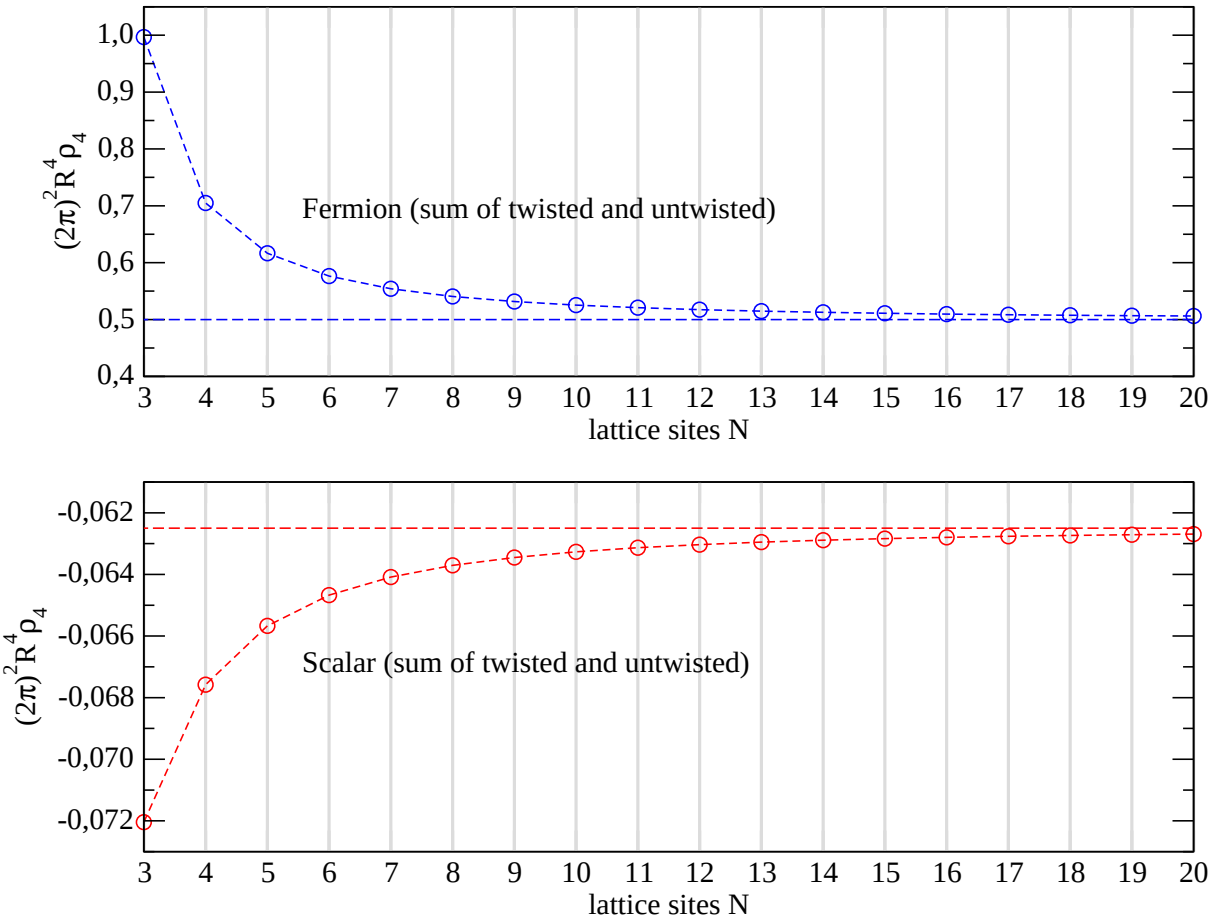

Figure 4.2: The Casimir energy densities for fermions (upper graph) and real scalars (lower graph). In this plot, R is fixed so that the lattice spacing decreases for increasing N. The dashed horizontal lines denote the continuum limit $N \to \infty$, which has for scalars the value $-\frac{1}{16}$ and for fermions $+\frac{1}{2}$.

$M_{\mathrm{s,f}}R$	1	10	100	1000	10^4	10^5
Scalar	$0,61$	$1,5 \cdot 10^{-4}$	$2,9 \cdot 10^{-12}$	$3,0 \cdot 10^{-20}$	$3,0 \cdot 10^{-28}$	$3,0 \cdot 10^{-36}$
Fermion	$0,74$	$3,5 \cdot 10^{-2}$	$3,7 \cdot 10^{-4}$	$3,8 \cdot 10^{-6}$	$3,7 \cdot 10^{-8}$	$3,7 \cdot 10^{-10}$

Table 4.2: The exponential suppression factors in Eqs. (4.24) and (4.25) of the Casimir energy densities for $N = 3$ lattice sites, where $M_{\mathrm{s,f}}$ denotes the bulk masses of the quantum fields.

4.5 Exponential Suppression by Massive Fields

So far, we have given results only in the case of vanishing bulk mass ($M_{\mathrm{s,f}} = 0$). For massive 5D fields we observe an approximately exponential suppression of the Casimir energy. This behaviour becomes obvious in the analytical calculation for a continuous ED, which is given in Sec. 3.2. But it is also achieved for the discretised case of this chapter, where in the limit of an infinite number of lattice sites ($N \to \infty$) we approach the values of the analytical formulas (3.24) and (3.25). To investigate the suppression behaviour depending on the mass $M_{\mathrm{s,f}}$ and the number N, we examine the ratio between the energy density of fields with mass $M_{\mathrm{s,f}}$ and that of massless fields. For scalar fields this ratio is defined by

$$\frac{S_1(M_{\mathrm{s}}R) + S_2(M_{\mathrm{s}}R)}{S_1(0) + S_2(0)}, \tag{4.24}$$

where the functions $S_{1,2}(N)$ are taken from Eq. (4.13) of Sec. 4.2. Analogously, using the functions $F_{1,2}(N)$ from Eq. (4.21) of Sec. 4.3, the ratio for fermionic fields reads

$$\frac{F_1(M_{\mathrm{f}}R) + F_2(M_{\mathrm{f}}R)}{F_1(0) + F_2(0)}. \tag{4.25}$$

Both ratios are plotted in Fig. 4.3 for a range of values of N and $M_{\mathrm{s,f}}R$. The suppression by a bulk mass is most minimal for small N. In the case of $N = 3$ lattice sites, the corresponding ratios are given in Table 4.2.

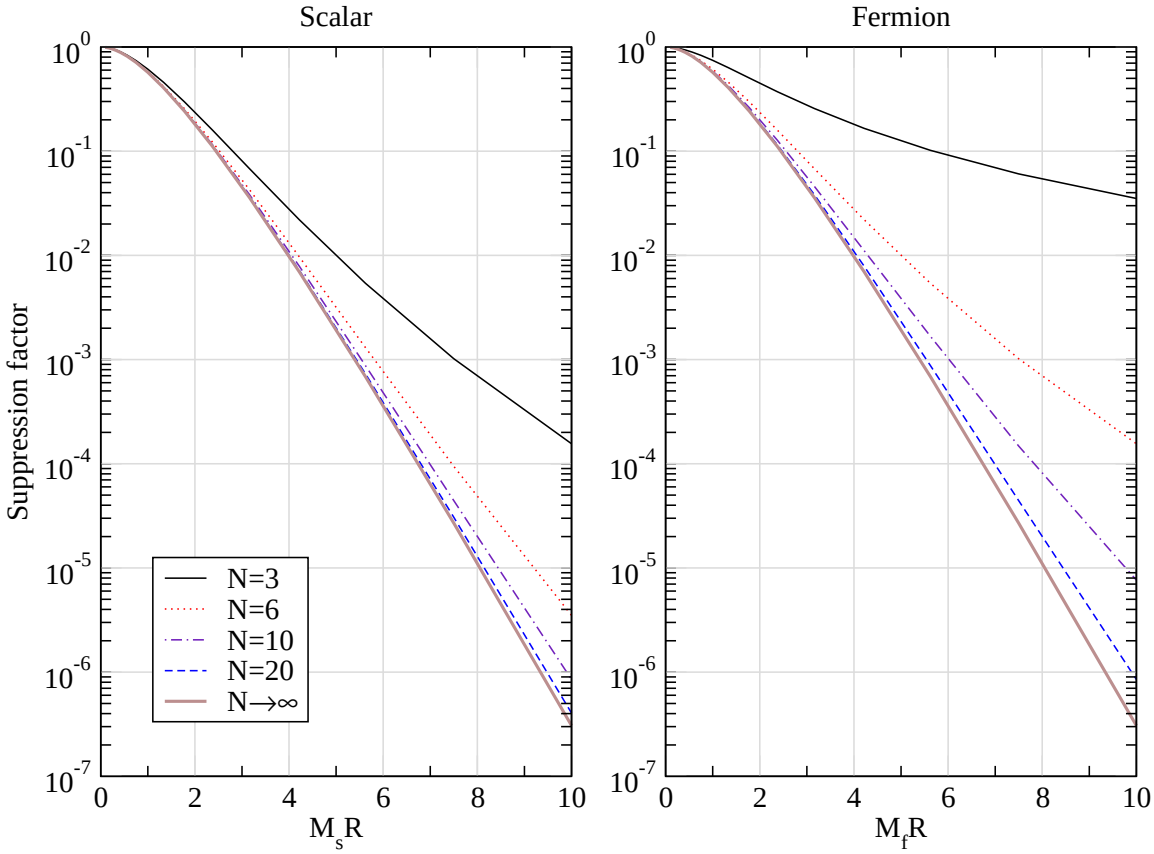

Figure 4.3: The ratios in Eqs. (4.24) and (4.25) of the Casimir energy density between massive and massless fields. The values for $N \to \infty$ are taken from the analytic formulas in Eqs. (3.24) and (3.25).

5 Vacuum Energy in Deconstruction

In this chapter we will discuss the vacuum energy of 4D quantum fields occurring in a deconstruction scenario. It is well known that the absolute value of the zero-point energy density $\int \mathrm{d}^3p \cdot \omega(p)$ of 4D quantum fields is formally divergent and completely unconstrained from a theory point of view. This means that without any further information we do not know how to assign a sensible and finite vacuum energy value to these fields. In Sec. 2.1 we already mentioned this problem and investigated the change of the vacuum energy density with respect to a renormalisation scale, but the absolute value still remained undetermined there.

Here, however, we propose a prescription how to treat this problem by using the correspondence of a discretised fifth dimension and deconstruction. For a 5D field obeying certain boundary conditions we are able to derive the part of its vacuum energy that depends on the boundary via the Casimir effect. Since in deconstruction the 5D field is described by many 4D fields it seems plausible to identify the vacuum energies of all the 4D fields with the Casimir energy density of the 5D field. Going this way we have found a definite and sensible prescription to determine the zero-point energies of quantum fields in the deconstruction framework. Due to the lack of alternatives to handle this problem, our idea represents at least a well motivated ansatz to obtain a reasonable result, in contrast to the naive cutoff method given in Eq. (2.1).

In the next section we will briefly introduce a deconstruction model that describes a discretised fifth dimension and give the values of masses and VEVs of the fields that appear in this framework. After that, we will use the results of the previous chapter to determine the vacuum energy of the 4D fields by using the prescription given above.

5.1 Deconstruction Model

In continuous EDs the maximum number of KK modes is usually restricted by an UV cutoff which reflects the fact that non-Abelian gauge theories in higher dimensions are non-renormalisable. Although this leads below the cutoff to a renormalisable effective 4D theory, the full higher-dimensional gauge-invariance is in general lost. To circumvent these problems the deconstruction framework has been proposed [29, 30] representing manifestly gauge-invariant and renormalisable 4D gauge theories, which reproduce higher-dimensional physics in their IR limit. These theories use the transverse lattice technique [64] as a gauge-invariant regulator to describe the EDs and yield viable UV completions extra-dimensional theories [65].

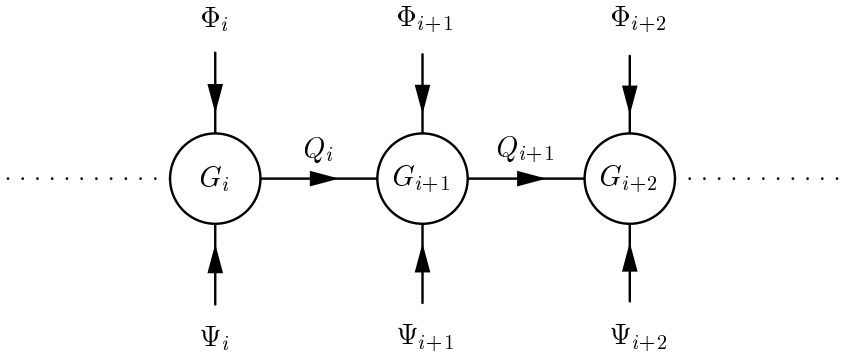

Figure 5.1: Part of the moose diagram, where the sites i, $i+1$ and $i+2$ are shown for a deconstructed extra dimension compactified on $\mathcal{S}^1$. Each circle G_i corresponds to the $U(1)_i$ gauge group and each arrow pointing towards (outwards) a circle represents a field with negative (positive) charge under this group [66].

Here, we consider a specific 5D deconstruction framework which was introduced in Ref. [66] and which represents a periodic model for a deconstructed 5D $U(1)$ gauge theory compactified on the circle $\mathcal{S}^1$. The model is defined by an $U(1)^N = \Pi_{i=1}^N U(1)_i$ product gauge group with N scalar link fields Q_i $(i = 1, \ldots, N)$, which carry the $U(1)$-charges $(q, -q)$ under the neighbouring groups $U(1)_i \times U(1)_{i+1}$. The identification $i + N = i$ establishes the periodicity of the lattice corresponding to untwisted quantum fields in the language of Sec. 3.2, whereas twisted quantum fields are described by an anti-periodic lattice with the condition $i + N = -i$. On the i^{th} lattice site, we put one Dirac fermion Ψ_i and one scalar Φ_i which carry both the charge $-q$ of the group $U(1)_i$. The fermions Ψ_i are SM-singlets and correspond to a right-handed bulk neutrino in the ADD scheme [67, 68]. As an illustration of this setup the corresponding "moose" [69] (or "quiver" [70]) diagram is shown in Fig. 5.1. Let us split up the Lagrangian of the model into several parts,

$$\mathcal{L} = \mathcal{L}_{\text{kin}}[\Phi_i, Q_i] + \mathcal{L}_{\text{kin}}[A_i^\mu] + \mathcal{L}_{\text{kin}}[\Psi_i] + \mathcal{L}_{\text{mass}}[\Psi_i, Q_i] - V,$$

where $\mathcal{L}_{\text{kin}}[A_i^\mu]$ and $\mathcal{L}_{\text{kin}}[\Psi_i]$ are the standard kinetic terms for the gauge bosons A_i^μ and the fermions Ψ_i given by

$$\begin{aligned} \mathcal{L}_{\text{kin}}[A_i^\mu] &= -\frac{1}{4}\sum_{n=1}^{N}(\partial_\mu A_{n\nu} - \partial_\nu A_{n\mu})^2, \\ \mathcal{L}_{\text{kin}}[\Psi_i] &= \sum_{n=1}^{N}\overline{\Psi}_n\gamma_\mu(\partial^\mu - ig_n A_n^\mu)\Psi_n. \end{aligned}$$

Moreover, the kinetic terms $\mathcal{L}_{\text{kin}}[\Phi_i, Q_i]$ for the scalars Φ_i and Q_i, which will later provide the gauge boson masses, can be written as

$$\mathcal{L}_{\text{kin}}[\Phi_i, Q_i] = \sum_{i=1}^{N}|(\partial_\mu + ig_i A_{i\mu})\Phi_i|^2 + \left|(\partial_\mu + ig_i A_{i\mu} - ig_{i+1}A_{(i+1)\mu})Q_i\right|^2, \qquad (5.1)$$

where g_i are the gauge couplings corresponding to the gauge group $U(1)_i$. Finally, the mass and mixing terms involving the fermions Ψ_i and the link fields Q_i are combined into

$$\mathcal{L}_{\text{mass}}[\Psi_i, Q_i] = \frac{u}{2} \cdot \sum_{n=1}^{N} \overline{\Psi}_{n\text{L}} \left[\frac{Q_n^\dagger}{u} \Psi_{(n+1)\text{R}} - \frac{Q_{n-1}}{u} \Psi_{(n-1)\text{R}} \right] + \text{h.c.}, \tag{5.2}$$

where $\Psi_{\text{L,R}} := \frac{1}{2}(1 \mp \gamma^5)$ denote the left- and right-handed components of the Dirac fermion Ψ. In the last line we have already introduced the universal real VEV $\langle Q_i \rangle = u$ of the link fields Q_i. At this point let us denote the VEV of the scalars Φ_i by $\langle \Phi_i \rangle = v$, which is also real and universal for all $i = 1 \dots N$. These properties of the VEV structure follow from the renormalisable potential V, which is not shown here since it not needed for the determination of vacuum energy in this setup. The potential has been discussed and minimised in great detail in Ref. [66], where it leads via a type-II seesaw mechanism [71] to the following values for the VEVs:

$$\langle Q_i \rangle = u \sim 10^{-2}\,\text{eV}, \;\; \langle \Phi_i \rangle = v \sim 10^{2}\,\text{GeV}.$$

Once Q_i and Φ_i have acquired their VEVs the gauge bosons $A_{i\mu}$ become massive via the Higgs mechanism. Assuming universal gauge couplings $g_i = g$ in the kinetic terms (5.1) of the scalars one finds the mass terms for the gauge bosons

$$g^2 \sum_{i=1}^{N} \left[v^2 A_{i\mu} A_i^\mu + u^2 (A_{i\mu} - A_{(i+1)\mu})^2 \right]. \tag{5.3}$$

After diagonalisation, the mass eigenvalues M_n of the gauge bosons read

$$M_n^2 = g^2 v^2 + 2 g^2 u^2 \left(1 - \cos 2\pi \frac{n}{N} \right), \quad n = 1, \dots, N, \tag{5.4}$$

which can be interpreted for $n \ll N$ as a linear KK spectrum $\sim n/R = gu \cdot n/N$ with a mass scale $u \sim 10^{-2}\,\text{eV}$. The scalar fields Φ_i provide in addition a constant bulk (or kink) mass of the order $v \sim 10^2\,\text{GeV}$. At this stage we can already observe the correspondence with the discretised boson spectrum from Eq. (4.2), by identifying the VEV u with the inverse lattice spacing a^{-1}, and respectively the VEV v with the bulk mass M_s.

Furthermore, we find in $\mathcal{L}_{\text{mass}}[\Psi_i, Q_i]$ from Eq. (5.2) terms of the type $Q_i^\dagger \overline{\Psi}_{i\text{L}} \Psi_{(i+1)\text{R}} + \text{h.c.}$ which yield fermion masses of order u when Q_i has taken on its VEV. In the next section we will see that the Ψ_i mass spectrum corresponds to the fermionic mass spectrum found in Eq. (4.17), where the fermionic Casimir effect was calculated. Also in this case we will be able to identify u with the inverse lattice spacing a^{-1} in the ED.

It is also possible to interpret the set of scalars Φ_i as one 5D massive scalar on a transverse lattice, since in the potential V there exist a bulk mass term and terms of the type $\sum_{i=1}^{N} M_\text{b}^2 \left| \Phi_i - Q_i \Phi_{i+1}/u \right|^2$ that can be interpreted as the discretised version of the continuum KK mass term $\int_0^R \text{d}y\, (\partial_5 \Phi)^2$. The resulting KK mass spectrum corresponds to the one for the gauge bosons in Eq. (5.4), but with an inverse lattice spacing of the order M_b and a constant kink mass $M_\Phi \sim 10^2\,\text{GeV}$.

Let us close this section with a summary of the relevant scales that follow from this model. For the gauge fields $A_{i\mu}$ and the fermions Ψ_i we find the inverse lattice spacing to be of the order $u \sim 10^{-2}\,\mathrm{eV}$ with an additional bulk gauge mass term of the order $v \sim 10^2\,\mathrm{GeV}$. The fermions do not have a bulk mass term. Finally, the scalars Φ_i with a bulk mass $M_\Phi \sim 10^2\,\mathrm{GeV}$ yield a lattice spacing given by $M_\mathrm{b} \sim (10^4 \ldots 10^5)\,\mathrm{eV}$.

5.2 Vacuum Energy in Deconstruction

In this section we show that by applying the correspondence between gauge theories in geometric and in deconstructed higher dimensions, it is possible to transfer the methods for calculating finite Casimir energy densities in higher dimensions to the 4D deconstruction setup. One therefore obtains an unambiguous and well-defined prescription to determine finite vacuum energies of 4D quantum fields which have a higher-dimensional correspondence. We will demonstrate this procedure explicitly with the deconstruction model given in the previous section, which finally yields a 4D vacuum energy density that is comparable with the observed value $\rho_\mathrm{obs} \sim 10^{-47}\,\mathrm{GeV}^4$.

Let us start with the energy density ρ of the 4D quantum fields in deconstruction with N KK modes which is schematically given by

$$\rho \propto \sum_{n=1}^{N} \int \mathrm{d}^3 p \cdot \sqrt{\vec{p}^2 + M_n^2}, \tag{5.5}$$

where the masses M_n depend on N, R, and the spin of the fields. Without any knowledge of the fifth dimension, it would not be clear how to put these UV divergent expressions into a sensible (finite) form. However, since we now interpret the KK tower in terms of an underlying higher-dimensional theory with certain boundary conditions, the 5D Casimir effect provides a well-known procedure to handle these UV divergences in four dimensions and yields a finite result.

We can make the correspondence even more definite by comparing the zero-point modes in Eq. (5.5), which follow from the deconstruction mass spectra, with the energy momentum relations (4.2) and (4.17) appearing in the Casmir calculations. In the previous section we have already found this relation explicitly by confronting the gauge boson/scalar masses from Eq. (5.4),

$$M_n^2 = g^2 v^2 + 2 g^2 u^2 \left(1 - \cos 2\pi \frac{n}{N}\right),$$

with Eq. (4.2),

$$m^2 = 2a^{-2}(1 - \cos 2\pi \frac{n}{N}) + M_\mathrm{s}^2.$$

Here, we directly observe that the inverse lattice spacing a^{-1} corresponds to gu, and respectively the bulk mass M_s to gv. For simplicity, we treat all bosons like real scalars since they differ only by their number of degrees of freedom, and for our purposes even this small factor 2 or 3 can be neglected. In this case the overall prefactor in Eq. (5.5)

is exactly given by that of Eq. (4.5) after integrating out the ED. This shows that the formal correspondence is exact for the bosons.

Now, we show this correspondence also for the fermions Ψ_i. Let us first mention that in this case the prefactor in Eq. (5.5) also exactly matches that of Eq. (4.18) after integrating out the ED. To determine the mass spectrum M_n for the Dirac spinor $\Psi_n = (\Psi_{n\mathrm{L}}, \Psi_{n\mathrm{R}})^{\mathrm{T}}$ we start with Eq. (5.2), where the link fields Q_i have acquired their VEVs u,

$$\mathcal{L}_{\mathrm{mass}}[\Psi_i, Q_i] \to \frac{u}{2} \cdot \sum_{n=1}^{N} \overline{\Psi}_{n\mathrm{L}} \left[\Psi_{(n+1)\mathrm{R}} - \Psi_{(n-1)\mathrm{R}}\right] + \mathrm{h.c.}.$$

This sum contains the boundary terms $-\frac{u}{2}\overline{\Psi}_{1\mathrm{L}}\Psi_{0\mathrm{R}}$ and $\frac{u}{2}\overline{\Psi}_{N\mathrm{L}}\Psi_{(N+1)\mathrm{R}}$, and $\Psi_{0\mathrm{R}}$ and $\Psi_{(N+1)\mathrm{R}}$ are defined by

$$\Psi_{mN+1} = T^m \cdot \Psi_1 \quad \text{and} \quad \Psi_0 = T^m \cdot \Psi_{mN}, \quad m \in \mathbb{Z},$$

where we distinguish between untwisted ($T = +1$) and twisted ($T = -1$) fermionic fields. Note that this is the discretised version of the continuum boundary condition

$$\Psi(y + mR) = T^m \cdot \Psi(y), \quad m \in \mathbb{Z}.$$

Now, the Lagrangian in matrix form reads

$$\mathcal{L}_{\mathrm{mass}}[\Psi_i] = \sum_{n,k=1}^{N} \overline{\Psi}_{n\mathrm{L}} M_{nk} \Psi_{k\mathrm{R}} + \mathrm{h.c.},$$

where the mass matrix M_{nk} and its square $M^2 = MM^\dagger = M^\dagger M$ are explicitly given by

$$M = \frac{u}{2}\begin{bmatrix} 0 & +1 & & & -T \\ -1 & 0 & +1 & & \\ & \ddots & \ddots & \ddots & \\ & & -1 & 0 & +1 \\ +T & & & -1 & 0 \end{bmatrix}, \quad M^2 = \frac{u^2}{4}\begin{bmatrix} 2 & 0 & -1 & & & -T & 0 \\ 0 & 2 & 0 & -1 & & & -T \\ -1 & 0 & 2 & 0 & -1 & & \\ & \ddots & \ddots & \ddots & \ddots & \ddots & \\ & & -1 & 0 & 2 & 0 & -1 \\ -T & & & -1 & 0 & 2 & 0 \\ 0 & -T & & & -1 & 0 & 2 \end{bmatrix}.$$

The squared masses m_n^2 of the fermions are found to be the eigenvalues of M^2. Thus, the mass spectrum for untwisted fields reads

$$m_n^2 = u^2 \sin^2 2\pi \frac{n}{N}, \quad n = 1, \ldots, N, \tag{5.6}$$

and for the twisted fields we obtain

$$m_n^2 = u^2 \sin^2 2\pi \frac{n - \frac{1}{2}}{N}, \quad n = 1, \ldots, N, \tag{5.7}$$

which is consistent with the spectra found in Ref. [63]. Note that only for odd N, both spectra become identical, which has already been discussed in the context of the odd-even

artefact in Sec. 4.4. With these mass spectra the Casimir energy of the fermions is (-8) times the Casimir energy of a real scalar, whereas in a non-lattice calculation the energies differ only by a factor of (-4) (see Sec. 4.4). This comes again from the well known phenomenon of fermion doubling in lattice theory.

Note that the fermionic spectrum given in Eq. (5.6) (and respectively Eq. (5.7) for twisted fields) is exactly that of Eq. (4.17),

$$m^2 = a^{-2} \sin^2 2\pi \frac{n}{N} + M_{\mathrm{f}}^2,$$

where the inverse lattice spacing a^{-1} is identified with the VEV u and vanishing bulk mass M_{f}.

We therefore conclude that with the prescription motivated in this section, we are able to assign the finite Casimir energy density as calculated in Secs. 4.2 and 4.3 to the vacuum energy densities of 4D quantum fields in deconstruction. Before we discuss the phenomenological consequences of this result, let us first treat the problem of fermion doubling.

One way to handle the fermion doubling is to add a Wilson term [72] to $\mathcal{L}_{\mathrm{mass}}[\Psi_i, Q_i]$. This leads to a modified fermion mass Lagrangian,

$$\mathcal{L}_{\mathrm{mass}} = u \cdot \sum_{n=1}^{N} \left[\overline{\Psi}_{n\mathrm{L}} \left(\frac{Q_n^\dagger}{u} \Psi_{(n+1)\mathrm{R}} - \Psi_{n\mathrm{R}} \right) - \overline{\Psi}_{n\mathrm{R}} \left(\Psi_{n\mathrm{L}} - \frac{Q_{n-1}}{u} \Psi_{(n-1)\mathrm{L}} \right) \right], \tag{5.8}$$

which yields with $\langle Q_n \rangle = u$ the mass matrix M. The squared masses m_n^2 of the fermions are now given by the eigenvalues of M^2, which is exactly the mass matrix for the bosons:

$$M = u \cdot \begin{bmatrix} -1 & +1 & & & 0 \\ & -1 & +1 & & \\ & & \ddots & \ddots & \\ & & & -1 & +1 \\ +T & & & & -1 \end{bmatrix}, \quad M^2 = u^2 \cdot \begin{bmatrix} 2 & -1 & & & -T \\ -1 & 2 & -1 & & \\ & \ddots & \ddots & \ddots & \\ & & -1 & 2 & -1 \\ -T & & & -1 & 2 \end{bmatrix}.$$

For the untwisted fields we get

$$m_n^2 = 2u^{-2} \left(1 - \cos 2\pi \frac{n}{N} \right), \quad n = 1 \ldots N, \tag{5.9}$$

and for the twisted ones n is replaced by $n - \frac{1}{2}$. These mass spectra are identical with the mass spectra of real scalars and yields the usual (continuum) factor (-4) in the vacuum energy density between the two field species. Looking at the above mass spectra, we remark that the spectrum (5.9) for scalars and Wilson-modified fermions does not contain a zero mode in the case of twisted fields.

Let us now discuss the overall value of vacuum energy density ρ originating from the deconstruction model of Sec. 5.1. According to the discussion in Sec. 4.4, the gauge bosons and scalars give a negative contribution to the CC. Without bulk masses its magnitude

field	inverse lattice spacing a^{-1}	bulk mass M	MR
scalars Φ_i	$M_\mathrm{b} \sim 10^4 - 10^5\,\mathrm{eV}$	$m \sim 10^2\,\mathrm{GeV}$	$N \cdot 10^6$
gauge bosons A_i	$u \sim 10^{-2}\,\mathrm{eV}$	$v \sim 10^2\,\mathrm{GeV}$	$N \cdot 10^{13}$
fermions Ψ_i	$u \sim 10^{-2}\,\mathrm{eV}$	0	0

Table 5.1: The 4D fields in the deconstruction scenario of Sec. 5.1, which can be interpreted as KK modes of a 5D field on a transverse lattice. The bulk mass is denoted by M, and $R = Na$ is the circumference of $\mathcal{S}^1_\mathrm{lat}$ with N sites and a lattice spacing a. For large values of MR the Casimir effect will be highly suppressed according to Fig. 4.3 and Table 4.2. Only the fermions contribute significantly to the CC.

would of the order R^{-4}, where the size R of the ED is given by $R = Na$. For a small number N of lattice sites this would induce a large negative contribution $|\rho| \gg \rho_\mathrm{obs}$ to the CC due to the small lattice spacing $a^{-1} = M_\mathrm{b} \sim 10^{4\ldots5}\,\mathrm{eV}$ for the scalars Φ_i. Fortunately, the scalars and also the gauge bosons are equipped with large bulk masses, which sufficiently suppress the Casimir energy thereby avoiding serious problems with observations. In contrast to this, the fermionic fields with KK masses of the order of the small VEV $u \sim 10^{-2}\,\mathrm{eV}$ induce a positive contribution $(u/N)^4 \sim (10^{-3}\,\mathrm{eV})^4$ to the CC which is of the observed order of magnitude already for a small number $N = \mathcal{O}(1)$ of lattice sites. In Table 5.1 we give the relevant quantities for the vacuum energy suppression of the fields. Finally, it should be noted that we have determined only the vacuum energy contributions of quantum fields in the deconstruction setup which have a higher-dimensional correspondence. Other sources of vacuum energy could still lead to a CC that is in contrast with its observed value. Further discussions about dark energy in the context of discretised space-times and theory spaces can be in Refs. [73, 74, 75].

6 Dark Energy and Discretised Gravity

Up to now, we have ignored gravity in the ED since in the usual approach of deconstruction gravity is assumed to have completely decoupled from the matter fields. In a gravitational ED, however, the gravity field has a discrete structure, too. By transferring the methods of deconstruction to this new setup one obtains an effective theory of a discretised gravitational ED [31, 32]. One has found that the gravitons that arise in such a framework exhibit a non-trivial feature in the form of a strong coupling behaviour that might occur significantly below the usual scale, where the effective theory breaks down. In addition, this new strong coupling scale depends on the size of the ED thereby leading to a so-called UV/IR-connection. In this chapter we will investigate the vacuum energy arising from the Casimir effect of massive quantum fields, where the strong coupling scale sets an upper limit for the bulk field masses. To avoid Casimir energy densities above the observed value of the CC large bulk field masses are needed for small EDs, but here they cannot be arbitrarily large due to the strong coupling. Because of this feature and the UV/IR-connection we are able to derive a lower bound on the size of the ED [76].

In the next section we will briefly introduce the effective theory of one discrete gravitational ED and the strong coupling scale arising in this model. Afterwards we will discuss the Casimir energy in this setup and derive the bounds on the fifth dimension.

6.1 Gravitational Extra Dimensions

Since we will perform the discretisation of a 6D gravitational model in great detail in Chap. 7 we keep the discussion of the 5D case relatively short. In the following we therefore present mainly results from the literature. For the 5D case of this chapter, an effective theory for a single discrete ED has been recently proposed [31, 32] by implementing gravity in theory space similar to the concept of deconstruction. In this model gravity remains continuous in the bulk.

Let us consider the theory space as given by the moose diagram shown in Fig. 6.1. Each of the sites shown as circles corresponds to one general coordinate invariance (GC) symmetry GC_i with $i = 1 \dots N$ and can be identified with the 4D metric $g^i_{\mu\nu}$ for this site. Every site i is connected to its neighbouring site $i+1$ by the link field $Y_{i\mu}$, which transforms as a vector under the two neighbouring GCs. This is shown as an arrow connecting the GCs in the diagram. Moreover, the theory space and thus the ED is compactified on a circle by the identification $i + N = i$. Finally, we have on each site the usual 4D Einstein–Hilbert

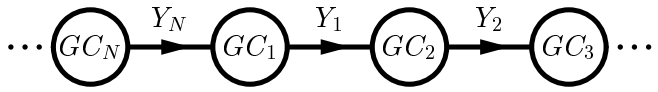

Figure 6.1: Part of the gravitational theory space for a discrete fifth dimension compactified on the circle $\mathcal{S}^1$. Each site corresponds to one general coordinate invariance GC_i $(i = 1, 2, \ldots, N)$, where two neighbouring sites i and $i+1$ are connected by one link field Y_i and we identify $i + N = i$.

action as described by

$$S^g_{\rm site} \;=\; \sum_{i=1}^{N} M_4^2 \int {\rm d}^4x\, \sqrt{|g^i|} R_{\rm 4D}(g^i), \tag{6.1}$$

where $R_{\rm 4D}(g^i)$ is the Ricci scalar on the site i, and M_4 denotes the universal Planck scale on the sites, which is related to the continuous Planck scale $M_{\rm Pl} = 1/\sqrt{8\pi G}$ by $M_4^2 = M_{\rm Pl}^2/N$ with G as the 4D Newton's constant. From Eq. (6.1) we observe, that the action $S^g_{\rm site}$ is invariant under the product group $\Pi_{i=1}^N GC_i$, which is explicitly broken to the diagonal GC by the gravitational interactions $S^g_{\rm link}$ between the sites. In our minimal discretisation with only nearest neighbour interactions, the action $S^g_{\rm link}$ has the form a Fierz-Pauli [77] mass term[1]

$$S^g_{\rm link} \;=\; \sum_{i=1}^{N} M_4^2 \int {\rm d}^4x\, \sqrt{|g^i|} m^2 (g^i_{\mu\nu} - g^{i+1}_{\mu\nu})(g^i_{\alpha\beta} - g^{i+1}_{\alpha\beta})(g^{i\mu\nu} g^{i\mu\nu} - g^{i\mu\alpha} g^{i\nu\beta}), \tag{6.2}$$

where the mass m corresponds to the inverse lattice spacing a^{-1}. The size of the fifth dimension is therefore given by $R = N/m$ and the 5D Planck scale by $M_5 = (M_{\rm Pl}^2/R)^{1/3}$, which defines the usual UV cutoff of the 5D theory. Let us now expand in the weak field limit the metrics $g^i_{\mu\nu}$ around flat space, $g^i_{\mu\nu} = \eta_{\mu\nu} + h^i_{\mu\nu}$, where $\eta_{\mu\nu}$ is the Minkowski metric. This leads to Fierz-Pauli graviton mass terms given by

$$S^{\rm FP}_{ij} = \int {\rm d}^4x\, M^2 m^2 (2\delta_{i,j} - \delta_{i,j+1} - \delta_{i,j-1})(h^i_{\mu\nu} h^{\mu\nu,j} - h^{\mu,i}_{\mu} h^{\nu,j}_{\nu}). \tag{6.3}$$

Note that this is the same mass matrix as for the gauge bosons and scalars in Sec. 5.1 implying the graviton mass spectrum

$$m_n^2 = 2m^2(1 - \cos(2\pi \frac{n}{N})) = 4m^2 \sin^2(\frac{\pi n}{N}), \quad n = 1, 2, \ldots, N. \tag{6.4}$$

This spectrum describes one diagonal zero-mode graviton which corresponds to the unbroken GC and a phonon-like spectrum of massive gravitons that approximates for $n \ll N$ a linear KK tower. At this level, the phenomenology of the model appears to be very similar to that of a deconstructed gauge theory. An important qualitative difference to deconstruction, however, reveals itself in the peculiar strong coupling effects of the theory.

[1] The Fierz-Pauli form for graviton mass terms ensures the absence of ghosts in the spectrum. For a recent discussion of ghosts in massive gravity, see Ref. [78]. For other aspects in this context see, e.g., Refs. [79, 80].

In Ref. [31] it was shown that the strong coupling behaviour is most conveniently discussed by making use of the Callan-Coleman-Wess-Zumino formalism for effective field theories [81]. Following this lead, the product symmetry group $\Pi_{i=1}^{N} GC_i$, which is broken by $S^g_{\rm link}$, can be formally restored in $S^g_{\rm link}$ by including Goldstone bosons. Therefore, one expands each link field around x^μ as $Y_i^\mu = x^\mu + \pi_i^\mu$, where the Goldstone bosons π_i^μ transform non–linearly under GC_i and GC_{i+1}. The massive Goldstone vector bosons, which have three degrees of freedom, are eaten by the massless gravitons with two degrees of freedom, to generate the five polarisations of the massive gravitons with the spectrum given by Eq. (6.4). Including the Goldstone bosons, the link action therefore acquires the form

$$\begin{aligned} S^g_{\rm link} &= \sum_{i=1}^{N} M_4^2 \int {\rm d}^4x \, \sqrt{|g^i|} m^2 (g^{i\mu\nu} g^{i\mu\nu} - g^{i\mu\alpha} g^{i\nu\beta}) && (6.5) \\ &\times \; (g^i_{\mu\nu} - \partial_\mu Y_i^\gamma \partial_\nu Y_i^\delta g^{i+1}_{\gamma\delta})(g^i_{\alpha\beta} - \partial_\alpha Y_i^\rho \partial_\beta Y_i^\sigma g^{i+1}_{\rho\sigma}). && (6.6) \end{aligned}$$

Let us further decompose the Goldstone bosons π_i^μ into its transverse A_i^μ and longitudinal ϕ_i components as $\pi_i^\mu = A_i^\mu + \partial_\mu \phi_i$. By using this form in Eq. (6.5) one finally obtains the interaction terms for the ϕ_i that are responsible for the strong coupling, they have the form

$$S^g_{\rm link} = \ldots (\partial^2 \phi)(\partial^2 \phi)(\partial^2 \phi). \tag{6.7}$$

Actually, the interactions of the lowest lying scalar longitudinal component ϕ of the Goldstone bosons lead to scattering amplitudes that quickly grow with the energy E of the scalars ϕ and lead to unitarity violation once the strong coupling scale is reached. For the present model it was found that the amplitude $\mathcal{A}(\phi\phi \to \phi\phi)$ for $\phi - \phi$ scattering is of the order $\mathcal{A} \sim E^{10}/\Lambda_4^{10}$, where

$$\Lambda_4 := \left(\frac{M_{\rm Pl}}{R^3} \right)^{1/4} \tag{6.8}$$

is the strong coupling scale of the theory, that is set by the triple vertex of ϕ as described by Eq. (6.7). From Eq. (6.8), it is seen that the UV cutoff scale Λ_4 of the effective theory depends on the IR scale R of the compactified ED. This phenomenon has been called UV/IR connection [32] since in a sensible effective theory for massive gravitons the lattice spacing $a = m^{-1}$ must always be larger than the minimal lattice spacing defined by $a_{\rm min} \sim \Lambda_4^{-1}$. This implies that the theory does not possess a naive continuum limit. In other words, for a given radius R, the effective theory is characterised by a highest possible number of lattice sites $N_{\rm max} = R\Lambda_4$, which limits how fine grained the lattice can be made.

In addition to the triple derivative coupling of ϕ, the Goldstone boson action contains other types of vertices, each of which can be associated with a characteristic strong coupling scale for that interaction [82]. As two such typical examples, we will consider the scales

$$\Lambda_3 = \left(\frac{M_{\rm Pl}}{R^2} \right)^{1/3} \quad \text{and} \quad \Lambda_5 = \left(\frac{M_{\rm Pl}}{R^4} \right)^{1/5}, \tag{6.9}$$

which we will later compare with Λ_4. It is important to note that here the existence of the strong coupling is qualitatively different from the UV cutoff in deconstructed gauge theories. The strong coupling scale in deconstruction associated with the non–linear sigma model approximation is of the order the inverse lattice spacing. Therefore deconstruction may provide, unlike the effective theory of massive gravitons discussed here, an UV completion of higher-dimensional gauge theories.

6.2 Bounds on the Size of the Extra Dimension

Let us now investigate the Casimir energies of matter fields propagating in the discrete fifth dimension introduced in the previous section. For this purpose, we treat the gravitational theory space as a flat background for quantum fields propagating in the space-time with a discretised fifth dimension. Since these Casimir energy densities contribute to the CC, we require that they lie below the observed value $\rho_{\rm obs} \sim 10^{-47}\,{\rm GeV}^4$, associated with the accelerated expansion of the universe. In Sec. 4.2 we have found that for massless bulk fields the 4D Casimir energy density ρ scales with the size R of the ED as $|\rho| \sim R^{-4}$, which would lead to a lower bound[2] $R \gtrsim (10^{-3}\,{\rm eV})^{-1} \sim 0,1\,{\rm mm}$. A much smaller size R becomes possible, if the bulk fields have nonzero masses M, which implies according to Sec. 4.5 an exponentially suppression for $M \gg R^{-1}$. In the discrete gravitational EDs, this suppression is only limited by the strong coupling scale Λ of the theory, since in a sensible effective field theory M should be smaller than the UV cutoff Λ. By virtue of the UV/IR connection, however, the cutoff Λ depends on R and can be much lower than the usual 4D Planck scale $M_{\rm Pl} \sim 10^{19}\,{\rm GeV}$. As a consequence, we expect from the Casimir effect a smallest possible value or lower limit on the size R, when M can at most be as large as the strong coupling scale Λ.

In the ED, the boundary conditions for the quantum fields can be periodic or anti–periodic corresponding to untwisted and twisted fields, respectively. We have found in Secs. 4.2 and 4.3 that the Casimir energy densities of these field configurations differ by a small factor and have opposite sign (ignoring the odd-even artefact). Following Eq. (4.12), the 4D Casimir energy density of a single untwisted real scalar field in the discretised fifth dimension can be written as

$$\rho_{\rm untwisted} = \frac{1}{2(2\pi)^3} \cdot \frac{4\pi}{8} \left[\sum_{n=1}^{N} m_n^4 \ln m_n - N \cdot \int_0^1 {\rm d}s \cdot m_s^4 \ln m_s \right], \tag{6.10}$$

where the ED has been integrated out. The mass spectrum m_n is given by Eq. (4.2) and reads $m_n^2 = 4m^2 \sin^2(\pi n/N) + M^2$. Furthermore, the variable s is treated in the integral as a continuous parameter which replaces n/N in the sine function. As long as the number of lattice sites is $N \gtrsim \mathcal{O}(10)$, the Casimir energy density on the transverse

[2] A scenario for obtaining the observed CC from a 5D Casimir effect of massless bulk matter fields with a sub–mm extra dimension has been proposed, e.g., in Ref. [83]. Current Cavendish–type experiments, however, put already very stringent upper bounds of the order $R \lesssim 0,1\,{\rm mm}$ on the possible size R of extra dimensions [84].

lattice in Eq. (6.10) differs less than $\lesssim 1\%$ from the value in the naive continuum limit $N \to \infty$, which is demonstrated in Fig. 4.3. In the remainder of this section, we will therefore employ the expressions for the Casimir energy densities of quantum fields in the continuum theory as discussed in Sec. 3.2. In this approximation, the vacuum energy density of a real (un)twisted scalar field reads

$$\rho_{\text{(un)twisted}} = \frac{\pm 1}{8(2\pi)^2} \frac{(2\pi)^5}{R^4} \int_x^\infty \mathrm{d}n \frac{(n^2 - x^2)^2}{\exp(2\pi n) \pm 1}, \tag{6.11}$$

where the plus and minus signs belong to twisted and untwisted fields, respectively, and $x = MR/(2\pi)$, in which M denotes the bulk mass of the scalar field. The integral in Eq. (6.11) can be performed exactly after neglecting the term ± 1 in the denominator. Hence, both densities differ only in an overall sign:

$$\rho_{\text{(un)twisted}} = \pm \frac{(MR)^2 + 3MR + 3}{(2\pi)^2 R^4} e^{-MR}. \tag{6.12}$$

When taking the sum of contributions for twisted and untwisted fields, the integrals must be added before carrying out the approximation, which gives

$$\rho_{\text{sum}} = -\frac{4(MR)^2 + 6MR + 3}{16(2\pi)^2 R^4} e^{-2MR}. \tag{6.13}$$

The corresponding energy densities of Dirac fermions are obtained by simply multiplying the scalar densities $\rho_{\text{(un)twisted}}$ by -4, where we assume that the fermion doubling has been taken care of, e.g., in the way discussed in Sec. 5.2. Note that the applied approximation works fine even in the limit of vanishing bulk masses $M \to 0$. The basic feature expressed in Eqs. (6.12) and (6.13) is that for large bulk masses $M \gg R^{-1}$, the energy density of massive matter fields becomes exponentially suppressed, which compensates for the large factor R^{-4} when R is comparatively small.

Now, we are in a position to calculate the Casimir energy densities with the bulk masses M set equal to the strong coupling scales Λ_3, Λ_4 and Λ_5 given in Eqs. (6.8) and (6.9). The effective field theory description suggests that these are the largest possible values that M can take in the gravitational theory space. If the UV cutoff Λ is much larger than $\sim R^{-1}$, the expressions in Eqs. (6.12) and (6.13) are dominated by the exponential damping factors, such that the Casimir energy densities are most strongly suppressed when M becomes of the order the strong coupling scale Λ, with $\Lambda = \Lambda_3, \Lambda_4, \Lambda_5$. Moreover, from Fig. 4.3 and Sec. 4.5 we know that this suppression is most effective, when the number of lattice sites N is maximised. Therefore we choose the inverse lattice spacing $m = N/R$ to be also of the order Λ.

Now the lower limit R_{min} on the size R of the ED emerges from requiring that the Casimir energy densities remain below the observed value $\rho_{\text{obs}} \sim 10^{-47}\,\text{GeV}^4$ of the dark energy density. The results for an untwisted scalar field and the sum of twisted and untwisted fields are plotted in Fig. 6.2. Since the smallest value R_{min} that R can take is due to the UV/IR connection a function of Λ, we have considered $R_{\text{min}}(\Lambda)$ for all three scales $\Lambda = \Lambda_3, \Lambda_4, \Lambda_5$. These values together with the corresponding maximum number of lattice

untwisted	$R_{\min}$	$\Lambda(R_{\min})$	$N = R_{\min} \cdot \Lambda(R_{\min})$
Λ_3	$6,1 \cdot 10^{-12}\,\mathrm{GeV}^{-1}$	$3,6 \cdot 10^{13}\,\mathrm{GeV}$	219
Λ_4	$9,0 \cdot 10^{-10}\,\mathrm{GeV}^{-1}$	$2,2 \cdot 10^{11}\,\mathrm{GeV}$	198
Λ_5	$1,1 \cdot 10^{-7}\,\mathrm{GeV}^{-1}$	$1,7 \cdot 10^{9}\,\mathrm{GeV}$	179

sum	$R_{\min}$	$\Lambda(R_{\min})$	$N = R_{\min} \cdot \Lambda(R_{\min})$
Λ_3	$8,2 \cdot 10^{-13}\,\mathrm{GeV}^{-1}$	$1,4 \cdot 10^{14}\,\mathrm{GeV}$	112
Λ_4	$6,6 \cdot 10^{-11}\,\mathrm{GeV}^{-1}$	$1,6 \cdot 10^{12}\,\mathrm{GeV}$	103
Λ_5	$4,4 \cdot 10^{-9}\,\mathrm{GeV}^{-1}$	$2,1 \cdot 10^{10}\,\mathrm{GeV}$	95

Table 6.1: The lower bounds $R_{\min}$ on the size R of the ED for an untwisted real scalar field and the sum of a twisted and an untwisted scalar. Additionally, the values of the strong coupling scale Λ and the number of lattice sites N are given when R is equal to $R_{\min}$. For the scale Λ, we considered each of the three choices $\Lambda = \Lambda_3, \Lambda_4, \Lambda_5$ from Eqs. (6.8) and (6.9). The lower bound $R_{\min}$ emerges from the requirement that the absolute Casimir energy density lies below the observed value ρ_{obs} of the DE density, when the bulk field mass M takes the largest possible value $M \sim \Lambda$.

sites $N = R_{\min} \cdot \Lambda(R_{\min})$, where $\Lambda(R_{\min})$ is the strong coupling scale associated with $R_{\min}$, are summarised in Tab. 6.1. Note that we can apply here the relations from the continuum theory, since the number N of lattice sites is of the order 10^2. Furthermore, the lattice calculation leads to energy densities (drawn as circles in Fig. 6.2), that agree very well with the values in the continuum theory. For $R_{\min}$ the values of the continuum and lattice formulas differ by about 15%, which is negligible, since the strong coupling scales $\Lambda_{3,4,5}$ from Eqs. (6.8) and (6.9) are order of magnitude estimates. For instance, the lattice calculation for an untwisted scalar field and $\Lambda = \Lambda_3$ gives $R_{\min} = 6.8 \cdot 10^{-12}\,\mathrm{GeV}^{-1}$, whereas the continuum approximation yields $R_{\min} = 6.1 \cdot 10^{-12}\,\mathrm{GeV}^{-1}$.

Let us now discuss the results. For the sum of a twisted and an untwisted field, we observe that the Casimir energy density of massive bulk fields exhibits a stronger suppression due to the different signs of both components. From Fig. 6.2, we read off that the minimal radius $R_{\min}$ of the discrete gravitational extra dimension lies in the range

$$(10^{12}\,\mathrm{GeV})^{-1} \lesssim R_{\min} \lesssim (10^{7}\,\mathrm{GeV})^{-1}, \tag{6.14}$$

where we typically find $\Lambda(R_{\min}) \sim 10^2 \times R_{\min}^{-1}$. For a radius R which is much smaller than the range given in Eq. (6.14), the Casimir energy densities of the bulk matter fields would significantly exceed ρ_{obs} and thus run into conflict with observation. Of course, there may be other possible sources of dark energy which might be responsible for the accelerated expansion of the universe, but it seems unlikely that they could exactly cancel the potentially large contributions from the Casimir effect in EDs.

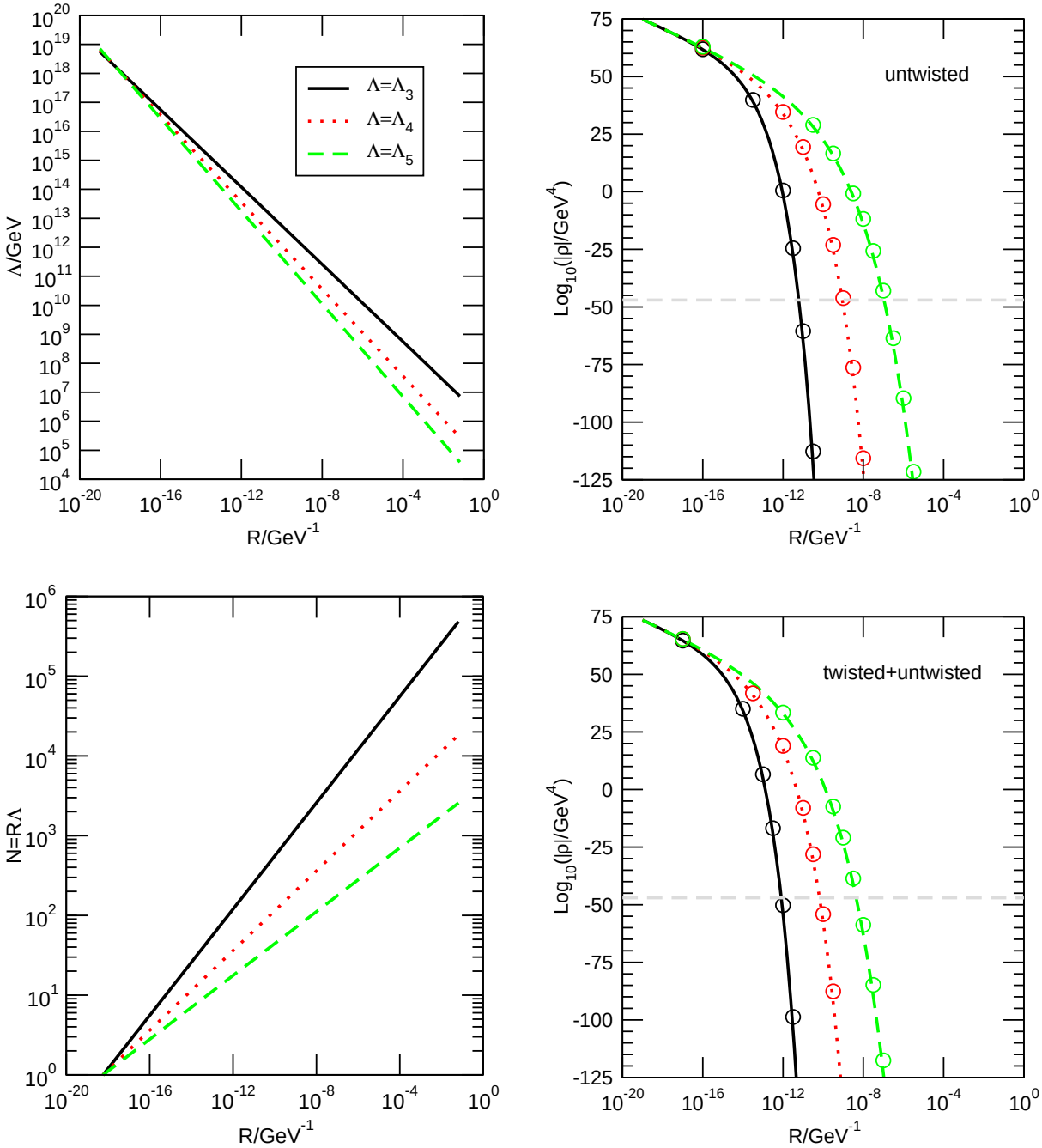

Figure 6.2: For the three choices $\Lambda = \Lambda_3, \Lambda_4, \Lambda_5$ of the strong coupling scale Λ from Eqs. (6.8) and (6.9), we have plotted the values of Λ, the Casimir energy densities ρ, and the corresponding number $N = R\Lambda$ of lattice sites as functions of the size R of the fifth dimension. The energy densities ρ are given for the untwisted scalar field, see Eq. (6.12), and for the sum of one untwisted and one twisted scalar field as given by Eq. (6.13). Note, that ρ is negative in both cases, and the bulk masses of the fields have their maximal values, given by Λ, according to Sec. 6.2. In the plots of ρ, the horizontal dashed line marks the observed value $\rho_{\text{obs}} \sim 10^{-47}\,\text{GeV}^4$ of the DE density and the circles represent exact lattice values from Eq. (6.10).

7 Discretised Curved Disk

This chapter is devoted to a special 6D model, where as before the 4D subspace is a flat Minkowski space-time. Both higher dimensions, however, form the discrete version of a disk with constant curvature. In the case of positive curvature, for example, the disk would be part of a 2-sphere. Moreover, we apply a very special discretisation, where on the disk boundary we place N lattice sites and only one site in the centre of the disk (Fig. 7.1). For gauge theories and gravitational EDs similar setups have been investigated before in Refs. [66, 85], but here we include the possibility that the disk has a constant curvature, too [86]. This more general case allows a flexible hierarchy in the mass structures of the effective 4D fields, which can be controlled entirely by the geometry parameters of the disk. Another motivation for the setup of this chapter was found in the context of multi-throat geometries, where the possibility of hiding large EDs was discussed [87].

In the following we will first discuss the 6D model in the continuum and show that it is a solution of Einstein's equations. Afterwards we explicitly derive the discretisation of the EDs and determine the mass spectrum for the effective 4D gravitons and the value for the effective 4D Planck mass. All these scales will be found to depend directly on the parameters of the curved disk. The explicit calculations also help to understand the 5D case of Sec. 6.1, especially the origin of the Fierz-Pauli graviton mass terms in Eq. (6.3) and the link action (6.2). Finally, we show how to implement fermions into this scenario, where we will find that the corresponding mass spectrum for the 4D fermions is directly related to the graviton spectrum. With these results we finally show a simple application to generate small fermion masses.

7.1 Curved Disk Geometry

Let us consider an effective field theory for massive gravitons, which arise after compactification of two gravitational EDs that have been discretised. We start out with a continuum theory, where 6D general relativity is compactified to four dimensions on a two-dimensional disk of constant curvature. In this space, the 6D coordinates are denoted by x^M with capital Latin letters $M = 0, 1, 2, 3, 5, 6$, while Greek letters appear in the usual 4D coordinates x^μ as $\mu = 0, 1, 2, 3$. The position of a point on the disk is described by the radial coordinate $r := x^5 \in [0, L]$ and the polar coordinate $\varphi := x^6 \in [0, 2\pi]$. The 6D Minkowski metric is given by $\eta_{MN} = \mathrm{diag}(1, -1, \ldots, -1)$. In the following, we consider a metric g_{MN} that is defined by the line element

$$\mathrm{d}s^2 = g_{\mu\nu}(x^M)\mathrm{d}x^\mu \mathrm{d}x^\nu - \frac{1}{1 - er^2}\mathrm{d}r^2 - r^2\mathrm{d}\varphi^2, \tag{7.1}$$

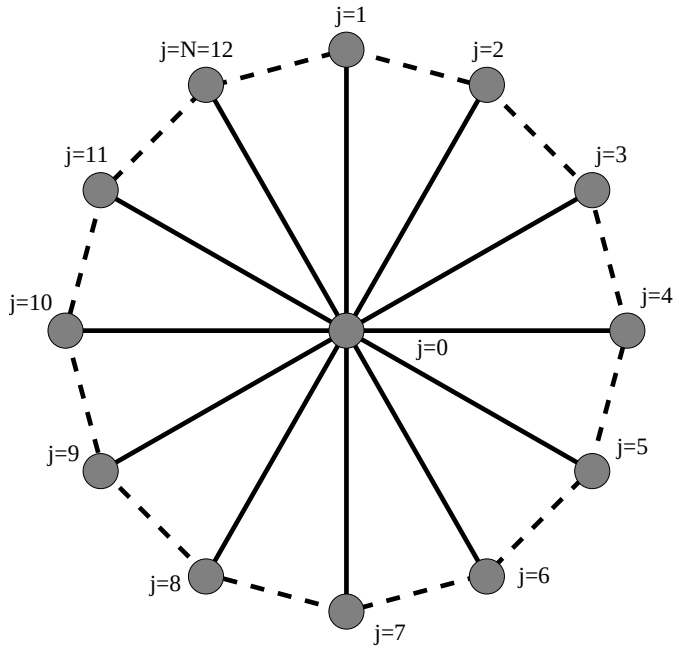

Figure 7.1: The curved disk model of Chap. 7 with a special discretisation, where N lattice sites are located on the boundary and only one site ($j = 0$) sits in the centre. In this example we chose $N = 12$. In the effective theory of massive 4D gravitons the solid lines in radial direction correspond to the mass scale $m_\star$ from Eq. (7.13), whereas m characterises the interactions in angular direction, which are shown as dashed lines.

where $1/\sqrt{|e|}$ is the curvature radius of the disk and $g_{\mu\nu}(x^M)$ the metric of the 4D subspace. Note that the parameter e controls the curvature of the disk, for $e > 0$ the disk is spherically curved, and $e < 0$ leads to a hyperbolic disk[1], respectively. $e = 0$ corresponds to a flat disk. From Eq. (7.1), we read off $g_{55} = -(1 - er^2)^{-1}$ and $g_{66} = -r^2$. We denote partial and covariant derivatives by commas and semicolons, respectively. Using $g_{55,5} = -2er/(1 - er^2)^2$ and $g_{66,5} = -2r$ we find for the non-zero Christoffel symbols

$$\begin{aligned}
\Gamma^\sigma_{\mu\nu} &= \overset{4D}{\Gamma}{}^\sigma_{\mu\nu}, \quad \Gamma^\mu_{\nu 5} = \frac{1}{2} g^{\mu\rho} g_{\nu\rho,5}, \quad \Gamma^\mu_{\nu 6} = \frac{1}{2} g^{\mu\rho} g_{\nu\rho,6}, \quad \Gamma^5_{\mu\nu} = -\frac{1}{2} g^{55} g_{\mu\nu,5}, \\
\Gamma^6_{\mu\nu} &= -\frac{1}{2} g^{66} g_{\mu\nu,6}, \quad \Gamma^5_{55} = \frac{1}{2} g^{55} g_{55,5} = \frac{er}{1 - er^2}, \\
\Gamma^5_{66} &= -\frac{1}{2} g^{55} g_{66,5} = -r(1 - er^2), \quad \Gamma^6_{56} = \frac{1}{2} g^{66} g_{66,5} = \frac{1}{r},
\end{aligned} \tag{7.2}$$

where $\overset{4D}{\Gamma}{}^\sigma_{\mu\nu} := \frac{1}{2} g^{\sigma\rho}(g_{\mu\rho,\nu} + g_{\rho\nu,\mu} - g_{\mu\nu,\rho})$. With our conventions the Riemann (curvature) tensor $R^A{}_{MND}$, the Ricci tensor R_{MN} and the Ricci scalar R are defined by

$$R^A{}_{MND} := \Gamma^A_{MD,N} - \Gamma^A_{MN,D} + \Gamma^A_{BN}\Gamma^B_{MD} - \Gamma^B_{MN}\Gamma^A_{BD},$$

$$R_{MN} := R^A{}_{MNA} = \Gamma^A_{MA,N} - \Gamma^A_{MN,A} + \Gamma^A_{BN}\Gamma^B_{MA} - \Gamma^B_{MN}\Gamma^A_{BA},$$

[1] Compact hyperbolic extra dimensions have been discussed, e.g., in Refs. [88, 89].

$$R := R_{MN} g^{MN}.$$

The 6D Einstein-Hilbert action[2] including a CC λ and some matter action S_{matter} reads

$$S = M_6^4 \int \mathrm{d}^6x \, \sqrt{|g|}(R - 2\lambda) + S_{\text{matter}}, \tag{7.3}$$

where $g = \det g_{MN}$ and M_6 denotes the 6D Planck scale. Note that in this chapter we denote the CC by the quantity λ, which has mass dimension two and is related to the vacuum energy density Λ via the Planck mass. The requirement that the variation δS with respect to the metric vanishes, leads to Einstein's equations

$$R_{MN} - \frac{1}{2} g_{MN} R + \Lambda g_{MN} = -\frac{1}{2M_6^4} T_{MN},$$

and the energy-momentum tensor T_{MN} follows from

$$\int \mathrm{d}^6x \sqrt{|g|} T_{MN} = 2 \frac{\delta S_{\text{matter}}}{\delta g^{MN}}.$$

Now we are interested in the Einstein-Hilbert action corresponding to the specific 6D metric given by Eq. (7.1). Under the 6D integral we therefore calculate $\sqrt{|g|}R = \sqrt{|g|}(g^{\mu\nu}R_{\mu\nu} + g^{55}R_{55} + g^{66}R_{66})$ in the following. The first term reads

$$\begin{aligned}
\sqrt{|g|} g^{\mu\nu} R_{\mu\nu} &= \sqrt{|g|} g^{\mu\nu} \big[\Gamma^\alpha_{\mu\alpha,\nu} - \Gamma^\alpha_{\mu\nu,\alpha} + \Gamma^\alpha_{\beta\nu}\Gamma^\beta_{\mu\alpha} - \Gamma^\beta_{\mu\nu}\Gamma^\alpha_{\beta\alpha} \\
&- \Gamma^5_{\mu\nu,5} + \Gamma^5_{\beta\nu}\Gamma^\beta_{\mu 5} + \Gamma^\alpha_{5\nu}\Gamma^5_{\mu\alpha} - \Gamma^5_{\mu\nu}\Gamma^A_{5A} \\
&- \Gamma^6_{\mu\nu,6} + \Gamma^6_{\beta\nu}\Gamma^\beta_{\mu 6} + \Gamma^\alpha_{6\nu}\Gamma^6_{\mu\alpha} - \Gamma^6_{\mu\nu}\Gamma^A_{6A} \big].
\end{aligned}$$

The derivative of the Christoffel symbol with respect to r (and similarly with respect to φ) can be written as

$$-\sqrt{|g|} g^{\mu\nu} \Gamma^5_{\mu\nu,5} = -\left[\sqrt{|g|} g^{\mu\nu} \Gamma^5_{\mu\nu} \right]_{,5} + \sqrt{|g|} g^{\mu\nu} \Gamma^A_{A5} \Gamma^5_{\mu\nu} - 2\sqrt{|g|} g^{\mu\alpha} \Gamma^\nu_{\alpha 5} \Gamma^5_{\mu\nu},$$

where on the right-hand side we have used $(\sqrt{|g|})_{,A} = \sqrt{|g|}\Gamma^B_{BA}$ in the second term and $g^{\mu\nu}{}_{,5} = -g^{\mu\alpha} g^{\nu\beta} g_{\alpha\beta,5} = -2 g^{\mu\alpha} \Gamma^\nu_{\alpha 5}$ in the third term. Thus we find

$$\sqrt{|g|} g^{\mu\nu} R_{\mu\nu} = \sqrt{|g|} R_{4\text{D}} - \left[\sqrt{|g|} g^{\mu\nu} \Gamma^5_{\mu\nu} \right]_{,5} - \left[\sqrt{|g|} g^{\mu\nu} \Gamma^6_{\mu\nu} \right]_{,6}$$

[2] In n space-time dimensions the Einstein-Hilbert action with Planck scale M_n reads

$$S = \int \mathrm{d}^n x \sqrt{|g|} M_n^{(n-2)} (R - 2\lambda) + S_{\text{matter}},$$

yielding Einstein's equations in the form

$$R_{MN} - \frac{1}{2} g_{MN} R + \lambda g_{MN} = -\frac{1}{2M_n^{(n-2)}} T_{MN}.$$

with R_{4D} denoting the usual 4D curvature scalar. Similarly we find for the other terms

$$\begin{aligned}
\sqrt{|g|}g^{55}R_{55} &= \sqrt{|g|}g^{55}\left[\Gamma^A_{5A,5} - \Gamma^A_{55,A} + \Gamma^A_{B5}\Gamma^B_{5A} - \Gamma^B_{55}\Gamma^A_{BA}\right] \\
&= \left[\sqrt{|g|}g^{55}\Gamma^A_{A5}\right]_{,5} - \left[\sqrt{|g|}g^{55}\Gamma^A_{55}\right]_{,A} \\
&+ \sqrt{|g|}g^{55}\big[2\Gamma^5_{55}\Gamma^A_{A5} - \Gamma^B_{B5}\Gamma^A_{A5} + \Gamma^B_{BA}\Gamma^A_{55} \\
&\quad -2\Gamma^5_{55}\Gamma^5_{55} + \Gamma^A_{B5}\Gamma^B_{A5} - \Gamma^B_{55}\Gamma^A_{BA}\big]. \\
&= \left[\sqrt{|g|}g^{55}\Gamma^A_{A5}\right]_{,5} - \left[\sqrt{|g|}g^{55}\Gamma^A_{55}\right]_{,A} \\
&+ \sqrt{|g|}g^{55}[\Gamma^\alpha_{\beta5}\Gamma^\beta_{\alpha5} - \Gamma^\alpha_{\alpha5}\Gamma^\beta_{\beta5} - 2\Gamma^\alpha_{\alpha5}\Gamma^6_{65}]
\end{aligned}$$

and

$$\begin{aligned}
\sqrt{|g|}g^{66}R_{66} &= \sqrt{|g|}g^{66}\left[\Gamma^A_{6A,6} - \Gamma^A_{66,A} + \Gamma^A_{B6}\Gamma^B_{6A} - \Gamma^B_{66}\Gamma^A_{BA}\right] \\
&= \left[\sqrt{|g|}g^{66}\Gamma^A_{A6}\right]_{,6} - \left[\sqrt{|g|}g^{66}\Gamma^A_{66}\right]_{,A} \\
&+ \sqrt{|g|}g^{66}\big[-2\Gamma^6_{56}\Gamma^5_{66} - \Gamma^B_{B6}\Gamma^A_{A6} + \Gamma^B_{BA}\Gamma^A_{66} \\
&\quad +\Gamma^A_{B6}\Gamma^B_{A6} - \Gamma^B_{66}\Gamma^A_{BA}\big]. \\
&= \left[\sqrt{|g|}g^{66}\Gamma^A_{A6}\right]_{,6} - \left[\sqrt{|g|}g^{66}\Gamma^A_{66}\right]_{,A} \\
&+ \sqrt{|g|}g^{66}[\Gamma^\alpha_{\beta6}\Gamma^\beta_{\alpha6} - \Gamma^\alpha_{\alpha6}\Gamma^\beta_{\beta6}].
\end{aligned}$$

Within these terms we collect all total derivatives that read altogether

$$\left[\sqrt{|g|}(-g^{\mu\nu}\Gamma^6_{\mu\nu} + g^{66}\Gamma^\alpha_{\alpha6})\right]_{,6} + \left[\sqrt{|g|}(-g^{\mu\nu}\Gamma^5_{\mu\nu} + g^{55}\Gamma^\alpha_{\alpha5} - g^{66}\Gamma^5_{66} + g^{55}\Gamma^6_{65})\right]_{,5},$$

where we now write the last two terms as

$$+ 2\sqrt{|g|}g^{55}\Gamma^\alpha_{\alpha5}\Gamma^6_{65} - 2\sqrt{|g|}g^{55}\Gamma^5_{55}\Gamma^6_{65}. \tag{7.4}$$

Here, we have used the relations $g^{66}\Gamma^5_{66} = -g^{55}\Gamma^6_{65}$ and $\Gamma^6_{65,5} = -(\Gamma^6_{65})^2$ following from Eqs. (7.2). Therefore, the first term in Eq. (7.4) cancels one term in $g^{55}R_{55}$ given above, and the last terms yields the cosmological term $\sqrt{|g|}(2e)$.

Finally, we are able to divide the 6D action (7.3) without matter into three parts,

$$S = S_{4D} + S_{\text{surface}} + S_{\text{mass}}, \tag{7.5}$$

where the (modified) Einstein-Hilbert action S_{4D} for the 4D subspace, the remaining surface terms S_{surface} and some terms S_{mass}, that will later become graviton mass terms, are respectively given by

$$S_{4D} := M_6^4 \int \mathrm{d}^6x\sqrt{|g|}\,(R_{4D} + 2e), \tag{7.6}$$

$$S_{\text{surface}} := M_6^4 \int \mathrm{d}^6x\,\left(2\left[\sqrt{|g|}g^{55}\Gamma^\alpha_{\alpha5}\right]_{,5} + 2\left[\sqrt{|g|}g^{66}\Gamma^\alpha_{\alpha6}\right]_{,6}\right) \tag{7.7}$$

$$\begin{aligned}
S_{\text{mass}} &:= M_6^4 \int \mathrm{d}^6x\sqrt{|g|}\,g^{55}[\Gamma^\alpha_{\beta5}\Gamma^\beta_{\alpha5} - \Gamma^\alpha_{\alpha5}\Gamma^\beta_{\beta5}]. \\
&+ M_6^4 \int \mathrm{d}^6x\sqrt{|g|}\,g^{66}[\Gamma^\alpha_{\beta6}\Gamma^\beta_{\alpha6} - \Gamma^\alpha_{\alpha6}\Gamma^\beta_{\beta6}].
\end{aligned} \tag{7.8}$$

Let us first consider S_{surface}, which reads in our setup

$$S_{\text{surface}} = M_6^4 \int \mathrm{d}^4x \int_0^{2\pi} \mathrm{d}\varphi \int_0^L \mathrm{d}r \left(\left[\sqrt{|g|} g^{55} g^{\mu\nu} g_{\mu\nu,5} \right]_{,5} + \left[\sqrt{|g|} g^{66} g^{\mu\nu} g_{\mu\nu,6} \right]_{,6} \right).$$

The φ-integral over the second term vanishes if we apply periodic boundary conditions, which is plausible for a disk, and the remaining term

$$S_{\text{surface}} = M_6^4 \int \mathrm{d}^4x \int_0^{2\pi} \mathrm{d}\varphi \left[\sqrt{|g|} g^{55} g^{\mu\nu} g_{\mu\nu,5} \right]_{r=0}^{r=L}, \tag{7.9}$$

can be also be removed by choosing appropriate boundary conditions at $r = 0$ and $r = L$. In addition, the lower limit would vanishes because of $\sqrt{|g|} g^{55} \propto r$ as long as $g_{\mu\nu}$ does not diverge at $r = 0$.

Furthermore, we write the mass term action in a simplified form given by

$$S_{\text{mass}} = M_6^4 \int \mathrm{d}^6x \sqrt{|g|} \sum_{c=5,6} \Big[-\frac{1}{4} g^{cc} g_{\mu\nu,c} (g^{\mu\nu} g^{\alpha\beta} - g^{\mu\alpha} g^{\nu\beta}) g_{\alpha\beta,c} \Big]. \tag{7.10}$$

Note that the naively discretised version of this equation would become in the 5D setup of Sec. 6.1 similar to Eq. (6.2), which will become more obvious in Sec. 7.5.

7.2 Solving Einstein's Equations

In this section we will find a simple solution of Einstein's equation for the 6D metric given by Eq. (7.1). For this purpose let us write the gravitational part of the 6D action (7.3) in the form

$$S = M_6^4 \int \mathrm{d}^6x \sqrt{|g|} \left[R - 2\lambda \cdot (g^{AB} n_{AB}) \right],$$

where we have introduced the tensor

$$n_{AB} := \mathrm{diag}(0, 0, 0, 0, \frac{1}{2} g_{55}, \frac{1}{2} g_{66}),$$

given in the coordinates of the previous section. The term involving λ is a modified cosmological term in the following sense. As long as we are working only with the action S as a number we can evaluate the expression $g^{AB} n_{AB} = n_A{}^A = 1$ and thus obtain standard 6D gravity with a 6D cosmological constant λ. However, if we want to derive Einstein's equations from the action functional $S[g_{AB}]$ we have to leave $g^{AB} n_{AB}$ unevaluated. The variational principle $\delta S / \delta g^{AB} = 0$ then gives 6D Einstein's equations

$$G_{MN} + g_{\mu\nu} \lambda = R_{MN} - \frac{1}{2} g_{MN} R + g_{\mu\nu} \lambda = 0$$

with a CC λ, that is located only within the whole 4D subspace described by the metric

$$g_{\mu\nu} := g_{MN} - 2 n_{MN} = \mathrm{diag}(g_{00}, g_{11}, g_{22}, g_{33}, 0, 0).$$

To calculate this we have used the relations $\frac{\delta(\sqrt{|g|}R)}{\delta g^{MN}} = \sqrt{|g|}G_{MN}$ and respectively

$$\begin{aligned}\frac{\delta(-2\lambda\sqrt{|g|}g^{AB}n_An_B)}{\delta g^{MN}} &= -2\lambda(-\frac{1}{2}\sqrt{|g|}g_{MN}g^{AB}n_{AB} + \sqrt{|g|}\delta^A_M\delta^B_N n_{AB}) \\ &= \lambda(g_{MN} - 2n_{MN}) = g_{\mu\nu}\lambda.\end{aligned}$$

We now apply the simple ansatz $g_{\mu\nu} = \eta_{\mu\nu} = \mathrm{diag}(1,-1,-1,-1)$ leading to

$$G_{MN} + g_{\mu\nu}\lambda = \begin{bmatrix} (-e+\lambda)\eta_{\mu\nu} & & \\ & 0 & \\ & & 0 \end{bmatrix},$$

which becomes a solution of Einstein's equations $G_{MN}+g_{\mu\nu}\lambda = 0$ by setting $\lambda = e$. In this case λ explicitly cancels the cosmological term in Eq. (7.6). In the next section we will investigate tensor fluctuations (gravitons) around the 4D Minkowski metric $\eta_{\mu\nu}$, which we have found to be a solution of Einstein's equations.

7.3 Massive 4D Gravitons

In Sec. 7.1 we have found the terms (7.10) that will become, as we show now, the mass terms for 4D gravitons. Let us first write S_{mass} in the form

$$\begin{aligned}S_{\mathrm{mass}} &= M_6^4 \int \mathrm{d}^4x \int \mathrm{d}\varphi\,\mathrm{d}r\,\sqrt{|g_4|}\Big[+ \frac{1}{4}r\sqrt{1-er^2}\partial_r g_{\mu\nu}(g^{\mu\nu}g^{\alpha\beta} - g^{\mu\alpha}g^{\nu\beta})\partial_r g_{\alpha\beta} \\ &\quad + \frac{1}{4}\frac{1}{r\sqrt{1-er^2}}\partial_\varphi g_{\mu\nu}(g^{\mu\nu}g^{\alpha\beta} - g^{\mu\alpha}g^{\nu\beta})\partial_\varphi g_{\alpha\beta}\Big],\end{aligned}$$

where we have used $\sqrt{|g|} = \sqrt{|g_4|}\sqrt{g_{55}g_{66}}$ in the second line. Then we introduce graviton fields $h_{\mu\nu}$ on a flat Minkowski metric $\eta_{\mu\nu}$ for the 4D subspace by the replacement

$$g_{\mu\nu} \to \eta_{\mu\nu} + h_{\mu\nu}.$$

Note that in our approach we ignore graviphoton and radion excitations, which could result from the g_{5M} and g_{6M} components of the metric. Since $\eta_{\mu\nu}$ is constant we have $g_{\mu\nu,A} \to h_{\mu\nu,A}$ and by expanding S_{mass} in second order in $h_{\mu\nu}$ we find

$$\begin{aligned}S_{\mathrm{mass}} &\to M_6^4 \int \mathrm{d}^4x \int \mathrm{d}\varphi\,\mathrm{d}r\,\Big[+ \frac{1}{4}r\sqrt{1-er^2}\partial_r h_{\mu\nu}(\eta^{\mu\nu}\eta^{\alpha\beta} - \eta^{\mu\alpha}\eta^{\nu\beta})\partial_r h_{\alpha\beta} \\ &\quad + \frac{1}{4}\frac{1}{r\sqrt{1-er^2}}\partial_\varphi h_{\mu\nu}(\eta^{\mu\nu}\eta^{\alpha\beta} - \eta^{\mu\alpha}\eta^{\nu\beta})\partial_\varphi h_{\alpha\beta}\Big].\end{aligned}$$

To obtain the discrete disk as described at the beginning of this chapter we perform the discretisation of the disk in the following way (Fig. 7.1). We put N points on the boundary and one point in centre of the disk so that only two points are lying in radial direction. The

coordinate distance between the centre point and every point on the boundary is given by the coordinate radius L of the disk, which in general differs from its proper radius. On the boundary we denote the graviton fields by $h^i_{\mu\nu}$ with $i = 1 \dots N$, and the position is given by $\varphi^i = i \cdot \Delta\varphi$, where $\Delta\varphi = 2\pi/N$ is the angular lattice spacing. The graviton field $h^0_{\mu\nu}$ in the centre carries the index 0, and the lattice spacing in radial direction is given by $\Delta r = L$. Explicitly, we discretise the disk by applying the following replacements to S_{mass}:

$$\begin{aligned}
\partial_r h(\varphi^i) &\to \frac{(h^i - h^0)}{\Delta r}, \\
\partial_\varphi h(\varphi^i) &\to \frac{(h^{i+1} - h^i)}{\Delta\varphi}, \\
\int \mathrm{d}r\, f(r) &\to \sum_{r=L} \Delta r \cdot f(L) = \Delta r \cdot f(L), \\
\int \mathrm{d}\varphi\, f(\varphi) &\to \sum_{i=1}^{N} \Delta\varphi \cdot f(\varphi^i).
\end{aligned} \tag{7.11}$$

Note that the integral $\int \mathrm{d}r$ is replaced by just one summation region of length L, where the summand is evaluated at the position $r = L$ to avoid problems with the derivative ∂_φ at $r = 0$. Thus we obtain for the mass terms on the discretised disk

$$\begin{aligned}
S_{\text{mass}} \;\to\; & M_6^4 \int \mathrm{d}^4x \sum_{i=1}^{N} \Delta\varphi \Delta r \\
\times\; & \left[+\frac{1}{4} L\sqrt{1 - eL^2} \cdot \frac{h^i_{\mu\nu} - h^0_{\mu\nu}}{\Delta r} (\eta^{\mu\nu}\eta^{\alpha\beta} - \eta^{\mu\alpha}\eta^{\nu\beta}) \frac{h^i_{\alpha\beta} - h^0_{\alpha\beta}}{\Delta r} \right. \\
& \left. + \frac{1}{4} \frac{1}{L\sqrt{1 - eL^2}} \cdot \frac{h^{i+1}_{\mu\nu} - h^i_{\mu\nu}}{\Delta\varphi} (\eta^{\mu\nu}\eta^{\alpha\beta} - \eta^{\mu\alpha}\eta^{\nu\beta}) \frac{h^{i+1}_{\alpha\beta} - h^i_{\alpha\beta}}{\Delta\varphi} \right],
\end{aligned}$$

which become more clear in the form

$$\begin{aligned}
S_{\text{mass}} \;\to\; & M_4^2 \int \mathrm{d}^4x \sum_{i=1}^{N} \\
\times\; & \left[+m_\star^2 \cdot (h^i_{\mu\nu} - h^0_{\mu\nu})(\eta^{\mu\nu}\eta^{\alpha\beta} - \eta^{\mu\alpha}\eta^{\nu\beta})(h^i_{\alpha\beta} - h^0_{\alpha\beta}) \right. \\
& \left. + m^2 \cdot (h^{i+1}_{\mu\nu} - h^i_{\mu\nu})(\eta^{\mu\nu}\eta^{\alpha\beta} - \eta^{\mu\alpha}\eta^{\nu\beta})(h^{i+1}_{\alpha\beta} - h^i_{\alpha\beta}) \right].
\end{aligned} \tag{7.12}$$

From the last line we observe immediately the relation to Eq. (6.2) that corresponds to the 5D case. Note that the actual graviton mass scale from the radial links, $m_\star$, and respectively from the angular links, m, depend on the 4D Planck mass M_4 of the observer's site (brane):

$$m_\star^2 := \frac{M_6^4}{M_4^2} \cdot \frac{1}{4} \cdot \frac{2\pi}{N} \cdot \sqrt{1 - eL^2}, \quad m^2 := \frac{M_6^4}{M_4^2} \cdot \frac{1}{4} \cdot \frac{N}{2\pi} \cdot \frac{1}{\sqrt{1 - eL^2}}. \tag{7.13}$$

However, the ratio of masses is independent of the Planck scales,

$$\frac{m_\star^2}{m^2} = \frac{(2\pi)^2}{N^2}(1 - eL^2), \tag{7.14}$$

which also shows that arbitrarily large hierarchies between $m_\star$ and m are possible by choosing eL^2 and N appropriately.

Therefore the 6D action of the curved disk with $\Lambda = e$,

$$S_{6\mathrm{D}} = M_6^4 \int \mathrm{d}^6x \, \sqrt{|g|} \left[R - 2\Lambda(g^{AB}n_{AB})\right],$$

becomes with the discretisation procedure from above and the expansion $g_{\mu\nu} \to \eta_{\mu\nu} + h_{\mu\nu}$

$$S_{6\mathrm{D}} \to M_6^4 \int \mathrm{d}^6x \sqrt{|g|} R_{4\mathrm{D}} + S_{\mathrm{mass}},$$

where S_{mass} is now given by Eq. (7.12).

7.4 4D Planck Scale on the Sites

Let us now turn to the determination of the 4D Planck mass M_4 on the sites. For this purpose we need to know the proper area of the curved disk that is given by

$$A := \int_0^{2\pi} \mathrm{d}\varphi \int_0^L \mathrm{d}r \sqrt{|g_{55}g_{66}|} = 2\pi \int_0^L \mathrm{d}r \frac{r}{\sqrt{1 - er^2}} = \begin{cases} \frac{2\pi}{e}(1 - \sqrt{1 - eL^2}), & e > 0 \\ \pi L^2, & e = 0 \\ \frac{2\pi}{|e|}(\sqrt{1 + |e|L^2} - 1), & e < 0. \end{cases} \tag{7.15}$$

For $|e|L^2 \ll 1$ we find that the area scales like $A = \pi L^2 + \mathcal{O}(eL^4)$ and for $e < 0$ the area grows approximately linearly with L for large values of eL^2: $A \approx 2\pi L/\sqrt{|e|}$. In the case $e > 0$ the coordinate range $r \in [0, 1/\sqrt{e}]$ covers one half of a 2-sphere with radius $1/\sqrt{e}$, thereby $r = 1/\sqrt{e}$ corresponds to the equator. The other half of the sphere can be described formally by the same metric and the coordinate range $r \in [-1/\sqrt{e}, 0]$, where $r \to 0$ with $r < 0$ means approaching the antipode. Thus the whole sphere has the usual area $4\pi/e$. Moreover, on the first half of the sphere the relation between the proper length s and the radial coordinate r is given by

$$s = \int_0^r \mathrm{d}r' \sqrt{|g_{55}|} = \int_0^r \mathrm{d}r' \frac{1}{\sqrt{1 - er^2}} \overset{e>0}{=} \left[\frac{1}{\sqrt{e}} \arcsin(\sqrt{e}r)\right]_0^r = \frac{1}{\sqrt{e}} \arcsin(\sqrt{e}r),$$

which is equal to the length of the arc on the right-hand side of Fig. 7.2.

For completeness we remark that in the hyperbolic disk case ($e < 0$) the proper distance s from the centre in radial direction is given by

$$s = \int_0^r \mathrm{d}r' \frac{1}{\sqrt{1 - er^2}} \overset{e<0}{=} \left[\frac{1}{\sqrt{|e|}} \operatorname{arsinh}(\sqrt{|e|}r)\right]_0^r = \frac{1}{\sqrt{|e|}} \operatorname{arsinh}(\sqrt{|e|}r),$$

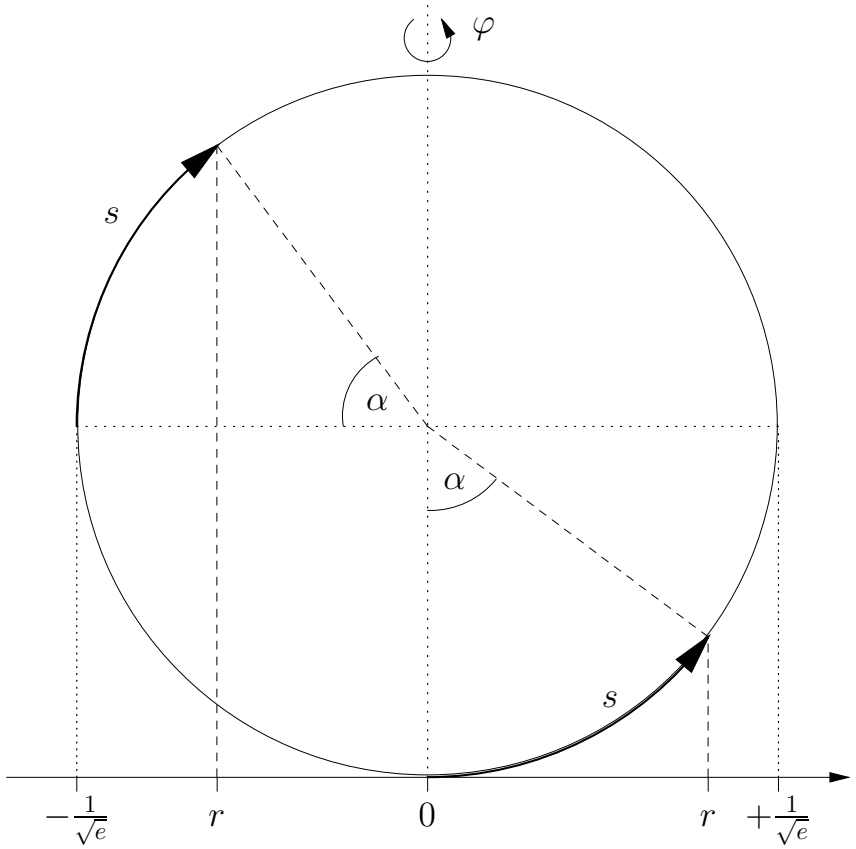

Figure 7.2: Illustration of the relation between the coordinate r and the corresponding proper length s for the spherically curved disk with $e > 0$. The first half of the sphere is described by the coordinate range $r \in [0, 1/\sqrt{e}]$, which covers the lower part of the sphere. The length s of the arc is given by $\alpha/\sqrt{e}$ with $\alpha = \arcsin(\sqrt{e}r)$. The upper part is covered by the range $r \in [-1/\sqrt{e}, 0]$, where $\alpha = \arcsin(\sqrt{e}r) + \pi/2$ and $r \leq 0$.

whereas for the flat case, $e = 0$, we simply find $s = r$.

We now proceed to discretise the term $M_6^4 \int \mathrm{d}^6x \sqrt{|g|} R_{4\mathrm{D}}$ from the modified 4D action (7.6). Since the extra-dimensional disk has a constant curvature it seems well motivated that also the 4D Planck scales M_4 should be constant and universal on all sites. Thus the $R_{4\mathrm{D}}$ terms of all $N+1$ sites have to take on the form

$$M_4^2 \sum_{i=0}^{N} \int \mathrm{d}^4x \ \sqrt{|g_4|} R_{4\mathrm{D}}\Big|_{\text{site } i} . \tag{7.16}$$

Since we cannot allow $R_{4\mathrm{D}}$ to depend on r and φ, we thus have

$$\sqrt{|g_4|} R_{4\mathrm{D}}\Big|_{\text{site } i} = \sqrt{|g_4|} R_{4\mathrm{D}}$$

for all sites i.

Now putting these parts together one finds that $M_6^4 \int \mathrm{d}^6x \sqrt{|g|} R_{4\mathrm{D}}$ has to be discretised

as

$$M_6^4 \underbrace{\int \mathrm{d}\varphi\, \mathrm{d}r\, \sqrt{|g_{55}g_{66}|}}_{\text{proper area } A} \int \mathrm{d}^4x\, \sqrt{|g_4|}R_{4\mathrm{D}} \;\rightarrow\; M_4^2 \sum_{i=0}^{N} \int \mathrm{d}^4x\; \sqrt{|g_4|}R_{4\mathrm{D}}\Big|_{\text{site } i} \tag{7.17}$$

$$= M_4^2 \sum_{i=0}^{N} \int \mathrm{d}^4x\, \sqrt{|g_4|}R_{4\mathrm{D}} \tag{7.18}$$

$$= M_4^2 (N+1) \int \mathrm{d}^4x\, \sqrt{|g_4|}R_{4\mathrm{D}}. \tag{7.19}$$

By comparing the left-hand side with the right-hand side the universal 4D site Planck scale is fixed,

$$M_4^2 = \frac{M_6^4 A}{N+1}, \tag{7.20}$$

where the proper disk area A as given in Eq. (7.15) is equally divided upon all sites. However, it is important to note that M_4 is not the (reduced) Planck scale $M_{\mathrm{Pl}} = 1/(8\pi G) \sim 10^{18}$ GeV that couples gravity to 4D matter. But M_{Pl} is determined by integrating out the EDs in the continuum, which means

$$M_6^4 \int \mathrm{d}^6x\, \sqrt{|g|}R_{4\mathrm{D}} = M_{\mathrm{Pl}}^2 \int \mathrm{d}^4x\, \sqrt{|g_4|}R_{4\mathrm{D}}.$$

From this we find as in the discretised 5D case of Sec. 6.1 the relation

$$M_{\mathrm{Pl}}^2 = M_6^4 A = (N+1)M_4^2. \tag{7.21}$$

In this section we have desisted from naively discretising the area integral $\int \mathrm{d}\varphi \mathrm{d}r\, \sqrt{|g_{55}g_{66}|}$ in $S_{4\mathrm{D}}$ since $\sqrt{g_{55}g_{66}} \propto r$ vanishes on the centre site and consequently there would not be a gravitational action. On the other hand, this strategy could be useful when considering a model, where the centre site just represents an auxiliary construction without physical relevance. However, we will not pursue this idea here any further.

Instead, we mention another possibility, where one could obtain a hierarchy between the centre and boundary sites. Let us consider for this purpose the spherically ($e > 0$) curved disk with L equal to its maximal value on both hemispheres of the sphere. In this case, we have a closed 2-sphere, where the centre sits on one point and all the boundary points sit on the antipode. This means effectively that there are only two points left. It might therefore appear "natural" to assign both points (centre and boundary) one half of the total area $2A$, which leads to

$$S = M_6^4 \int \mathrm{d}^6x \sqrt{|g|}R_{4\mathrm{D}} \rightarrow M_6^4 \left[A \int \mathrm{d}^4x\, \sqrt{|g_4|}R_0 + \sum_{i=1}^{N} \frac{A}{N} \int \mathrm{d}^4x\; \sqrt{|g_4|}R_{4\mathrm{D}}\Big|_{\text{site } i} \right].$$

We thus see that the squared 4D Planck mass on one boundary site would just be one N^{th} of the squared 4D Planck mass in the centre.

7.5 Graviton Mass Spectrum

Up to now we have determined the mass term action for 4D gravitons that follows from the discrete 6D model under consideration. Let us now determine the actual mass spectrum. First we apply the graviton expansion $g_{\mu\nu} = \eta_{\mu\nu} + h_{\mu\nu}$ of the 4D metric $g_{\mu\nu}$ also in the 4D curvature scalar $R_{4\mathrm{D}}$ that occurs in the gravitational terms $M_4^2 \sum_{i=0}^{N} \int \mathrm{d}^4x \, \sqrt{|g_4|} R_{4\mathrm{D}}$ for all sites. This leads to the kinetic terms for each graviton and was found to have the form [77, 90]

$$\sqrt{|g|}R_{4D} = \sqrt{|g_{55}\, g_{66}|}\frac{1}{4}(\partial^\mu h^{\nu\kappa}\partial_\mu h_{\nu\kappa} - \partial^\mu h \partial_\mu h - 2h^\mu h_\mu + 2h^\mu \partial_\mu h) + \mathcal{O}(h_{\mu\nu}^3), \qquad (7.22)$$

where the following relations have been used:

$$h := h^\mu{}_\mu, \quad h_\nu := \partial^\mu h_{\mu\nu}, \quad h^{\mu\nu} := \eta^{\mu\alpha}\eta^{\nu\beta}h_{\alpha\beta},$$
$$g^{\mu\nu} = \eta^{\mu\nu} - h^{\mu\nu} + h^{\mu\kappa}h_\kappa^\nu + \mathcal{O}(h_{\mu\nu}^3).$$

Up to second order in $h_{\mu\nu}$ we find that the whole graviton action, following from Eqs. (7.22) and (7.12), is given by

$$\begin{aligned} S_{\text{graviton}} &= M_4^2 \sum_{i=0}^{N} \int \mathrm{d}^4x \, \frac{1}{4}(\partial^\mu h^{i\nu\kappa}\partial_\mu h^i_{\nu\kappa} - \partial^\mu h^i \partial_\mu h^i - 2h^{i\mu}h^i_\mu + 2h^{i\mu}\partial_\mu h^i) \\ &+ M_4^2 \sum_{i=1}^{N} \int \mathrm{d}^4x \\ &\times \big[+m_\star^2 \cdot (h^i_{\mu\nu} - h^0_{\mu\nu})(\eta^{\mu\nu}\eta^{\alpha\beta} - \eta^{\mu\alpha}\eta^{\nu\beta})(h^i_{\alpha\beta} - h^0_{\alpha\beta}) \\ &\quad + m^2 \cdot (h^{i+1}_{\mu\nu} - h^i_{\mu\nu})(\eta^{\mu\nu}\eta^{\alpha\beta} - \eta^{\mu\alpha}\eta^{\nu\beta})(h^{i+1}_{\alpha\beta} - h^i_{\alpha\beta})\big], \end{aligned} \qquad (7.23)$$

where the mass scales $m_\star$ and m have been determined in Eq. (7.13).

Next we have to diagonalise the graviton mass terms by a unitary transformation. As mentioned in Sec. 7.4 we choose the site Planck scales M_4 to be universal and fixed as in Eq. (7.20). Then the squared $(N+1)$-dimensional mass matrix M^2 in the basis $(h^0_{\mu\nu}, h^1_{\mu\nu}, \ldots, h^N_{\mu\nu})$ has the following form

$$M^2 = m_\star^2 \begin{pmatrix} N & -1 & -1 & \cdots & -1 \\ -1 & 1 & & & \\ -1 & & 1 & & \\ \vdots & & & \ddots & \\ -1 & & & & 1 \end{pmatrix} + m^2 \begin{pmatrix} 0 & 0 & 0 & \ldots & 0 \\ 0 & 2 & -1 & & -1 \\ 0 & -1 & 2 & \ddots & \\ \vdots & & \ddots & \ddots & -1 \\ 0 & -1 & & -1 & 2 \end{pmatrix}, \qquad (7.24)$$

where the first matrix proportional to $m_\star$ originates from the interactions in radial direction. The second matrix comes from the angular interactions and is very similar to the gauge boson mass matrix described by Eq. (5.3). Fortunately, both matrices can be diagonalised simultaneously by a unitary transformation. When we denote the graviton

mass eigenstates by $H^n_{\mu\nu}$ corresponding to the mass M_n, we find the following relations for the eigenvectors:

$$H^0_{\mu\nu} = \frac{1}{\sqrt{N+1}} \sum_{i=0}^{N} h^i_{\mu\nu}, \tag{7.25}$$

$$H^p_{\mu\nu} = \frac{1}{\sqrt{N}} \sum_{i=1}^{N} \left[\sin(2\pi i \tfrac{p}{N}) + \cos(2\pi i \tfrac{p}{N})\right] \cdot h^i_{\mu\nu}, \tag{7.26}$$

$$H^N_{\mu\nu} = \frac{1}{\sqrt{N(N+1)}} \left[-N \cdot h^0_{\mu\nu} + \sum_{i=1}^{N} h^i_{\mu\nu}\right], \tag{7.27}$$

where $p = 1 \ldots N-1$. The eigenvalues M_n are respectively given by

$$M_0^2 = 0 \tag{7.28}$$

$$M_p^2 = m_\star^2 + 4m^2 \sin^2 \frac{\pi p}{N}, \tag{7.29}$$

$$M_N^2 = (N+1) m_\star^2. \tag{7.30}$$

From these results we observe that the zero-mode $H^0_{\mu\nu}$ has a flat profile and is equally located on all sites, whereas the mode $H^N_{\mu\nu}$ with squared mass $(N+1)m_\star^2$ is peaked on the centre site with equal support on the boundary sites. The $N-1$ modes $H^p_{\mu\nu}$ with $p = 1 \ldots N-1$ are located only on the boundary with a typical discrete KK mass spectrum like Eq. (4.2) that has been shifted by $m_\star^2$. In the limit $m \ll m_\star$ the masses of the states $H^p_{\mu\nu}$ from Eq. (7.26) become degenerate, and for $N \gg 1$ the mode $H^N_{\mu\nu}$ becomes very heavy.

Finally, we remark that a scenario related to ours has been discussed recently in the context of multi-throat geometries [87]. It was shown that large EDs can be hidden in the sense that the occurrence of massive KK modes is shifted to energies much higher than the compactification scale of the ED, which helps evading limits on KK particles and other bounds [25, 26, 27]. This behaviour can be observed here for the modes $H^{n>0}_{\mu\nu}$ in the limit $m_\star \gg m$, too.

7.6 Fermions on the Disk

Let us now investigate the incorporation of Dirac fermions into the discretised disk model of Sec. 7.1. As in the graviton case we start with a 6D Dirac fermion Ψ in the continuum. Using the vielbein formalism [91], the corresponding action S on the curved disk reads [16]

$$S = \int \mathrm{d}^6x \sqrt{|g|} \left[\frac{1}{2} i \left(\overline{\Psi} G^A V_A^M \nabla_M \Psi - \overline{\nabla_M \Psi} V_A^M G^A \Psi\right)\right], \tag{7.31}$$

where we denote 6D Lorentz indices by $A, B, \ldots$ and general coordinate indices by $M, N, \ldots$, respectively. Moreover, we call G^A the 6D Dirac matrices, and for the barred spinor $\overline{\Psi}$ we

use the abbreviation $\overline{\Psi} = \Psi^\dagger G^0$. The vielbein components $V_A^M(x^N)$ follow from the relation $g_{MN} = V_M^A V_N^B \eta_{AB}$, which connects the Lorentz coordinate system with the general coordinate system. For the diagonal metric given by Eq. (7.1),

$$\mathrm{d}s^2 = g_{\mu\nu}(x^M)\mathrm{d}x^\mu \mathrm{d}x^\nu - \frac{1}{1-er^2}\mathrm{d}r^2 - r^2\mathrm{d}\varphi^2, \tag{7.32}$$

we find $V_M^A = \delta_M^A$ with the exceptions $V_{M=5}^{A=5} = \sqrt{|g_{55}|}$ and $V_{M=6}^{A=6} = \sqrt{|g_{66}|}$. To avoid confusion with indices we denote the inverse vielbein components by

$$V_5 := V_{A=5}^{M=5} = \sqrt{|g^{55}|} \;\text{ and }\; V_6 := V_{A=6}^{M=6} = \sqrt{|g^{66}|},$$

respectively. On a curved space-time the covariant derivative $\nabla_M = \partial_M + \Gamma_M$ for spinors contains in addition to the usual partial derivative ∂_M also the spin connection

$$\Gamma_M = \frac{1}{8}[G^A, G^B]V_A^N V_{BN;M}. \tag{7.33}$$

To determine the form of the 6D γ-matrices [62] let us first look at the 4D case, where the γ-matrices are given by

$$\gamma^0 = \begin{bmatrix} 0 & 1_2 \\ 1_2 & 0 \end{bmatrix},\ \gamma^k = \begin{bmatrix} 0 & \sigma^k \\ -\sigma^k & 0 \end{bmatrix},\ \gamma^5 = i\gamma_0\gamma_1\gamma_2\gamma_3 = \begin{bmatrix} -1 & 0 \\ 0 & +1 \end{bmatrix},$$

where $k = 1\ldots3$ and σ^k denote the Pauli matrices. This set of matrices has the properties

$$(\gamma^0)^\dagger = \gamma^0,\ (\gamma^k)^\dagger = -\gamma^k,\ (\gamma^5)^\dagger = \gamma^5,\ \{\gamma^5, \gamma^\mu\} = 0$$

with the anti-commutator $\{\Box, \Box\}$. In five dimensions the number of spinor components is still four and the corresponding γ-matrices are simply given by $\Gamma^0 = \gamma^0$, $\Gamma^k = \gamma^k$ and $\Gamma^5 = i\gamma^5 = -(\Gamma^5)^\dagger$.

In six dimensions, however, the Dirac algebra is 8-dimensional. Here, we use the following set of γ-matrices

$$\begin{aligned} G^0 &= \begin{bmatrix} 0 & 1_4 \\ 1_4 & 0 \end{bmatrix} = (G^0)^\dagger, \\ G^n &= \begin{bmatrix} 0 & \Gamma^0\Gamma^n \\ -\Gamma^0\Gamma^n & 0 \end{bmatrix} = -(G^n)^\dagger, \quad n = 1,2,3,5, \\ G^6 &= \begin{bmatrix} 0 & \Gamma^0 \\ -\Gamma^0 & 0 \end{bmatrix} = -(G^6)^\dagger, \end{aligned}$$

which fulfil the Cifford algebra $\{G^A, G^B\} = 2\eta^{AB} \cdot 1_8$. Furthermore, in 6D one can also define a chirality matrix G_c by

$$G_c = G^0G^1G^2G^3G^5G^6 = \begin{bmatrix} -1_4 & 0 \\ 0 & 1_4 \end{bmatrix} = G_c^\dagger,$$

which satisfies $G_c^2 = 1$ and $\{G_c, G^A\} = 0$.

From the form of the vielbeins and the γ-matrices it follows that the terms $V_{BN;M}$ that occur in the spin connection[3] Γ_M vanish except for $V_{(B=6,N=5);6} = 1$ and $V_{(B=5,N=6);6} = -r\sqrt{1-er^2}$, which leads to

$$\begin{aligned}\Gamma_6 &= \frac{1}{8}[G^5,G^6]V_5V_{B=6,N=5;6} + \frac{1}{8}[G^6,G^5]V_6V_{B=5,N=6;6} \\ &= \frac{1}{4}[G^5,G^6]\sqrt{1-er^2} = \frac{1}{2}iV_5\begin{bmatrix}\gamma^5 & 0\\ 0 & \gamma^5\end{bmatrix} = -\Gamma_6^\dagger,\end{aligned}$$

while all other components $\Gamma_{M\neq 6}$ vanish. Finally, we observe that in the action (7.31) the term involving Γ_6,

$$\frac{1}{2}i\left(\overline{\Psi}G^6V_6\Gamma_6\Psi - \overline{\Gamma_6\Psi}G^6V_6\Psi\right),$$

vanishes because of $\overline{\Gamma_6\Psi}G^6 = \Psi^\dagger\Gamma_6^\dagger G_0G_6 = \overline{\Psi}G^6\Gamma_6$.

Let us now diagonalise the action by the substitution $\Psi := G^6\Phi$, which yields $\overline{\Psi} = -\Phi^\dagger G^6G^0$ and respectively

$$i\overline{\Psi}G^AV_A^M\nabla_M\Psi = i\Phi^\dagger\begin{bmatrix}-\Gamma^0 & 0\\ 0 & \Gamma^0\end{bmatrix}\left[G^0\partial_0 + G^k\partial_k + V_5G^5\partial_5 + V_6G^6\partial_6\right]G^6\Phi$$

in the action (7.31). It turns out that all the products G^AG^6 are block diagonal and if we decompose the eight-component spinor $\Phi = (\Phi_a,\Phi_b)^{\mathrm{T}}$ into two four-component spinors Φ_a, Φ_b the last line reads

$$\begin{aligned}i\left[\overline{\Phi_a},\overline{\Phi_b}\right] \times \Bigg[&\begin{pmatrix}\gamma^0 & 0\\ 0 & \gamma^0\end{pmatrix}\partial_0 + \begin{pmatrix}-\gamma^k & 0\\ 0 & \gamma^k\end{pmatrix}\partial_k \\ &+\begin{pmatrix}-i\gamma^5 & 0\\ 0 & +i\gamma^5\end{pmatrix}V_5\partial_5 + \begin{pmatrix}1 & 0\\ 0 & -1\end{pmatrix}V_6\partial_6\Bigg] \times \begin{bmatrix}\Phi_a\\ \Phi_b\end{bmatrix}\end{aligned}$$

with $\overline{\Phi_{a,b}} = \Phi_{a,b}^\dagger\gamma^0$. From this one can read off that Φ_a corresponds to Φ_b but with negative energy, therefore we will work only with Φ_b in the following. If we now denote the left- and right-handed components of Φ_b by $\Phi_{\mathrm{L,R}} := \frac{1}{2}(1\mp\gamma^5)\Phi_b$, then the full action for Φ_b can be written in the form

$$\begin{aligned}S &= \int \mathrm{d}^6x\sqrt{|g|}\Big[\frac{1}{2}i\left(\overline{\Phi_b}\gamma^\mu\partial_\mu\Phi_b - \overline{\partial_\mu\Phi_b}\gamma^\mu\Phi_b\right) \\ &- V_5\frac{1}{2}\left(\overline{\Phi_{\mathrm{L}}}\partial_5\Phi_{\mathrm{R}} - \overline{\Phi_{\mathrm{R}}}\partial_5\Phi_{\mathrm{L}} - \overline{\partial_5\Phi_{\mathrm{L}}}\Phi_{\mathrm{R}} + \overline{\partial_5\Phi_{\mathrm{R}}}\Phi_{\mathrm{L}}\right) \\ &- iV_6\frac{1}{2}\left(\overline{\Phi_{\mathrm{L}}}\partial_6\Phi_{\mathrm{R}} + \overline{\Phi_{\mathrm{R}}}\partial_6\Phi_{\mathrm{L}} - \overline{\partial_6\Phi_{\mathrm{L}}}\Phi_{\mathrm{R}} - \overline{\partial_6\Phi_{\mathrm{R}}}\Phi_{\mathrm{L}}\right)\Big].\end{aligned}$$

In the last line let us further transform both middle terms by an integration by parts and apply periodicity conditions with respect to the φ-coordinate:

$$\int_0^{2\pi}\mathrm{d}\varphi\left(\overline{\Phi_{\mathrm{R}}}\partial_6\Phi_{\mathrm{L}} - \overline{\partial_6\Phi_{\mathrm{L}}}\Phi_{\mathrm{R}}\right) = \left[\overline{\Phi_{\mathrm{R}}}\Phi_{\mathrm{L}} - \overline{\Phi_{\mathrm{L}}}\Phi_{\mathrm{R}}\right]_0^{2\pi} - \int_0^{2\pi}\mathrm{d}\varphi\left(\overline{\partial_6\Phi_{\mathrm{R}}}\Phi_{\mathrm{L}} - \overline{\Phi_{\mathrm{L}}}\partial_6\Phi_{\mathrm{R}}\right).$$

[3]Note that we use subscript indices for the spin connection Γ_M and superscript indices for the 5D γ-matrices Γ^A.

And for both middle terms in the second line we respectively obtain

$$\begin{aligned}\int_0^L \mathrm{d}r\sqrt{|g_{55}g_{66}|}V_5\left(-\overline{\Phi_\mathrm{R}}\partial_5\Phi_\mathrm{L}-\overline{\partial_5\Phi_\mathrm{L}}\Phi_\mathrm{R}\right) &= \left[-r\overline{\Phi_\mathrm{R}}\Phi_\mathrm{L}-r\overline{\Phi_\mathrm{L}}\Phi_\mathrm{R}\right]_0^L \\ &- \int_0^L \mathrm{d}r\left(-\overline{\Phi_\mathrm{R}}\Phi_\mathrm{L}-\overline{\Phi_\mathrm{L}}\Phi_\mathrm{R}\right) \\ &- \int_0^L \mathrm{d}r\cdot\sqrt{|g_{66}|}\left(-\overline{\partial_5\Phi_\mathrm{R}}\Phi_\mathrm{L}-\overline{\Phi_\mathrm{L}}\partial_5\Phi_\mathrm{R}\right).\end{aligned}$$

By using the same discretisation prescription

$$-\int_0^L \mathrm{d}r\left(-\overline{\Phi_\mathrm{R}}\Phi_\mathrm{L}-\overline{\Phi_\mathrm{L}}\Phi_\mathrm{R}\right)\to L\left[\overline{\Phi_\mathrm{R}}\Phi_\mathrm{L}+\overline{\Phi_\mathrm{L}}\Phi_\mathrm{R}\right]_{r=L}$$

as given in Eq. (7.11) for the gravitons in Sec. 7.3, we find that only the terms in the last line will survive in the end.

Since 6D spinors have mass dimension $\frac{5}{2}$ we have to rescale them in order to obtain usual 4D spinors. As in the graviton case we will integrate the kinetic terms over the EDs and also apply a similar discretisation procedure as in Sec. 7.4, which means

$$\int \mathrm{d}^6x\sqrt{|g|}\frac{1}{2}i\overline{\Phi_b}\gamma^\mu\partial_\mu\Phi_b\to\sum_{j=0}^{N}\frac{A}{N+1}\int \mathrm{d}^4x\frac{1}{2}i\overline{\Phi_b^j}\gamma^\mu\partial_\mu\Phi_b^j,$$

where A is the proper area of the EDs as given in Eq. (7.15). Finally we absorb the factor $A/(N+1)$ into the fermion fields $\chi := \Phi_b\sqrt{A/(N+1)}$ and subsequently apply the discretisations

$$\begin{aligned}\partial_5\chi &\to (\chi^j-\chi^0)/\Delta r, \\ \partial_6\chi &\to (\chi^{j+1}-\chi^j)/\Delta\varphi, \\ \int \mathrm{d}r\mathrm{d}\varphi\cdot f &\to \sum_{j=1}^{N}\Delta r\Delta\varphi\cdot f^j,\end{aligned} \tag{7.34}$$

where we also use $\Delta r = L$ and $\Delta\varphi = 2\pi/N$. Note that in radial direction we cannot use a symmetric derivative as in Sec. 4.3 since there are only two lattice points available. For the derivative in radial direction we will later on consider a more symmetric form. As a result we obtain the action for $N+1$ 4D fermions,

$$\begin{aligned}S &= \sum_{j=0}^{N}\int \mathrm{d}^4x\frac{1}{2}i\left(\overline{\chi^j}\gamma^\mu\partial_\mu\chi^j-\overline{\partial_\mu\chi^j}\gamma^\mu\chi^j\right) \\ &- \sum_{j=1}^{N}\int \mathrm{d}^4x\cdot m_\star\left(\overline{\chi_\mathrm{L}^j}(\chi_\mathrm{R}^j-\chi_\mathrm{R}^0)+(\overline{\chi_\mathrm{R}^j}-\overline{\chi_\mathrm{R}^0})\chi_\mathrm{L}^j\right) \\ &- \sum_{j=1}^{N}\int \mathrm{d}^4x\cdot i\cdot m\left(\overline{\chi_\mathrm{L}^j}(\chi_\mathrm{R}^{j+1}-\chi_\mathrm{R}^j)-(\overline{\chi_\mathrm{R}^{j+1}}-\overline{\chi_\mathrm{R}^j})\chi_\mathrm{L}^j\right),\end{aligned}$$

where the mass scales read

$$\begin{aligned} m_\star &:= \Delta r \Delta\varphi \sqrt{|g_{55} g_{66}|} V_5 \frac{N+1}{A} \frac{1}{\Delta r} = \frac{2\pi(N+1)L}{NA}, \\ m &:= \Delta r \Delta\varphi \sqrt{|g_{55} g_{66}|} V_6 \frac{N+1}{A} \frac{1}{\Delta\varphi} = \frac{(N+1)L}{A\sqrt{1-eL^2}}. \end{aligned}$$

Note that the ratio $m_\star/m$ is the same as in Eq. (7.14) for the gravitons. However, the mass terms are different and can be written symbolically in the form

$$M = m_\star \cdot \begin{bmatrix} & \chi_{\rm R}^0 & \chi_{\rm R}^1 & \chi_{\rm R}^2 & \cdots \\ \overline{\chi_{\rm L}^0} & 0 & 0 & 0 & \\ \overline{\chi_{\rm L}^1} & -1 & 1 & & \\ \overline{\chi_{\rm L}^2} & -1 & & 1 & \\ \vdots & \vdots & & & \ddots \end{bmatrix} + im \cdot \begin{bmatrix} & \chi_{\rm R}^0 & \chi_{\rm R}^1 & \chi_{\rm R}^2 & \cdots \\ \overline{\chi_{\rm L}^0} & 0 & 0 & 0 & \\ \overline{\chi_{\rm L}^1} & 0 & -1 & 1 & \\ \overline{\chi_{\rm L}^2} & 0 & & -1 & 1 \\ \vdots & \vdots & & & \ddots \end{bmatrix}.$$

In order to find the mass eigenvalues we apply a bi-unitary transformation meaning that left- and right-handed fields transform differently. Thus the states χ and the mass eigenstates ψ are related by

$$\begin{aligned} \overline{\chi_{\rm L}^0} &= \overline{\psi_{\rm L}^0} \\ \overline{\chi_{\rm L}^j} &= \frac{1}{\sqrt{N}} \sum_{n=1}^{N} \exp(+2\pi i \cdot j \frac{n}{N}) \overline{\psi_{\rm L}^n} \\ \chi_{\rm R}^0 &= \frac{1}{\sqrt{N+1}} \psi_{\rm R}^0 - \frac{N}{\sqrt{N(N+1)}} \psi_{\rm R}^N \\ \chi_{\rm R}^j &= \frac{1}{\sqrt{N}} \sum_{n=1}^{N-1} \exp(-2\pi i \cdot j \frac{n}{N}) \psi_{\rm R}^n + \frac{1}{\sqrt{N+1}} \psi_{\rm R}^0 + \frac{1}{\sqrt{N(N+1)}} \psi_{\rm R}^N. \end{aligned} \tag{7.35}$$

Expressed by the mass eigenstates ψ the action S for $N+1$ 4D Dirac fermions reads

$$\begin{aligned} S &= \sum_{j=0}^{N} \int {\rm d}^4x \left[\frac{1}{2} i \left(\overline{\psi^j} \gamma^\alpha \partial_\alpha \psi^j - \overline{\partial_\alpha \psi^j} \gamma^\alpha \psi^j \right) \right. \\ &- \sum_{j=1}^{N-1} \int {\rm d}^4x \cdot \overline{\psi_{\rm L}^j} \psi_{\rm R}^j [m_\star + im(e^{-2\pi i \frac{n}{N}} - 1)] + \overline{\psi_{\rm R}^j} \psi_{\rm L}^j [m_\star - im(e^{2\pi i \frac{n}{N}} - 1)] \\ &- \left. m_\star \sqrt{N+1} \left(\overline{\psi_{\rm L}^N} \psi_{\rm R}^N + \overline{\psi_{\rm R}^N} \psi_{\rm L}^N \right) \right]. \end{aligned}$$

From this result we read off that there is one massless fermion ψ^0, one heavy fermion ψ^N with mass $m_\star\sqrt{N+1}$ and $N-1$ fermions $\psi^1, \ldots, \psi^{N-1}$ with complex masses, whose squared absolute values read

$$|m_\star + im(e^{-2\pi i \frac{n}{N}} - 1)|^2 = m_\star^2 + 4m^2 \sin^2(\frac{\pi n}{N}) + 2m_\star m \sin(\frac{2\pi n}{N}).$$

In contrast to the graviton case from Eq. (7.29), here we find an additional interference term $2m_\star m \sin(\frac{2\pi n}{N})$ in the mass spectrum. Since this looks a bit strange we propose a slightly modified discretisation procedure for the angular direction. Instead of $\partial_6\chi \to (\chi^{j+1} - \chi^j)/\Delta\varphi$ from Eq. (7.34) we choose the following prescription on a formal level

$$\partial_6 \to i \cdot \frac{\chi^{j+\frac{1}{2}} - \chi^{j-\frac{1}{2}}}{\Delta\varphi}.$$

This does not change anything with the zero mode or the heavy mode, but the transformations in Eqs. (7.35) lead to modified complex masses for the modes $\psi^1 \dots \psi^{N-1}$. Their squared absolute values read in this case

$$|m_\star + im(2\sin\frac{\pi n}{N})|^2 = m_\star^2 + 4m^2\sin^2(\frac{\pi n}{N}).$$

Here we see that the interference terms from above do not exist and the fermion mass spectrum has exactly the same structure as the gravitons.

7.7 Small Fermion Masses

Here, we finish this chapter with a simple application, where the results for the fermions on the discretised curved disk can be applied directly to generate small fermion masses. For this purpose let us assume that our known 4D world is located on the centre site of the disk. At this place the particle standard model may couple to the 4D component $\chi_{\rm R}^0$ of the 6D Dirac field via a Yukawa coupling schematically given by $\overline{L}\langle H\rangle\chi_{\rm R}^0$, where $\overline{L}$ is a left-handed lepton doublet and $\langle H\rangle$ is the VEV of the Higgs doublet, respectively. In addition we consider a large number N of lattice sites so that the heaviest mode Φ^N decouples due to its large mass $m_\star\sqrt{N+1}$. From Eq. (7.35) it follows that the right-handed fermion $\chi_{\rm R}^0$ on the centre site essentially consists only of the zero-mode $\psi_{\rm R}^0$ with a weight factor $1/\sqrt{N+1}$. Thus the Yukawa coupling of the left-handed SM doublet L with the right-handed fermion $\chi_{\rm R}^0$ leads to a suppression of the SM neutrino mass,

$$\overline{L}\langle H\rangle\chi_{\rm R}^0 \to \frac{1}{\sqrt{N+1}}\nu_{\rm L}\langle H\rangle\psi_{\rm R}^0.$$

For example, the number $N \sim 10^{24}$ might explain the lightness of the SM neutrinos [86]. For related applications in this context see also Ref. [85]. Finally, we mention that this mass suppression mechanism can be considered as a discrete version of the wave function suppression mechanism in continuous higher dimensions from Ref. [68].

8 Summary and Conclusions

In this thesis we have investigated the dark energy problem from two different perspectives that both involve vacuum energy, or equivalently the CC, as the major dark energy candidate. In the first part we have started with scaling laws for the CC originating from RGEs in quantum field theory and quantum gravity. However, since these theories do not fix the physical interpretation of the corresponding renormalisation scale, some typical scales occurring in the context of cosmology have been chosen to fit into this role. In this sense we have considered the Hubble rate in addition to the scales characterised by the cosmological event and particle horizons. In the end, this leads to a time-dependent CC implying a non-trivial scaling of the matter energy density with the cosmic scale factor. Solving Einstein's equations therefore becomes more complicated, but the solutions we found exhibit some very interesting features.

In the late-time epoch of the cosmological evolution we have found, apart from the well known de Sitter final states, also power-law and super-exponential solutions for the scale factor. Additionally, we have observed in some cases future singularities of the big rip and big crunch type, which usually appear only in more exotic dark energy models. In detail we have discussed in this analysis all combinations of scaling laws and renormalisation scale identifications and solved Einstein's equations analytically and numerically. As a result we have determined the fate of the universe for each case and studied the influence of the parameters on the solutions. By doing this it happened that some final states occur only for certain scaling laws or scale interpretations. Finally, the running of Newton's constant was taken into account in one case, which we treated numerically in more detail. In conclusion, the results found in this thesis feature several very different solutions for the cosmological late-time evolution. Based on this outcome the analysis may help to discriminate between different combinations of scaling laws and scales.

The second part of the work consists of an investigation of vacuum energy in higher dimensions, where we make use of the fact that the zero-point energy of quantum fields depends on boundary conditions. Starting from the Casimir effect in a continuous higher-dimensional space-time, where the Casimir energy density was determined and compared with results from the literature, we have adjusted the calculations to the case of discrete EDs. Within a detailed analysis we have discussed the influence of boundary conditions and the number of lattice sites on the value of the Casimir energy density, which contributes to the effective 4D CC. Special emphasis was placed on the effect of bulk field masses, which open up the possibility to considerably suppress the corresponding vacuum energy contribution. In addition, we have discussed the differences between the bosonic and fermionic case and observed some typical lattice artefacts for fermions.

A nice motivation for discrete EDs comes from the model building sector in the form

of deconstruction. Representing its most important property, this framework describes discretised EDs on the basis of 4D quantum fields thereby avoiding problems that appear in continuous higher dimensions. As quantum fields in this setup are not subject to boundary conditions their zero-point energy is a priori completely unconstrained. At this stage we have proposed a prescription to solve this problem by employing the correspondence between the discrete 5D setup and deconstruction. Therefore the vacuum energy of all 4D fields in deconstruction has been identified with the finite Casimir energy of the corresponding 5D quantum field. Within a specific model we have demonstrated this idea on a formal level for bosons and fermions. By using the suppression mechanism of large field masses in this setup, we have also shown that the vacuum energy contributions lie below or around the observed value of the CC.

Even if the strong condition of tiny CC contributions might be satisfied for arbitrary small EDs by implementing sufficiently large bulk masses, we have found that this might not be true for discrete gravitational EDs. In these models there usually exists a strong coupling scale that depends on the size of the ED thereby implying an upper limit for the mass scales in the theory. Due to this UV/IR connection one has lost the ability to arbitrarily suppress the Casimir energy by considering large bulk masses. In this context, a lower limit on the ED size emerges. By applying our results for the Casimir effect we have found the minimal size $R_{\min}$ to be roughly in the range $(10^{12}\,\mathrm{GeV})^{-1} \ldots (10^{7}\,\mathrm{GeV})^{-1}$. As a consequence, one can exclude, e.g., Planck scale sized EDs in this framework.

Motivated by the appearance of massive gravitons in discrete gravitational dimensions our last subject of investigation consists of a 6D model, where both EDs form a discretised two-dimensional curved disk. After discussing the disk in the continuum, we have applied a special discretisation procedure that features 4D gravitons with an interesting mass spectrum. The explicitly performed calculation of the masses has led, for instance, to the observation of a gap between the zero mode and the finite KK tower. As the main result of this subject, both mass scales appearing in this spectrum were found to be completely adjustable by the parameters of the curved disk. In contrast to a flat disk, here it is the curvature of the disk that makes this flexibility possible. In the future, it will be interesting to explore some applications and the strong coupling scale in this setup or more generalised scenarios [86]. As a foretaste, we have finally shown in this work the explicit implementation of fermions, which could be directly applied to generate small fermion masses.

As our final conclusion let us mention that, despite many possible candidates for the source of the accelerated expansion of the universe, the CC should be the first one to look at. We have seen in this thesis that quantum effects lead not only to a dependence on boundary conditions as given by discrete EDs, but they may also induce a time-dependence. By investigating both subjects we have found new insights for cosmology and the structure of our space-time.

Acknowledgements

At first, I would like to thank Manfred Lindner for great support, collaboration and the freedom in doing my research. Furthermore, I wish to thank my collaborators Marc-Thomas Eisele, Mathias Garny, Tomas Hällgren and Gerhart Seidl for excellent teamwork and fruitful discussions. I also thank Markus Michael Müller for accepting the sunshine in our office and for the nice coffee discussions. Moreover, I want to express my appreciation to all members and guests of our group for the excellent atmosphere during the last years. Also, I acknowledge financial support in terms of a doctorate grant by the Freistaat Bayern. Finally, my biggest thanks go to my parents for their great support.

Bibliography

[1] Supernova Search Team Collaboration, A. G. Riess et al., Astron. J. 116, 1009 (1998), astro-ph/9805201; J. L. Tonry et al., Astrophys. J. **594**, 1 (2003), astro-ph/0305008.

[2] Supernova Cosmology Project Collaboration, S. Perlmutter et al., Astrophys. J. 517, 565 (1999), astro-ph/9812133; R. A. Knop et al., Astrophys. J. **598**, 102 (2003), astro-ph/0309368.

[3] SDSS Collaboration, M. Tegmar*k* et al., Phys. Rev. D 69, 103501 (2004), astro-ph/0310723.

[4] S. P. Boughn and R. G. Crittenden, Nature **427**, 45 (2004), astro-ph/0404470.

[5] S. Hannestad, astro-ph/0509320.

[6] D. N. Spergel et al., astro-ph/0603449.

[7] P. J. E. Peebles and B. Ratra, Rev. Mod. Phys. **75** (2003) 559, astro-ph/0207347.

[8] V. Sahni, Lect. Notes Phys. **653** (2004) 141, astro-ph/0403324.

[9] T. Padmanabhan, Phys. Rept. **380** (2003) 235, hep-th/0212290; T. Padmanabhan, gr-qc/0503107.

[10] L. Perivolaropoulos, astro-ph/0601014.

[11] E. J. Copeland, M. Sami and S. Tsujikawa, hep-th/0603057.

[12] S. Weinberg, Rev. Mod. Phys. **61** (1989) 1.

[13] C. Wetterich, Nucl. Phys. B **302**, 668 (1988); B. Ratra and P. J. E. Peebles, Phys. Rev. D **37**, 3406 (1988).

[14] J. D. Barrow, Class. Quant. Grav. **21** (2004) L79, gr-qc/0403084; S. Nojiri, S. D. Odintsov, S. Tsujikawa, Phys. Rev. D **71** (2005) 063004, hep-th/0501025; M. Sami, A. Toporensky, P. V. Tretjakov, S. Tsujikawa, Phys. Lett. B **619** (2005) 193, hep-th/0504154; P. Tretyakov, A. Toporensky, C. Cattoen, M. Visser, gr-qc/0508045; Y. Shtanov, V. Sahni, gr-qc/0510104.

[15] R. R. Caldwell, M. Kamionkowski and N. N. Weinberg, Phys. Rev. Lett. 91 (2003) 071301, astro-ph/0302506.

[16] N. D. Birrell and P. C. W. Davies, "Quantum Fields In Curved Space," Cambridge, UK: Univ. Pr. (1982) 340p.

[17] I. L. Shapiro, J. Sola, Phys. Lett. B **475** (2000) 236, hep-ph/9910462; I. L. Shapiro, J. Sola, JHEP **0202** (2002) 006, hep-th/0012227; I. L. Shapiro, J. Sola, C. Espana-Bonet, P. Ruiz-Lapuente, Phys. Lett. B **574** (2003) 149, astro-ph/0303306; C. Espana-Bonet, P. Ruiz-Lapuente, I. L. Shapiro, J. Sola, JCAP **0402** (2004) 006, hep-ph/0311171; I. L. Shapiro, J. Sola, astro-ph/0401015; I. L. Shapiro, J. Sola, H. Stefancic, JCAP **0501** (2005) 012, hep-ph/0410095; J. Grande, J. Sola and H. Stefancic, gr-qc/0604057.

[18] A. Babic, B. Guberina, R. Horvat, H. Stefancic, Phys. Rev. D **65** (2002) 085002, hep-ph/0111207; B. Guberina, R. Horvat, H. Stefancic, Phys. Rev. D **67** (2003) 083001, hep-ph/0211184; A. Babic, B. Guberina, R. Horvat, H. Stefancic, Phys. Rev. D **71** (2005) 124041, astro-ph/0407572; B. Guberina, R. Horvat, H. Stefancic, JCAP **0505** (2005) 001, astro-ph/0503495.

[19] I. L. Buchbinder, S. D. Odintsov and I. L. Shapiro, "Effective action in quantum gravity," Bristol, UK: IOP (1992) 413 p.

[20] M. Reuter, Phys. Rev. D **57** (1998) 971, hep-th/9605030; A. Bonanno and M. Reuter, Phys. Rev. D **65** (2002) 043508, hep-th/0106133; M. Reuter, H. Weyer, JCAP **0412** (2004) 001, hep-th/0410119.

[21] M. Reuter, C. Wetterich, Phys. Lett. B **188** (1987) 38; M. Reuter, hep-th/0012069; A. Bonanno, M. Reuter, Int. J. Mod. Phys. D **13** (2004) 107, astro-ph/0210472; A. Bonanno, G. Esposito, C. Ruban, Gen. Rel. Grav. **35** (2003) 1899, hep-th/0303154; M. Reuter, H. Weyer, hep-th/0311196; A. Bonanno, G. Esposito, C. Rubano, gr-qc/0403115; M. Reuter, H. Weyer, Phys. Rev. D **70** (2004) 124028, hep-th/0410117.

[22] O. Bertolami, J. M. Mourao, J. Perez-Mercader, Phys. Lett. B **311** (1993) 27; E. Elizalde, S. D. Odintsov, I. L. Shapiro, Class. Quant. Grav. **11** (1994) 1607, hep-th/9404064; O. Bertolami, J. Garcia-Bellido, Int. J. Mod. Phys. D **5** (1996) 363, astro-ph/9502010; E. Elizalde, C. O. Lousto, S. D. Odintsov, A. Romeo, Phys. Rev. D **52** (1995) 2202, hep-th/9504014; A. A. Bytsenko, L. N. Granda, S. D. Odintsov, JETP Lett. **65** (1997) 600, hep-th/9705008; E. Verlinde, H. Verlinde, JHEP **0005** (2000) 034, hep-th/9912018; C. Rubano, P. Scudellaro, Gen. Rel. Grav. **37** (2005) 521, astro-ph/0410260; H. W. Hamber, R. M. Williams, Phys. Rev. D **72** (2005) 044026, hep-th/0507017.

[23] H. B. G. Casimir, Kon. Ned. Akad. Wetensch. Proc. **51** (1948) 793.

[24] T. Appelquist and A. Chodos, Phys. Rev. Lett. **50**, 141 (1983); Phys. Rev. D **28**, 772 (1983).

[25] E.G. Adelberger, B.R. Heckel and A.E. Nelson, hep-ph/0307284; C.D. Hoyle, U. Schmidt, B.R. Heckel, E.G. Adelberger, J.H. Gundlach, D.J. Kapner, H.E. Swanson, Phys. Rev. Lett. **86** (2001) 1418, hep-ph/0011014; EÖT-WASH Group, E.G. Adelberger, et al., hep-ex/0202008.

[26] S. Cullen and M. Perelstein, Phys. Rev. Lett. **83** (1999) 268, hep-ph/9903422; V. Barger, T. Han, C. Kao, and R.J. Zhang, Phys. Lett B **461** (1999) 34, hep-ph/9905474; S. Hannestad and G.G. Raffelt, Phys. Rev. Lett. **87** (2001) 051301, hep-ph/0103201; C. Hanhart, D.R. Philips, S. Reddy, and M.J. Savage, Nucl. Phys. B **595** (2001) 335, nucl-th/0007016.

[27] S. Hannestad and G.G. Raffelt, Phys. Rev. Lett. **88** (2001) 071301, hep-ph/0110067; S. Hannestad and G.G. Raffelt, Phys. Rev. D **67** (2003) 125008, hep-ph/0304029.

[28] A. Perez, Class. Quant. Grav. **20** (2003) R43, gr-qc/0301113; D. Rideout, S. Zohren, gr-qc/0606065.

[29] N. Arkani-Hamed, A.G. Cohen, and H. Georgi, Phys. Rev. Lett. **86** (2001) 4757, hep-th/0104005.

[30] C. T. Hill, S. Pokorski, and J. Wang, Phys. Rev. D **64** (2001) 105005, hep-th/0104035.

[31] N. Arkani-Hamed, H. Georgi, and M. D. Schwartz, Annals Phys. **305** (2003) 96, hep-th/0210184.

[32] N. Arkani-Hamed and M. D. Schwartz, Phys. Rev. D **69** (2004) 104001, hep-th/0302110.

[33] F. Bauer, Class. Quant. Grav. **22** (2005) 3533, gr-qc/0501078.

[34] F. Bauer, gr-qc/0512007.

[35] J. Sola, H. Stefancic, Phys. Lett. B **624** (2005) 147, astro-ph/0505133; J. Sola, H. Stefancic, astro-ph/0507110.

[36] E.V. Gorbar, I.L. Shapiro, JHEP **0302** (2003) 021, hep-ph/0210388; I.L. Shapiro, hep-th/0412115.

[37] O. Lauscher, M. Reuter, Phys. Rev. D **65** (2002) 025013, hep-th/0108040; O. Lauscher, M. Reuter, Class. Quant. Grav. **19** (2002) 483, hep-th/0110021; D. F. Litim, Phys. Rev. Lett. **92** (2004) 201301, hep-th/0312114; A. Bonanno, M. Reuter, hep-th/0410191; A. Bonanno, G. Esposito, C. Rubano, Int. J. Mod. Phys. A **20** (2005) 2358, hep-th/0511188.

[38] A. Bonanno, M. Reuter, Phys. Lett. B **527** (2002) 9, astro-ph/0106468; E. Bentivegna, A. Bonanno, M. Reuter, JCAP **0401** (2004) 001, astro-ph/0303150; A. Bonanno, G. Esposito, G. Rubano, P. Scudellaro, astro-ph/0507670.

[39] M. Reuter, F. Saueressig, JCAP **0509** (2005) 012, hep-th/0507167.

[40] H. W. Hamber, R. M. Williams, Nucl. Phys. B **435**, 361 (1995), hep-th/9406163; H. W. Hamber, R. M. Williams, Phys. Rev. D **59**, 064014 (1999), hep-th/9708019; H. W. Hamber, Phys. Rev. D **61**, 124008 (2000), hep-th/9912246.

[41] G. W. Gibbons, S. W. Hawking, Phys. Rev. D **15** (1977) 2738; T. Padmanabhan, Phys. Rept. **406** (2005) 49, gr-qc/0311036.

[42] T. M. Davis, C. H. Lineweaver, astro-ph/0310808.

[43] A. Gregori, hep-th/0207195; A. Gregori, hep-th/0402126.

[44] T. Padmanabhan, Phys. Rept. **406** (2005) 49, gr-qc/0311036; hep-th/0406060.

[45] L. Parker, Phys. Rev. Lett. **21** (1968) 562.

[46] H. Stefancic, Phys. Rev. D **71** (2005) 084024, astro-ph/0411630; S. Nojiri, S.D. Odintsov, S. Tsujikawa, Phys. Rev. D **71** (2005) 063004, hep-th/0501025.

[47] J.P. Uzan, AIP Conf. Proc. **736** (2005) 3, astro-ph/0409424.

[48] S. Nojiri, S. D. Odintsov, Phys. Lett. B **595** (2004) 1, hep-th/0405078; E. Elizalde, S. Nojiri, S. D. Odintsov, Phys. Rev. D **70** (2004) 043539, hep-th/0405034.

[49] E. M. Barboza Jr., N. A. Lemos, gr-qc/0606084.

[50] T. Kaluza, Sitzungsber. Preuss. Akad. Wiss. Berlin (Math. Phys.) **1921**, 966 (1921); O. Klein, Z. Phys. **37**, 895 (1926); Surveys High Energ. Phys. **5**, 241 (1986).

[51] E. Cremmer and B. Julia, Phys. Lett. B **80** (1978) 48; J. Sherk and J. Schwarz, Nucl. Phys. B **153** (1979) 61.

[52] I. Antoniadis, Phys. Lett. B **246** (1990) 377; I. Antoniadis, C. Munoz, M. Quiros, Nucl. Phys. B **397** (1993) 515, hep-ph/9211309; I. Antoniadis, K. Benakli, M. Quiros, Phys. Lett. B **331** (1994) 313, hep-ph/9403290; J. Lykken, Phys. Rev. D **54** (1996) 3693, hep-th/9603133; I. Antoniadis, S. Dimopoulos, G. Dvali, Nucl. Phys. B **516** (1998) 70, hep-ph/9710204; J. Lykken, L. Randall, J. High Energy Phys. **0006** (2000) 014, hep-th/9908076.

[53] I. Antoniadis, C. Bachas, D. C. Lewellen and T. N. Tomaras, Phys. Lett. B **207** (1988) 441; I. Antoniadis, N. Arkani-Hamed, S. Dimopoulos and G.R. Dvali, Phys. Lett. B **436** (1998) 257, hep-ph/9804398.

[54] E. Ponton, E. Poppitz, JHEP **0106**, 019 (2001), hep-ph/0105021; E. Elizalde, S. Nojiri, S.D. Odintsov, S. Ogushi, Phys. Rev. D **67**, 063515 (2003), hep-th/0209242.

[55] P. Candelas and S. Weinberg, Nucl. Phys. B 237 (1984) 397.

[56] M.J. Sparnaay, Physica 24 (1958) 751.

[57] M. Bordag, U. Mohideen and V. M. Mostepanenko, Phys. Rept. **353**, 1 (2001), quant-ph/0106045.

[58] K. A. Milton, J. Phys. A **37** (2004) R209, hep-th/0406024.

[59] C.J. Isham, Proc. R. Soc. Lond. A. **362** (1978) 383; C.J. Isham, Proc. R. Soc. Lond. A. **364** (1978) 591; S.J. Avis and C.J. Isham, Nucl. Phys. B **156** (1979) 441.

[60] A. A. Saharian, hep-th/0002239.

[61] R. Kantowski and K.A. Milton, Phys. Rev. D 36 (1987) 3712.

[62] A. Pilaftsis, Phys. Rev. D 60 (1999) 105023, hep-ph/9906265.

[63] C.T. Hill and A.K. Leibovich, Phys. Rev. D 66 (2002) 016006, hep-ph/0205057.

[64] W.A. Bardeen and R.B. Pearson, Phys. Rev. D 14 (1976), 547; W.A. Bardeen, R.B. Pearson and E. Rabinovici, Phys. Rev. D 21 (1980) 1037.

[65] H.C. Cheng, C.T. Hill, S. Pokorski, J. Wang, Phys. Rev. D 64 (2001) 065007, hep-th/0104179; H.C. Cheng, K.T. Matchev, J. Wang, Phys. Lett. B 521 (2001) 308, hep-ph/0107268; A. Falkowski, C. Grojean, S. Pokorski, Phys. Lett. B 535 (2002) 258, hep-ph/0203033; L. Randall, Y. Shadmi, N. Weiner, J. High Energy Phys. 0301 (2003) 055, hep-th/0208120; E. Dudas, A. Falkowski, S. Pokorski, Phys. Lett. B 568 (2003) 281, hep-th/0303155.

[66] F. Bauer, M. Lindner, and G. Seidl, JHEP **0405** (2004) 026, hep-th/0309200.

[67] N. Arkani-Hamed, S. Dimopoulos, G.R. Dvali, Phys. Lett. B **429** (1998) 263, hep-ph/9803315; Phys. Rev. D **59** (1999) 086004, hep-ph/9807344; I. Antoniadis, N. Arkani-Hamed, S. Dimopoulos, G.R. Dvali, Phys. Lett. B **436** (1998) 257, hep-ph/9804398.

[68] N. Arkani-Hamed, S. Dimopoulos, G. R. Dvali and J. March-Russell, Phys. Rev. D 65 (2002) 024032, hep-ph/9811448; K.R. Dienes, E. Dudas, and T. Gherghetta, Nucl. Phys. B **557** (1999) 25, hep-ph/9811428.

[69] H. Georgi, Nucl. Phys. B **266** (1986) 274.

[70] M.R. Douglas and G. Moore, hep-th/9603167.

[71] R.N. Mohapatra and G. Senjanović, Phys. Rev. Lett. **44** (1980) 912; Phys. Rev. D **23** (1981) 165; J. Schechter and J.W.F. Valle, Phys. Rev. D **22** (1980) 2227; G. Lazarides, Q. Shafi, and C. Wetterich, Nucl. Phys. B **181** (1981) 287.

[72] K.G. Wilson, Phys. Rev. D 10 (1974) 2445.

[73] N. Arkani-Hamed, A.G. Cohen and H. Georgi, JHEP **0207**, 020 (2002), hep-th/0109082.

[74] G. Cognola, E. Elizalde, S. Nojiri, S. D. Odintsov, S. Zerbini, Mod. Phys. Lett. A **19**, 1435 (2004) hep-th/0312269. S. Nojiri, S. D. Odintsov, Phys. Lett. B **590**, 295 (2004), hep-th/0403162. G. Cognola, E. Elizalde, S. Zerbini, hep-th/0506082.

[75] N. Kan and K. Shiraishi, Class. Quant. Grav. **20**, 4965 (2003), gr-qc/0212113.

[76] F. Bauer and G. Seidl, Phys. Lett. B 624 (2005) 250, hep-ph/0506184.

[77] M. Fierz and W. Pauli, Proc. Roy. Soc. Lond. A **173** (1939) 211.

[78] P. Creminelli, A. Nicolis, M. Papucci and E. Trincherini, JHEP **0509**, 003 (2005), hep-th/0505147.

[79] N. Boulanger, T. Damour, L. Gualtieri and M. Henneaux, Nucl. Phys. B **597**, 127 (2001) hep-th/0007220; N. Boulanger, Fortsch. Phys. **50**, 858 (2002), hep-th/0111216.

[80] T. Damour, I.I. Kogan and A. Papazoglou, Phys. Rev. D **66**, 104025 (2002), hep-th/0206044; C. Deffayet and J. Mourad, Class. Quant. Grav. **21**, 1833 (2004), hep-th/0311125.

[81] S.R. Coleman, J. Wess and B. Zumino, Phys. Rev. **177** (1969) 2239; C.G. Callan, S.R. Coleman, J. Wess and B. Zumino, Phys. Rev. **177** (1969) 2247.

[82] M.D. Schwartz, Phys. Rev. D **68** (2003) 024029, hep-th/0303114.

[83] K.A. Milton, R. Kantowski, C. Kao and Y. Wang, Mod. Phys. Lett. A **16**, 2281 (2001), hep-ph/0105250; K.A. Milton, Grav. Cosmol. **9**, 66 (2003), hep-ph/0210170.

[84] C. D. Hoyle, D. J. Kapner, B. R. Heckel, E. G. Adelberger, J. H. Gundlach, U. Schmidt and H. E. Swanson, Phys. Rev. D **70** (2004) 042004, hep-ph/0405262.

[85] T. Hällgren, T. Ohlsson and G. Seidl, JHEP **0502** (2005) 049, hep-ph/0411312.

[86] F. Bauer, T. Hällgren and G. Seidl, in preparation.

[87] H.D. Kim, JHEP **0601** (2006) 090, hep-th/0510229.

[88] N. Kaloper, J. March-Russell, G. D. Starkman and M. Trodden, Phys. Rev. Lett. 85 (2000) 928, hep-ph/0002001.

[89] I. P. Neupane, Class. Quant. Grav. **21** (2004) 4383, hep-th/0311071.

[90] G. 't Hooft and M.J.G. Veltman, Annales Poincare Phys. Theor. A **20** (1974) 69; M.J.G. Veltman, in "Les Houches 1975: Methods in Field Theory", North-Holland, Amsterdam (1976); P. Van Nieuwenhuizen, Phys. Rept. **68** (1981) 189.

[91] S. Weinberg, "Gravitation and Cosmology: Principles and Applications of the General Theory of Relativity", Wiley, New York (1972).